NOTICE

The quality of this microform is heavily dependent upon the quality of the original thesis submitted for microfilming. Every effort has been made to ensure the highest quality of reproduction possible.

If pages are missing, contact the university which granted the degree.

Some pages may have indistinct print especially if the original pages were typed with a poor typewriter ribbon or if the university sent us an inferior photocopy.

Reproduction in full or in part of this microform is governed by the Canadian Copyright Act, R.S.C. 1970, c. C-30, and subsequent amendments.

AVIS

La qualité de cette microforme dépend grandement de la qualité de la thèse soumise au microfilmage. Nous avons tout fait pour assurer une qualité supérieure de reproduction.

S'il manque des pages, veuillez communiquer avec l'université qui a conféré le grade.

La qualité d'impression de certaines pages peut laisser à désirer, surtout si les pages originales ont été dactylographiées à l'aide d'un ruban usé ou si l'université nous a fait parvenir une photocopie de qualité inférieure.

La reproduction, même partielle, de cette microforme est soumise à la Loi canadienne sur le droit d'auteur, SRC 1970, c. C-30, et ses amendements subséquents.

FLAT PLATE BUFFETING IN YAWED WIND WITH POSSIBLE APPLICATIONS TO BRIDGES

by

Kichiro Kimura

A dissertation submitted to the University of Ottawa
in partial fulfillment of the requirements
for the degree of Doctor of Phiiosophy.
Department of Civil Engineering
University of Ottawa

ISBN 0-315-75065-0

UNIVERSITÉ D'OTTAWA
UNIVERSITY OF OTTAWA

ABSTRACT

The wind resistant design of bridges becomes more realistic if the directionality of wind is incorporated into the analysis. However, the necessary information about the bridge response under wind with yaw angle, namely, under a wind not perpendicular to the bridge longitudinal axis, has not been obtained to this date.

This thesis is concerned with the buffeting response of cantilever models under yawed turbulent wind. The employed cantilever models can be thought as a simple version of a cable-stayed bridge under construction which is known to be extremely vulnerable to the wind action. It has been also indicated that these structures reveal relatively large response under yawed wind.

Models with various cross-sections were tested under different flow conditions and the buffeting response was measured taking the yaw angle as a parameter. The response was mostly in the first vertical bending mode. For the flat plate cross-section models, the effect of the model width was found to be most significant. The wider the model was, the larger the response was found to be under the wind from the free end direction. Even the largest response was sometimes observed under the wind parallel to the model axis from free end direction. A simple response prediction by taking the cosine component of the wind velocity, which has been used from time to time, was found to give generally smaller values than the actual model response.

The conventional buffeting analysis was modified so that the response of the cantilever structure under yawed wind can be predicted. Wind velocity components normal to the side and the end of the model were taken as the effective wind velocities, and the response was calculated separately corresponding to each effective wind velocity. The modified buffeting analysis was applied to the flat plate cross-section models. The analytical results generally explained the experimental findings regarding the effect of the wind yaw angle.

ACKNOWLEDGEMENT

The author would like to express his deepest gratitude to his supervisor, Dr. H. Tanaka for his guidance and encouragement all through the period of this study.

The gratitude is also extended to Mr. R.L. Wardlaw, the former Head of the Low Speed Aerodynamics Laboratory, National Research Council Canada, for a number of occasions for the discussion on the subject matter and also for his kind arrangement to give access to the experiment facilities for the author's convenience. The author is also grateful to Dr. R.J. Kind of Carleton University for his generosity to let the author use the wind tunnel at his laboratory. Technical discussion with the member of the Low Speed Aerodynamics Laboratory particularly Drs. J. Xie, S.J. Zan and N.G. Ball has been always very helpful. The time spent with Dr. T. Yoshimura, a visiting professor from Kyushu Sangyo University, was instructive and helpful particularly regarding the wind tunnel testing.

The assistance of the entire Low Speed Aerodynamics Laboratory staff and the Mechanical Engineering and Aeronautics Library personnel is gratefully acknowledged. Among all, Mr. M.G. Savage took extensive care within his capacity in order to help the author. Mr. V. Maloney at the machine shop provided useful ideas about the model design. The author is grateful to Mr. Maloney and his staff for their efforts and assistance in manufacturing the models. Discussions with friends at University of Ottawa were useful, in particular, the names of Mr. L. Phillips and Mrs. S. Resende-Ide should be mentioned for their suggestions and encouragements. Finally, the gratitude must be extended to Drs. M. Ito and Y. Fujino, the former supervisors of the author at the University of Tokyo, for their warm encouragement all through the study.

The financial support was provided by the Natural Science and Research Council through the supervisor, University of Ottawa Scholarships, Japan Education Association (Nihon Ikuei Kai) scholarship, FINIPED, Civil Engineering Alumni Association of the University of Tokyo and also by the author's parents. All of this support is gratefully acknowledged.

TABLE OF CONTENTS

LIST OF SYMBOLS

The following is a list of commonly appearing symbols. Symbols used only once are defined in the text where they are used.

AR	aspect ratio (Section 4.2.7)
b	model width (Fig. 3.2)
B	typical dimension of the section (deck width)
C_L	lift coefficient (Fig. 2.1)
C_D	drag coefficient (Fig. 2.1)
C_M	moment coefficient (Fig. 2.1)
d	model depth
D	aerodynamic drag force (Fig. 2.1)
f	frequency
f_r	natural frequency of the r-*th* mode
F	force
F_r	generalized force for the r-*th* mode(eqn. (2.15))
h_a	aerodynamic damping ratio
h_s	structural damping ratio
h_T	total damping ratio
$\|H_r(f)\|^2$	mechanical admittance for the r-*th* mode(eqn. (2.25))
I_u, I_w	turbulence intensities (eqns. (2.28) and (2.29))
K, K′	reduced frequency, $K = B\omega/U$, $K' = Bf/U$
l	model length (Fig. 3.2)

L	aerodynamic lift force (Fig. 2.1)
L	scale of isotropic turbulence (Section 2.3.5)
L_y^w, L_x^u, etc.	scales of turbulence (Section 2.3.5)
m	distributed mass
M	aerodynamic pitching moment (Fig. 2.1)
M_r	generalized mass for the r-*th* mode (eqn. 2.16)
q	generalized coordinate (eqn. 2.13)
r.m.s.	root-mean-square
S	power spectrum
S_u, S_w	power spectra of u and w-component
S_q	power spectrum in terms of generalized coordinate
S_{uu}, S_{ww}	cross spectra of u and w-component
U	mean wind speed
U_e	effective wind velocity (Section 4.2.1)
U_r	relative wind velocity (Figs. 2.2 and 2.3)
$\|X_L^w(fB/U)\|^2$	aerodynamic admittance (Section 2.3.6)
u, v, w	fluctuating wind velocity component (Fig. 3.2)
x, y, z	coordinates taken with reference to the wind direction (Fig. 3.2). These coordinates agree with structural coordinates when no wind yaw angle is considered (Section 2.3).
x′, y′, z′	coordinate taken with reference to the structure (Fig. 3.2)
α	angle of attack (Fig. 2.1)
α'	instantaneous angle of attack (Fig. 2.2)

β	wind yaw angle (Figs. 2.5 and 3.2)
θ	torsional displacement
ρ	air density
σ	overall r.m.s. response
ϕ	mode shape (eqn. (2.13))
ω	circular frequency
ω_r	natural circular frequency for the r-*th* mode

Subscripts

b	buffeting force
s	self-excited force
r	r-*th* mode
u	u-component
w	w-component
q	generalized coordinate
z, z′	z or z′-direction
α	differentiation with respect to α
C	cosine case (Section 4.2.1)
S	sine case (Section 4.2.1)
:l	"linear" case (Section 4.2.7)
:n	"nonlinear" case (Section 4.2.7)

Other

" · "	differentiation with respect to time

Chapter 1. INTRODUCTION

1.1. Brief History of Research on the Wind Induced Dynamic Response of Bridges

Dynamic response of bridges caused by wind action has been drawing bridge engineers' attention for more than half a century since the dramatic failure of the original Tacoma Narrows bridge in 1940. Before this disaster, the wind resistant design of bridges had only counted the static wind load. The Tacoma Narrows bridge for example was designed to withstand the static wind loading equivalent to the wind speed of 60 m/sec. However, the bridge revealed a violent torsional motion which led to the failure of the main span under a moderately strong wind. The wind speed was reported to be only 19 m/sec. The cause of the phenomenon was not clear then, but it was apparent that the wind-induced *dynamic* response played a principal role in the incident (Scanlan, 1980; Tanaka, 1988).

After this incident, a technique of scaled bridge model testing in wind tunnel was introduced in order to investigate the dynamic behaviour of cable supported bridges under wind action. The earliest contributions were made by Farquharson et al. (1950-54) and by Scruton (1952) et al. The important results from these studies are as follows (Davenport et al., 1969a): 1) The aerodynamic instability phenomena such as observed on the Tacoma Narrows bridge can be reproduced by using a scaled "full model"; 2) The critical wind speed for aerodynamic instability can be estimated by using a "sectional model" with reasonable accuracy. Full bridge models are intended to model the whole bridge structure including the towers and cable system with correctly scaled mechanical characteristics as well as the exact geometrical shapes (Wardlaw, 1979). Generally speaking, the aerodynamic forces acting on bridge deck system are considered to be dominant in the overall aerodynamic forces. Therefore, the requirement of exact geometrical modelling of towers and cables is sometimes relaxed even for full models. Sectional models usually consider only the aerodynamic forces acting on bridge decks, and are intended to model a typical bridge deck section "sliced out" of the suspended structure. The sliced out

rigid section which should have a correct geometrical configuration is usually spring-supported across the wind tunnel with its span normal to the wind. Mechanical characteristics are controlled by the supporting system. By using a slice of the bridge deck as a model, the sectional model replaces the original problem with a two-dimensional problem. So, it is also important to keep the two-dimensionality of the flow over the sectional model. The model constructions in these early studies more or less set the standard for the wind tunnel testing for bridge aerodynamics since then. These tests have been carried out mostly in conventional aeronautical wind tunnels which generate uniform flows with very low turbulence, because the wind tunnel testing techniques had been well developed in aeronautics since the beginning of this century and most wind tunnels were constructed for aeronautical use. The cost of a wind tunnel experiment using a full bridge model tends to be expensive because of the complex model construction and also because of the need of a large wind tunnel in order to have a model that duplicates enough details to reproduce the aerodynamic characteristics of the prototype. It is relatively inexpensive and less time consuming to carry out a sectional model testing, and the procedure to determine the critical wind speed for the aerodynamic instabilities using sectional models in an uniform flow with very low turbulence has been accepted as a popular method.

In the 1960's, the importance of considering more realistic wind condition for bridge response was pointed out (Davenport, 1962b). Uniform flow with very low turbulence commonly used in the aeronautical wind tunnels is by no means similar to natural wind for bridge structures where wind is often considered to be an atmospheric boundary layer flow with three-dimensional structure of the turbulence. The wind also does not necessarily approach with an angle normal to the longitudinal bridge axis. In order to consider these effects, a sectional model has some inherent difficulties because of its two-dimensional characteristics. On the other hand, a full model in artificially created boundary layer flow as a simulated natural wind may well represent much more realistic situations. Experiments with this viewpoint began to be conducted using full bridge models with simulated natural wind conditions (for example, Davenport et al., 1969a, 1969b; Melbourne, 1980; Irwin and Schuyler, 1977; Davenport and King, 1982; Gamble and Irwin, 1985; Zan, Yamada and Tanaka, 1986; Zan, 1987b; Ferraro and Irwin, 1989, Davenport and King, 1990). The model bridge responses were found to be influenced greatly by the

existence of turbulence in the approaching flow. However, as stated previously, experiments using full models are expensive, time consuming and technically more difficult. In order to overcome these difficulties, the concept of the "taut strip model" was proposed (Davenport, 1974). The stiffness of taut strip models is given by two or more taut wires stretched in the model span-wise direction between anchor blocks. Bridge deck section modules imitating the bridge deck configuration are attached to the taut wires forming the geometrical shape and mass distribution of the model. Taut strip models can be tested more easily compared with full models because of their simple structures. Despite the fact that taut strip models only reveal a half sine wave mode shape as the fundamental mode, the response of the model can be used as the essential information to predict the prototype bridge response. Test results using taut strip models in turbulent boundary layer flow provided good agreement with observed full scale bridge motions (Davenport et al., 1980; Tanaka and Davenport, 1983). Advantages and disadvantages of this particular method have been extensively discussed elsewhere (Tanaka, 1987). It should be pointed out that there is also another viewpoint regarding the use of sectional models, where such models are used as a device to provide the essential information on the aerodynamic characteristics of bridge decks (Scanlan, 1983, 1987). If that is the case, the correct modelling of the geometrical shape is essentially the only requirement for the model, and by employing the analytical approach together with the information obtained from the experiment, the prototype response can be predicted.

These extensive experimental studies have given considerable insight on the characteristics of bridge dynamic behaviour under wind action. Together with analytical studies which try to explain the mechanism of the phenomena, the understanding of the subject is so advanced that now a suspension bridge having a centre span of 2000 m can be a realistic project. However, complete understanding of the phenomena is yet to be achieved.

1.2. Wind Induced Dynamic Behaviour of Bridges

There are various types of wind induced dynamic response of bridge decks and they may

be classified as follows (Tanaka, 1988):

- Vortex induced oscillation
- Self-excited oscillations
  - Vertical bending instability
  - Torsional instability
  - Coupled flutter
- Buffeting motion

The mechanism of the vortex induced oscillation is still not completely understood but it is basically attributed to the periodic vortices shed from the aerodynamically bluff bridge decks. The vortex shedding frequency is usually proportional to the wind speed. Thus, the fluctuation of the aerodynamic forces induced by these vortices causes a resonant response at a specific wind speed where the vortex shedding frequency coincides with a natural frequency of the bridge. When such motion occurs, the shedding frequency may be locked-in to the frequency of the motion over a limited range of wind speed and the resonance continues in that range. The motion of the bridge deck also has an effect over the magnitude of the exciting forces which show a strong nonlinearity with the amplitude of the motion. For small amplitude motions, the exciting force increases with the amplitude of the motion. However, if the motion amplitude exceeds a certain limit, the exciting force alters into a damping force. Thus the vortex induced oscillation usually shows limited amplitude response within a narrow range of wind velocity. This type of response is often observed in relatively low wind speed.

The self-excited oscillations occur when energy transfer from the flow to the structural system occurs because of the movement of the bridge deck. The vertical bending instability and torsional instability are single-degree-of-freedom flutters associated with the negative damping due to anti-symmetrical flow separation or delayed flow re-attachment around a moving bluff bridge deck. The collapse of the original Tacoma Narrows bridge is considered to be because of torsional instability. Coupled flutter occurs with unseparated flow conditions around a streamlined bridge deck and is caused by the energy transfer from the flow due to the coupled

vertical and torsional motion with a phase lag. A critical wind speed for the coupled flutter is generally higher than that of the single-degree-of-freedom flutters. These self-excited oscillations are divergent amplitude oscillations. The response amplitude often grows up rapidly if the wind speed rises to or beyond the critical wind speed.

The buffeting motion is generally defined as a random bridge response caused by the unsteady loading due to velocity fluctuations in the oncoming flow (Simiu and Scanlan, 1985). In bridge aerodynamics, atmospheric turbulence is the usual cause of the velocity fluctuation in the oncoming flow. Much more detailed explanation is given later in the thesis. Turbulence in the flow also affects the characteristics of the aerodynamic behaviour such as vortex induced and self-excited oscillations of structures (Wardlaw, Tanaka and Utsunomiya, 1983).

1.3. Scope of the Research

In this research, the buffeting motion which may be observed particularly in bridge structures is studied and special attention is given to the response under wind with yaw angle; or, in other words, under wind coming from an average direction not perpendicular to the bridge longitudinal axis. In this thesis, the wind yaw angle is defined as the horizontal angle of mean wind velocity from the direction normal to the bridge axis. The reason why this particular subject was chosen is as follows:

There are several types of dynamic phenomena which are observed as bridge response under wind action. The most dangerous phenomena are the self-excited oscillations which cause divergent amplitude response once they happen and the probable results are disasters like the Tacoma Narrows. This kind of phenomena must be avoided, and the bridge designers certainly do so as much as possible by the aid of present knowledge such as conducting wind tunnel tests. The vortex induced oscillation is less dangerous because it is generally speaking a limited amplitude oscillation. Although the phenomenon may cause serviceability problems or fatigue damage, the problem can be often solved successfully by changing the cross-sectional shape of

the bridge decks by applying various aerodynamic devices. On the other hand, the buffeting motion can occur in any bridge no matter how the bridge deck sections are designed. And the bridge response may grow more and more under higher wind speeds. This phenomenon may not cause immediate collapse of the bridge, but could lead to serious fatigue damage. This is the reason why the buffeting motion is considered as a serious topic in this study. Actually, the Severn bridge in U.K. has been reported to be suffering serious fatigue damages although its deck shape was carefully designed by extensive wind tunnel tests to avoid self-excited and vortex induced oscillations. These damages have been attributed mostly to the buffeting motion.

The wind induced response of long-span bridges has been extensively studied for decades as stated before. One of the assumptions, however, usually made in these studies is that the wind approaches in the direction normal to the bridge axis. This assumption is almost intuitively agreeable with the understanding that the bridge response should be most sensitive to the wind normal to the bridge axis and the worst case, therefore, is thus being studied. However, this is only a critical case. The wind direction is almost constantly changing in reality. If a little more realistic prediction of probable bridge response is to be made in relation to the local wind climate, such as an expected annual peak response level or the probability of exceeding certain response levels for a given return period, this directionality of wind needs to be taken into account and the response under wind with various yaw angles becomes a necessary information.

Also, there are cases in which wind yaw angle other than normal to the bridge axis should be treated with special care. An example is a cable-stayed bridge during its construction and particularly when the balanced cantilever method is employed as is often the case in North America. This is known to be an extremely flexible structure susceptible to wind action. It is, of course, because of its overall structural stiffness. However, it is not only susceptible to a normal wind but the structure also seems to be equally vulnerable to a yawed wind. An aeroelastic model test of a cable-stayed bridge during its construction stage gave comparably high level of response under a wind angle of 30° as the same model under a normal wind (Zan, 1987a). In this case, the existence of unsupported free ends seems to be responsible for the high response. Similar phenomena have been observed in the case of cantilevered roofs (Barnard,

1981).

There have been some research works that studied the response of bridges under wind other than normal to the bridge longitudinal axis but more is needed to obtain a general idea of how the wind yaw angle affects the bridge response. The purpose of this study is to extract more insights on the buffeting analysis and the special focus is on the consideration of the wind yaw angle on the buffeting response of structures.

The thesis first attempts a literature review of previous studies on the buffeting motion of bridges and the effects of wind yaw angles. The procedure of conventional buffeting analysis is also explained. Then results of the present experimental study are reported. The behaviour of a cantilever supported model which is considered to be a very much simplified model of a cable-stayed bridge under construction is examined in turbulent wind with various wind yaw angles. The theoretical explanation of the model behaviour is also attempted. The conventional buffeting analysis is modified so that the response under yawed wind can be treated. The results of experimental and theoretical studies are compared and discussed. Finally, some concluding remarks are made on what has been obtained through the research.

Novel contributions by the author through the present study can be summarized as follows:

(1) Conspicuous buffeting response of cantilever supported structures under wind with yaw angle was studied experimentally and its characteristics were clarified.
(2) The conventional buffeting analysis was modified to include the effect of wind yaw angle. The results indicated that the experimental observations were reasonably well explained.

The modified analysis still has some room for possible improvements which will be discussed in the thesis. However, the purpose of the study is to increase the understanding of bridge response under yawed wind, and those improvements seem to be neither essential for the purpose nor reliable without further investigation. In the present study, the model response is

predicted by using acceptable assumptions within a current knowledge, and it gives a basis for the direction of further study. Nevertheless, the modified analysis that has been used explains the essential part of the phenomena observed in the experiment.

1.4. Objective of the Thesis

The objective of this thesis is to clarify the effect of wind yaw angle on buffeting response of structures such as bridges. Cantilevered structures are chosen to be studied because the effect of wind yaw angle seems to be more important for this type of structure. In order to simplify the problem, structures with flat plate cross-sections and the buffeting response in vertical bending are mostly considered. The result of the thesis will be applied to more practical cases such as a cable-stayed bridge under construction.

Chapter 2. PREVIOUS STUDIES

2.1. Introduction

In this chapter, previous research studies related to the present study are reviewed. First, the development of research work on the buffeting problem is briefly surveyed. Then, typical procedures for the buffeting analysis for vertical bridge deck motion is explained which forms the basis of the theoretical studies in Chapter 4. Finally, the previous researches which considered the effect of wind yaw angle are reviewed.

2.2. Buffeting Analysis

In the early 1950's, Liepmann (1952) treated the buffeting problem of two-dimensional aerofoils. The statistical concepts were introduced and the fluctuating lift on aerofoils was obtained by spectral analysis with the knowledge of statistical theories of isotropic turbulence. The same approach was applied to beams and plates by Eringen (1957). The development of the theory for aerofoils in turbulent flow is well described by Blake (1986, p.741).

These results were applied to civil engineering structures of slender, line-like form such as long-span suspension bridges, tall masts and overhead power lines by Davenport (1962a). The effects of the wind gustiness on civil engineering structures were underlined for the first time, and the formulation to predict the buffeting response was successfully established by reducing the expressions for spectra and cross-spectra of the atmospheric turbulence for its application. Assumptions adopted for this formulation are as follows:

(1) The most serious effects are likely to be felt under a wind normal to the longitudinal structural axis.

(2) Small changes of wind direction in relation to the axis of the structure have little or no effect on the loading.

(3) The structure is so slender that only the two-dimensional flow condition can be applied to each span-wise section rather than considering the three-dimensional interactions.

(4) Turbulent fluctuation of velocity components are so small compared to the mean velocity that the fluctuating loads on the structure can be expressed as linear functions of the gust velocity.

The third assumption is the so-called "strip theory" approximation (Dowell et al., 1989), which means that the load acting on each span-wise section is assumed to be equal to the load under two-dimensional flow (or flow over a structure of an infinite span length having the same cross-sectional shape) at the same wind angle of attack. Hence, the strip theory assumes that the aerodynamic forces acting on a section are dependent only on the flow pattern that is determined by the cross-sectional shape, including the angle of attack, of the section.

These four assumptions have been generally well accepted for the buffeting analysis of line-like structures. Another widely used assumption is a "quasi-steady" approximation which assumes that the aerodynamic forces acting on a structure at any instant are the same as those that would act on the structure under a steady flow having the same relative velocity to the structure at this particular instant. Therefore, when the quasi-steady approximation is employed, the aerodynamic forces are assumed to be independent of the time history of the flow pattern and the structural motion in the past. With this approximation, the aerodynamic forces at any instant depend only on the representative relative wind velocity at that instant. The quasi-steady approximation seems to be reasonable when the concerned flow fluctuation wave length which can be expressed as U/f is large compared to the width of the structure; where U is the mean wind speed and f is the frequency of the flow fluctuation which is caused by either the movement of the structure or turbulence in the oncoming flow. When U/f is large compared to the size of the structure, the flow around the structure approaches steady state. However, for large structures such as bridges, the wave length of the flow fluctuation to be considered may not be large enough compared with the width of the structure for the application of the quasi-steady

approximation. For this case, in order to account for the effect of non-uniformity of the flow around the cross-section, some corrections are required, and the so-called aerodynamic admittance is introduced as a correction factor for the quasi-steady approximation. The aerodynamic admittance is considered to be the transfer function from fluctuating wind velocity power spectra to the aerodynamic loading power spectra of the section in the frequency domain. For bodies with non-streamlined cross-sections, it is impossible to obtain the aerodynamic admittance theoretically with the present knowledge of mathematical analysis in fluid mechanics and they must be determined experimentally.

Assuming that the aerodynamic admittance for a truss girder of a suspension bridge can be evaluated by determining the total cross-correlation of the fluctuating vel[illegible] over the area, Davenport (1962b) derived a rapidly decaying function from the quasi-steady value of one to zero. This function derived as a transfer function from the longitudinal velocity component of turbulence to fluctuating drag force had a similar form as the Sears' admittance function (Sears, 1941) which is a transfer function from vertical velocity component of turbulence to fluctuating lift force derived from the two-dimensional aerofoil theory. The Sear's admittance function is often referred to as the Sears function. Davenport assumed that the aerodynamic admittances between other combinations of fluctuating velocity and loading components would be expressed by similar functions. With this assumption, the aerodynamic loading power spectra on the section can be obtained from the fluctuating wind velocity power spectra. By applying modal analysis, the response power spectrum in terms of generalized coordinates for the bridge natural mode is expressed by the product of aerodynamic load power spectrum, mechanical admittance, and so-called joint acceptance that represents the effectiveness of the spatially distributed load in exciting the natural mode. The joint acceptance is obtained as the double integral of the product of the mode shapes and square-root coherence of the loading at two span-wise locations over the entire span. The square-root coherence of the loading is equal to that of the fluctuating wind velocity if the strip theory approximation is assumed. It was empirically approximated with an exponential decay form by Davenport (1962a).

Vickery (1965) measured fluctuating drag forces on plates and prisms placed normal to

a grid generated turbulent flow. The theoretical derivation of the aerodynamic admittance for a lattice plate was attempted, and compared with a more empirical expression for it. The shape of the empirical function is almost the same as what Davenport derived, except the function generally takes slightly higher values.

Scanlan (1978, 1984; Scanlan and Gade, 1977) included the self-excited forces in the buffeting analysis of cable-suspended bridges. Self-excited forces are expected to be measured by sectional model tests. The aerodynamic admittance was not used in his study, however, a direct measurement of the buffeting forces via sectional model tests was suggested instead. Irwin (1977) considered the vibration modes involving coupled torsional and lateral motion and based his analysis on Davenport's analysis. Aerodynamic damping was considered using the quasi-steady approximation and compared with measurements from sectional model tests. Cross-spectra derived from the isotropic turbulence theory were used for the analysis and the aerodynamic admittance was obtained using these cross-spectra in the same manner as Davenport did. Research is still going on for the determination of the bridge deck aerodynamic admittance (for example, Jancauskas and Melbourne, 1986; Xie, Savage and Tanaka, 1989), and it can be pointed out that they could be quite different from the Sears function. An experimental result in which the aerodynamic admittance has the value even beyond 7 in some cases has been reported (Kumarasena, Ehsan and Scanlan, 1989). This was attributed to the effect of the wake behind the aerodynamically bluff bridge deck section. On the other hand, some results agreed fairly well with the Sears function (Davenport and King, 1982).

The applicability of buffeting theories have been examined in several cases. Holmes (1977) compared his analytical result with a full bridge model test in turbulent flow. The comparison was reasonably good. A better agreement was obtained by considering empirically determined aerodynamic damping and the Sears function type aerodynamic admittance. The buffeting analysis by Irwin (1977) stated above showed an excellent agreement with experimental results from the aeroelastic test of a suspension bridge in a simulated turbulent wind. Soo and Scanlan (1983) calculated the buffeting response from the same experiment, and the results overestimated the experimental results by some 20 to 40%. This discrepancy was attributed to

non-application of the aerodynamic admittance. A theoretical calculation result considering the self-excited aerodynamic forces and the Sears function type aerodynamic admittance showed a reasonable agreement with experimental results of taut strip models which had flat plate and box sections in turbulent boundary layer flow (Tanaka and Davenport, 1982). A theoretical result by Davenport and King (1982) agreed quite well with the results of a full bridge model test of a cable-stayed bridge in turbulent flow. In this calculation, measured values from a sectional model test were used for the aerodynamic damping and aerodynamic admittance.

Thus, the methods for predicting buffeting response of long span bridges by utilizing data obtained from sectional model tests have been well developed. However, all of these methods consider only the wind normal to the bridge axis and cannot be applied immediately to the cases with yawed wind.

2.3. Procedure of Buffeting Analysis

A typical procedure of the conventional buffeting analysis is illustrated in this section. Of course, the conventional buffeting analysis in this section does not consider wind yaw angles; i.e., the wind is assumed to come perpendicular to the bridge axis. A basic assumption of the buffeting analysis is that the aerodynamic forces acting on the bridge deck in motion under a turbulent wind can be expressed as a linear summation of the self-excited aerodynamic forces and buffeting aerodynamic forces. The self-excited aerodynamic forces are caused by the movement of the body whereas the buffeting aerodynamic forces are based on the velocity fluctuation of the oncoming flow. Both of the self-excited and buffeting aerodynamic forces are usually expressed as linear functions of the bridge deck motion or fluctuating wind velocity by assuming that the velocity of the motion and the wind velocity fluctuation are much smaller than the mean wind velocity in magnitude. Aerodynamic forces which play important roles in the bridge response are usually the lift force and torsional moment around the longitudinal axis of the bridge deck. Only the aerodynamic force components acting on the bridge deck are considered here.

2.3.1. Self-Excited Force Components

Following the analysis of Scanlan, it is now a common practice to express the self-excited aerodynamic lift force and pitching moment acting on a two-dimensional body of unit length as follows (Scanlan and Tomko, 1971):

$$L = \left(\frac{1}{2}\rho U^2\right)(2B)\left(KH_1^* \frac{\dot{z}}{U} + KH_2^* B \frac{\dot{\theta}}{U} + K^2 H_3^* \theta\right) \tag{2.1}$$

$$M = \left(\frac{1}{2}\rho U^2\right)(2B^2)\left(KA_1^* \frac{\dot{z}}{U} + KA_2^* B \frac{\dot{\theta}}{U} + K^2 A_3^* \theta\right) \tag{2.2}$$

where L and M are the aerodynamic lift force and pitching moment respectively (Fig. 2.1); ρ is the air density; U is the mean wind speed; B is the bridge deck width; z and θ are the vertical and torsional displacements of the bridge deck; and " $\dot{}$ " indicates the derivative with respect to time. K is called the reduced frequency which is defined as $K = B\omega/U$, where ω is the circular frequency of the motion. The coefficients H_i^* and A_i^* are called flutter derivatives which are functions of the reduced frequency K. In the expression above, the aerodynamic inertial terms which are proportional to $\ddot{z}$ and $\ddot{\theta}$ are neglected because the contributions of these terms to the motion of bridge decks are usually very small compared with the large inertial term in the equation of the motion. In the view of the fact that only the vertical response of a flat plate is considered in Chapter 4, and also because the description here is to explain a typical procedure for the buffeting calculation, the discussion will be also limited to the vertical motion. Then the above expression of self-excited forces will be reduced to only one term which relates $\dot{z}$ to L. Furthermore, if the quasi-steady approximation is applied, for example, to the two-dimensional situation of a flat plate vibrating in the vertical direction under a horizontal wind shown in Fig. 2.2, the unsteady aerodynamic force acting on the moving body of a unit length in the vertical direction can be replaced by (Okauch, Ito and Miyata, 1977)

$$F_z(t) = \frac{1}{2}\rho BU_r^2[C_L\cos\alpha'(t) + C_D\sin\alpha'(t)]$$
$$= \frac{1}{2}\rho BU^2[C_L + C_D\tan\alpha'(t)]\sec\alpha'(t) \qquad (2.3)$$

where $F_z(t)$ is the quasi-steady aerodynamic force which is a function of time t, acting in vertical direction z; B is a typical dimension of the body (usually width of the plate); U_r is the relative wind velocity shown in Fig. 2.2; C_L and C_D are the aerodynamic lift and drag coefficients respectively and $\alpha'(t)$ is the instantaneous angle of attack. The instantaneous or temporal angle of attack $\alpha'(t)$ shown in Fig. 2.2 is the relative angle of attack at a particular instance when the aerodynamic force is to be expressed. The expressions for aerodynamic coefficients are given in Fig. 2.1. The relationship $U = U_r\cos\alpha'(t)$ is used in eqn. (2.3). In order to approximate the self-excited aerodynamic force, F_{zs}, caused by a small amplitude body motion, the slope of F_z to α' around zero temporal angle of attack is to be calculated. Differentiation of F_z with respect to α' becomes

$$\frac{dF_z}{d\alpha'} = \frac{1}{2}\rho BU^2[\sec\alpha'(\frac{dC_L}{d\alpha} + C_D\sec^2\alpha') + \sec\alpha'\tan\alpha'(C_L + C_D\tan\alpha' + \frac{dC_D}{d\alpha})] \qquad (2.4)$$

where the relationships by the quasi-steady approximation, $dC_L/d\alpha' = dC_L/d\alpha$ and $dC_D/d\alpha' = dC_D/d\alpha$, are used. Then, $dF_z/d\alpha'$ at $\alpha' = 0$ becomes

$$\left[\frac{dF_z}{d\alpha'}\right]_{\alpha'=0} = \frac{1}{2}\rho BU^2(\frac{dC_L}{d\alpha} + C_D) \qquad (2.5)$$

The vertical velocity of the body movement $\dot{z}(t)$ causes the apparent angle of attack relative to the body which is equal to $\alpha'(t) = \tan^{-1}[-\dot{z}(t)/U]$ (Fig. 2.2). Using the approximation of $\alpha'(t) \cong -\dot{z}(t)/U$, the self-excited aerodynamic force in vertical direction per unit length, when the body is vibrating in vertical direction with small amplitude, can be approximated as

$$F_{sz}(t) \equiv \left[\frac{dF_z}{d\alpha'}\right]_{\alpha'=0} \alpha'(t) = -\frac{1}{2}\rho BU\left(\frac{dC_L}{d\alpha} + C_D\right)\dot{z}(t) \tag{2.6}$$

Eqn. (2.6) gives the quasi-steady expression of the self-excited aerodynamic force in vertical direction caused by the vertical movement of the body. For a flat plate, C_D is negligible compared with $dC_L/d\alpha'$ and the expression becomes simply

$$F_{sz}(t) = -\frac{1}{2}\rho BU\frac{dC_L}{d\alpha}\dot{z}(t) \tag{2.7}$$

2.3.2. Buffeting Force Components

The two-dimensional unsteady aerodynamic force in the vertical direction in a fluctuating flow is now to be expressed using the quasi-steady approximation. The flow having horizontal mean velocity and no movement of the body is considered (Fig. 2.3). The role of $-\dot{z}(t)$ in the case of self-excited forces in Section 2.3.1 is simply replaced by w(t) in this case, provided that u(t) is much smaller than U and its contribution to the temporal angle of attack α' is negligible. Here, w(t) and u(t) are the fluctuating velocity components in z and x direction respectively. Then, by replacing $-\dot{z}(t)$ with w(t) in eqn. (2.6), the aerodynamic buffeting force induced by the w-component in vertical direction for unit length of the body is

$$F_{sbw}(t) = \frac{1}{2}\rho BU\left(\frac{dC_L}{d\alpha} + C_D\right)w(t) \tag{2.8}$$

The aerodynamic force for unit length caused by u(t) can be expressed as

$$F_{zu}(t) = \frac{1}{2}\rho B U_r^2 C_L$$
$$= \frac{1}{2}\rho B [U + u(t)]^2 C_L \qquad (2.9)$$
$$\equiv \frac{1}{2}\rho B [U^2 + 2Uu(t)] C_L$$

where approximation is made by assuming that the fluctuating velocity components u(t) is much smaller than the mean velocity U in magnitude. By taking the fluctuating part of eqn. (2.9), the aerodynamic buffeting force in the vertical direction caused by the u-component becomes simply:

$$F_{zbu}(t) = \rho B U C_L u(t) \qquad (2.10)$$

Finally, by adding eqns. (2.8) and (2.10), the aerodynamic buffeting force in the vertical direction, F_{zb}, is expressed as

$$F_{zb}(t) = F_{zbw} + F_{zbu}$$
$$= \frac{1}{2}\rho B U [(\frac{dC_L}{d\alpha} + C_D) w(t) + 2C_L u(t)] \qquad (2.11)$$

In the case of a flat plate, C_D is negligible compared with $dC_L/d\alpha$ and C_L at zero angle of attack is zero. Hence the eqn. (2.11) reduces to

$$F_{zb}(t) = \frac{1}{2}\rho B U \frac{dC_L}{d\alpha} w(t) \qquad (2.12)$$

2.3.3. Equation of Motion

The equation of motion for the vertical response, z, for a line-like structure that represents a bridge deck as shown in Fig. 2.4 is considered here. Applying modal analysis, the vertical response at any point of the structure can be expressed as

$$z(y,t) = \sum_r \phi_r(y) q_r(t) \tag{2.13}$$

where $\phi_r(y)$ is the r-*th* mode shape function given in a dimensionless manner and $q_r(t)$ is the generalized coordinate for the r-*th* mode having the same dimension of deflection as z. $\phi_r(y)$ is a function of the space coordinate y alone and $q_r(t)$ is a function of t. By introducing eqn. (2.13) to the equation of motion for the line-like structure, a set of equations as follows is obtained:

$$\ddot{q}_r + 2h_{sr}\omega_r \dot{q}_r + \omega_r^2 q_r = F_{zr}/M_r \ , \quad r = 1,2,\cdots,N \tag{2.14}$$

where h_{sr} is the structural damping ratio; ω_r is the natural circular frequency; F_{zr} is the generalized force; M_r is the generalized mass, all for the r-*th* mode and N is the number of the modes considered in the analysis. F_{zr} and M_r are calculated as

$$F_{zr}(t) = \int_0^l F_z(y,t)\phi_r(y)\,dy \tag{2.15}$$

$$M_r = \int_0^l m(y)\phi_r^2(y)\,dy \tag{2.16}$$

where m(y) is the distribution of mass along the structure and l is the span length. Eqn. (2.14) is the equation of motion for the r-*th* mode, and there are N of them as given in eqn. (2.14). By introducing the modal analysis, the structural response in the r-*th* mode can be calculated by solving eqn. (2.14) just as a single-degree-of-freedom system, because the equations of motion for different modes are not coupled to each other if the coupling term for the damping is negligible. This assumption has been well accepted in many cases and will be used here, too.

Now, the aerodynamic force should be introduced into the equation of motion. As stated in the beginning of Section 2.3, the aerodynamic force acting on a structure is assumed to be the linear summation of the self-excited force and buffeting force. However, the treatment of each force is different. It is because the buffeting force will be treated as the external force and be placed the right hand side of eqn. (2.14), whereas the self-excited force which is dependent on

$\dot{z}$ can be treated as the damping term which is the second term in the left hand side of eqn. (2.14). Let us consider again the fluctuating component of the aerodynamic force in the vertical direction for a flat plate. By applying the strip theory approximation, the external force acting at a span-wise section y is simply expressed by the two-dimensional aerodynamic force based on the angle of attack at that particular span-wise location. The generalized buffeting force can be obtained from eqns. (2.12) and (2.15) as

$$\begin{aligned} F_{zbr} &= \int_0^l F_{zb}(y,t)\phi_r(y)\,dy \\ &= \frac{1}{2}\rho BU\frac{dC_L}{d\alpha}\int_0^l w(y,t)\phi_r(y)\,dy \end{aligned} \tag{2.17}$$

where F_{zbr} is the generalized buffeting force for the r-*th* mode, and the cross-section of the structure and the mean wind velocity are assumed to be constant along the span of the structure. In order to obtain the self-excited force equivalent to the damping term in eqn. (2.14), $F_{zs}(t)$ in eqn. (2.7) should be multiplied by $-\phi_r(y)$, divided by M_r, and integrated over the span length. Applying the strip theory approximation and substituting eqn. (2.13), the following expression equivalent to the r-*th* mode damping term is obtained:

$$\begin{aligned} \frac{\int_0^l [-\phi_r(y)]F_{zs}(y,t)\,dy}{M_r} &= \frac{\frac{1}{2}\rho BU\frac{dC_L}{d\alpha}}{M_r}\int_0^l \phi_r(y)\dot{z}(y,t)\,dy \\ &= \frac{\frac{1}{2}\rho BU\frac{dC_L}{d\alpha}}{M_r}\int_0^l \phi_r(y)\left[\sum_k \phi_k(y)\dot{q}_k(t)\right]dy \\ &= \frac{\frac{1}{2}\rho BU\frac{dC_L}{d\alpha}}{M_r}\int_0^l \phi_r^2(y)\,dy\;\dot{q}_r(t) \\ &= \frac{\frac{1}{2}\rho BU\frac{dC_L}{d\alpha}}{m}\dot{q}_r(t) \end{aligned} \tag{2.18}$$

where the cross-section, mean wind velocity and distributed mass m are assumed to be constant along the span of the structure, and the orthogonality of the mode shapes is utilized. Comparing eqn. (2.18) with the second term of the left hand side of eqn. (2.14), an equivalent expression as the damping ratio for the self-excited aerodynamic force, which is called aerodynamic damping ratio for the r-*th* mode, h_{ar}, can be obtained as

$$h_{ar} = \frac{\rho BU \frac{dC_L}{d\alpha}}{4m\omega_r} \tag{2.19}$$

Then the total damping ratio for the r-*th* mode h_{Tr} can be expressed as

$$h_{Tr} = h_{sr} + h_{ar} \tag{2.20}$$

Using eqns. (2.17) and (2.20) for the r-*th* mode, the equation of motion for a line-like structure with a flat plate section under turbulent wind can be written as

$$\begin{aligned} \ddot{q}_r + 2h_{Tr}\omega_r \dot{q}_r + \omega_r^2 q_r &= F_{zbr}/M_r \\ &= \frac{\frac{1}{2}\rho BU \frac{dC_L}{d\alpha}}{M_r} \int_0^l w(y,t)\phi_r(y)\,dy \end{aligned} \tag{2.21}$$

2.3.4. Response Power Spectrum

Eqn. (2.21) is the equation of motion for a linear system under random force proportional to w(y,t), which can be conveniently treated by the spectral analysis, where both the response and external force due to fluctuating velocity are expressed in terms of power spectra. The Fourier transform of eqn. (2.21) becomes

$$\int_{-\infty}^{\infty}[\ddot{q}_r + 2h_{Tr}\omega_r\dot{q}_r + \omega_r^2 q_r]e^{-i\omega t}dt = \int_{-\infty}^{\infty}[\frac{\frac{1}{2}\rho BU\frac{dC_L}{d\alpha}}{M_r}\int_0^l w(y,t)\phi_r(y)dy]e^{-i\omega t}dt \tag{2.22}$$

where i is the imaginary unit and ω is the circular frequency. By changing the order of the integration of the right hand side of the equation and performing the Fourier transform, the equation can be expressed as

$$[-\omega^2 + i2h_{Tr}\omega_r\omega + \omega_r^2]Q_r(\omega) = \frac{\frac{1}{2}\rho BU\frac{dC_L}{d\alpha}}{M_r}\int_0^l W(y,\omega)\phi_r(y)dy \tag{2.23}$$

where $Q_r(\omega)$ and $W(y,\omega)$ are the Fourier transforms of $q_r(t)$ and $w(y,t)$, respectively. By multiplying the complex conjugate of each side of eqn. (2.23) to corresponding side and dividing each side by T which is the length of time under consideration, and taking the limit of $T \to \infty$, eqn. (2.23) yields to

$$S_{qr}(f) = \frac{\left(\frac{1}{2}\rho BU\frac{dC_L}{d\alpha}\right)^2}{\omega_r^4 M_r^2}|H_r(f)|^2\int_0^l\int_0^l S_{ww}(y,y',f)\phi_r(y)\phi_r(y')dydy' \tag{2.24}$$

where $S_{qr}(f)$ is the power spectrum of the generalized coordinate q_r; f is the frequency; $|H_r(f)|^2$ is called the mechanical admittance which is expressed as

$$|H_r(f)|^2 = \frac{1}{[1-(f/f_r)^2]^2 + 4h_{Tr}^2(f/f_r)^2} \tag{2.25}$$

where f_r is the natural frequency for the r-*th* mode. $S_{ww}(y,y',f)$ in eqn. (2.24) is the cross-spectrum of w(y,t) and w(y′,t). The spectra and admittance in eqn. (2.24) are expressed as functions of frequency f instead of circular frequency ω. Eqn. (2.24) gives the relationship between the cross-spectrum of fluctuating wind velocity and the power spectrum of response generalized coordinate. Therefore, once the cross-spectrum of the fluctuating velocity and other characteristics of the structure are given, the response power spectrum can be obtained from the equation. Variance of the response is simply the integration of the response power spectrum over the whole frequency range, and the r.m.s. (root-mean-square) response is the square-root of the variance. The actual deflectional response of the structure can be obtained from the response in generalized coordinates via the relationship given by eqn. (2.13). Corresponding stresses, strains, etc. can be also calculated from the results.

2.3.5. Cross-Correlation of Fluctuating Wind Velocity

By assuming the isotropy of the flow field, the cross-correlations of fluctuating wind velocity components can be analytically expressed. Here, the isotropy is defined as the condition which is statistically independent of direction. Therefore, in an isotropic turbulence, the statistical characteristics which are the only information obtained for turbulent flow are invariant under the rotation of the coordinate system and under reflection with respect to the coordinate planes (Bradshaw, 1971; Hinze, 1975). The assumption of isotropy automatically requires homogeneity which means that the statistical characteristics do not change according to the position in space. This assumption of homogeneous isotropic turbulence makes the theoretical treatment relatively easier, and thus studies for the isotropic turbulence have been extensively conducted. Although an exactly homogeneous isotropic turbulence does not exist in reality, some turbulent flows can be well assumed as isotropic, and even for non-isotropic turbulent flows, small eddies in the flow constitute almost isotropic condition. Therefore the results from the isotropic turbulence are often applied to the actual cases as a good approximation.

For an isotropic turbulence, von Kármán suggested three-dimensional spectra which

incorporate two theoretical expressions of energy spectra for different range (Hinze, 1975, p.244). Based on these widely used, so-called von Kármán spectra, the corresponding power spectra of turbulence which are equivalent to the measurable power spectra in wind tunnels can be expressed as (Irwin, 1977)

$$S_u(f) = \frac{4\sigma_u^2 L_x^u/U}{[1+70.78(fL_x^u/U)^2]^{5/6}} \tag{2.26}$$

$$S_w(f) = \frac{(2\sigma_w^2 L_z^w/U)[1+188.8(fL_z^w/U)^2]}{[1+70.78(fL_z^w/U)^2]^{11/6}} \tag{2.27}$$

where $S_u(f)$ and $S_w(f)$ are the power spectra for u and w fluctuating velocity component; u and w are as defined in Section 2.3.2; and σ_u and σ_w are the r.m.s. values of u and w. Usually, σ_u and σ_w are given in terms of turbulence intensities I_u and I_w, which are defined as

$$I_u = \sigma_u/U \tag{2.28}$$

$$I_w = \sigma_w/U \tag{2.29}$$

L_x^u and L_z^w are the integral scales of turbulence. L_x^u is defined as

$$L_x^u = \int_0^\infty R_{uu}(x)\,dx \tag{2.30}$$

where $R_{uu}(x)$ is the correlation coefficient defined as

$$R_{uu}(x) = \overline{u(s)u(s+x)}/\sigma_u^2 \tag{2.31}$$

in which the overscore denotes the average value. Similarly, L_z^w and the correlation coefficient of w-component in z-direction are

$$L_z^w = \int_0^\infty R_{ww}(z)\,dz \tag{2.32}$$

$$R_{ww}(z) = \overline{w(s)w(s+z)}/\sigma_w^2 \tag{2.33}$$

The integral scales of turbulence will be called simply the scales of turbulence in this thesis. The scales of turbulence in other directions can be also defined similarly, for example,

$$L_y^w = \int_0^\infty R_{ww}(y)\,dy \tag{2.34}$$

$$R_{ww}(y) = \overline{w(s)w(s+y)}/\sigma_w^2 \tag{2.35}$$

For an isotropic turbulence, it is known that

$$L_x^u = L_y^v = L_z^w = L \tag{2.36}$$

$$L_y^u = L_z^u = L_z^v = L_x^v = L_x^w = L_y^w = L/2 \tag{2.37}$$

where v is the fluctuating velocity component in y-direction. As shown in eqns. (2.36) and (2.37), the value L of the scales of turbulence in eqn. (2.36) is double the value in eqn. (2.37) for isotropic turbulence. Although the value of $L_x^u = L_z^w$ is just assigned as L from the derivation above, the scales of turbulence in eqns. (2.26) and (2.27) are written not using the single parameter L so that the expression of spectra would give better approximations for non-isotropic turbulence. A similar idea was suggested by Irwin (1977).

Harris (1971) and Roberts and Surry (1973) derived an expression for the cross-spectrum of u at two locations separated by Δy, $S_{uu}(\Delta y,f)$, assuming the isotropy and the von Kármán spectrum, which is

$$S_{uu} = \frac{2^{1/6} S_u}{\Gamma(5/6)}[\eta^{5/6} K_{5/6}(\eta) - \frac{\eta^{11/6}}{2} K_{1/6}(\eta)] \tag{2.38}$$

where Γ is the gamma function, $K_{5/6}$ and $K_{1/6}$ are the modified Bessel functions of the second kind, η is a dimensionless parameter given by

$$\eta = \frac{\Delta y}{2L_y^u} B_1 \sqrt{1 + (2\pi/B_1)^2 (2L_y^u f/U)^2}$$

where

$$B_1 = \sqrt{\pi}\, \frac{\Gamma(5/6)}{\Gamma(1/3)}$$

Jackson, Graham and Maull (1973) and Irwin (1977) extended the derivation above, and derived an expression for the cross-spectrum for the w-component with the distance Δy, which becomes

$$S_{ww} = \frac{2^{1/6} S_w}{\Gamma(5/6)} \left\{ \eta^{5/6} K_{5/6}(\eta) - \frac{\eta^{11/6} K_{1/6}(\eta)}{1 + \frac{8}{3}(2\pi/B_1)^2 (2L_y^w f/U)^2} \right\} \tag{2.39}$$

where

$$\eta = \frac{\Delta y}{2L_y^w} B_1 \sqrt{1 + (2\pi/B_1)^2 (2L_y^w f/U)^2}$$

The scales of turbulence in the expressions of η above, $2L_y^u$ and $2L_y^w$, correspond to the single parameter L for the case of an isotropic turbulence. The derivation of the expressions for the cross-spectra above is given in detail by Irwin (1977).

Once the intensities and scales of turbulence are given or measured, the theoretical cross-spectrum for w-component can be obtained by eqns. (2.27) and (2.39). Assuming the strip theory and the quasi-steady approximation, eqn. (2.24) can then be used to obtain the response spectra once the characteristics of the structure are known.

2.3.6. Aerodynamic Admittance

For the analysis given above, the quasi-steady approximation has been adopted. As mentioned in Section 2.2, for the accurate evaluation of the buffeting response, effects of the unsteady flow pattern caused by the fluctuating wind velocity around the cross-sections sometimes have to be taken into account. For this purpose, the aerodynamic admittance is introduced as a transfer function in the frequency domain from the fluctuating velocity to the aerodynamic buffeting load on the cross-section. The intensity of the unsteadiness is probably well expressed in terms of the ratio of the typical dimension of the section, B, to the gust wave length U/f, therefore the aerodynamic admittance should be readily given as a function of the reduced frequency $K' = fB/U$ in the frequency domain.

The aerodynamic admittance is defined under two-dimensional conditions. For example, in case of a two-dimensional body under a wind with fluctuating velocity component w, the relationship between the power spectrum of the aerodynamic buffeting force in vertical direction, $S_{zb}(f)$, and the power spectrum of w, $S_w(f)$, can be obtained from eqn. (2.12) as

$$S_{zb}(f) = \left(\frac{1}{2}\rho BU\frac{dC_L}{d\alpha}\right)^2 S_w(f) \tag{2.40}$$

This is an expression assuming the quasi-steady condition. The aerodynamic admittance should be included in the relationship as

$$S_{zb}(f) = \left(\frac{1}{2}\rho BU\frac{dC_L}{d\alpha}\right)^2 |X_L^w(fB/U)|^2 S_w(f) \tag{2.41}$$

where the effects of unsteady flow for the relationship between w-component and lift force are considered by the aerodynamic admittance $|X_L^w(fB/U)|^2$. For aerofoils or flat plates, the theoretical aerodynamic admittance between the w-component and the lift force has been given by Sears (1941) and that between the u-component and the lift force is given by Horlock (1968). For bodies having aerodynamically bluff cross-sections that cause flow separations, the aerodynamic admittance can be determined by experiments, measuring the transfer function between the fluctuating wind velocity component and the aerodynamic buffeting forces. The aerodynamic admittance is usually considered for the two-dimensional turbulence condition. Recently some researchers are using special equipment for the generation of two-dimensional turbulence and measuring the aerodynamic admittance. If a normal three-dimensional turbulence is used, some correction for the smaller spatial correlation in the cross-wind direction should be made.

A linear relationship holds between two-dimensional and three-dimensional aerodynamic forces if the strip theory approximation is applied. Therefore, introducing the aerodynamic admittance to eqn. (2.24), the power spectrum of the generalized coordinate for line-like structures considering the unsteady flow effects is given by

$$S_{qr}(f) = \frac{\left(\frac{1}{2}\rho BU\frac{dC_L}{d\alpha}\right)^2}{\omega_r^4 M_r^2} |H_r(f)|^2 |X_L^w(fB/U)|^2 \int_0^l\int_0^l S_{ww}(y,y',f)\phi_r(y)\phi_r(y')\,dy\,dy' \tag{2.42}$$

2.4. Effects of Yaw Angle on Bridge Response

In the area of bridge aerodynamics, some experimental work considering the effects of wind yaw angle on the response can be found. However, little clear physical explanation has been given to the mechanism of the phenomena.

Scruton (1951) studied the response of a full bridge model of a suspension bridge under yawed wind in the early 1950's. The critical wind speeds for the vertical and torsional vortex induced oscillations in smooth flow were observed to be higher when the wind was inclined to the normal direction. The response in the turbulent yawed wind was also examined, but the comparison is difficult because of the non-homogeneity of the flow field.

Vincent (1958) analyzed the response of a full scale bridge during storms probably caused by vortices or buffeting. The vertical response was correlated with the wind speed and direction. The effect of the wind direction was apparent where "moderate winds blowing at right angles to the bridge excite greater oscillation than do violent winds nearly parallel to the bridge." He suggested that if the velocity component normal to the bridge longitudinal axis was taken as the representative wind speed, the bridge response with any wind direction could be expressed by the same relationship of the representative wind speed.

Davenport et al. (1969a) conducted an experiment using a full model of a suspension bridge in turbulent yawed wind including its erection stages. The objective was to obtain data to predict the bridge response level vs. return period by jointly integrating experimental response data and wind climate statistics. Generally speaking, the buffeting response in the vertical bending mode of the completed bridge model became considerably smaller under yawed wind. However, for some erection stages, the response did not decrease as much with the increase of wind yaw angles. The response in low turbulent flow showed even less sensitivity to the wind yaw angle. The response spectra of the completed bridge were found to be generally of a similar nature regardless of the yaw angle. Another study by the same authors (1969b) examined the vertical and lateral bending response of a concrete bridge model in turbulent yawed wind. The

test was carried out only for the completed bridge. The bridge response was found to diminish gradually with the increase in yaw angle. Peak torsional response of a taut strip model tested in turbulent wind (Davenport, Isyumov and Tanaka, 1976) showed a more pronounced sensitivity to change in wind direction (Fig. 2.5). The response with a wind angle of 20° from the normal was found to be almost a half in magnitude of that with normal wind. Davenport (1977) suggested a similarity of the result with the full scale observations of Vincent (1958).

Irwin and Schuyler (1977) found that a velocity component taken normal to the bridge axis seemed to provide a reasonable measure for the critical flutter speed for torsional instability observed with a full suspension bridge model in smooth flow. Melbourne (1980) conducted a full model test for a cable-stayed bridge in boundary layer turbulence. He studied the effect of yaw angle, and a peak vertical displacement was found to be proportional to the cosine component of wind angle taken from normal to the deck. Tanaka and Davenport (1982) further studied the effect of yaw angle using taut strip models in boundary layer turbulence. The effect of yaw angle was generally well-represented by taking a velocity component perpendicular to the bridge axis as the representative velocity when the flow is relatively smooth. However for highly turbulent wind, the actual model response with yaw angle was found to be underestimated by applying this assumption. The approach of taking a normal velocity component to the bridge axis as the representative wind speed has also been employed as a simple assumption for the prediction of flutter-induced extreme response by Lepage and Irwin (1985) and Irwin (1987b). In this thesis, let us call this approach the "cosine rule" for convenience sake. With the cosine rule, if the actual wind speed is replaced by the representative wind speed normal to the bridge axis, the response vs. representative wind speed relationship is assumed to be the same under any wind direction. Figs. 2.5. and 2.6. are shown with this concept. There has been also a reliability analysis of a cable-stayed bridge by calculating vortex induced response assuming the effective width of the bridge road deck to be taken in the direction of wind (Matsumoto and Prenninger, 1989).

Recently, Xie et al. (1991) developed a buffeting analysis of long span bridges under yawed wind by introducing a concept of effective values of mean wind velocity, deck width, and

turbulence correlation length. This approach seems to be one of the most comprehensive at present. However, it is still necessary to decide more clearly how much of the contribution from each component should be expected. Furthermore, there is an indication that the situation may change very much if the bridge has unsupported free ends since the three-dimensionality of the structure seems to have a significant effect.

Concerning cable-stayed bridges under construction, which actually have free ends, there are some analytical studies to calculate the wind-induced response, such as by Xie and Xiang (1985), Irwin (1987a), Khalil and Bush (1987) and Zan and Wardlaw (1987). Experimental works have been done by Gamble and Irwin (1985), Xiang, Xie and Lin (1988), Arzoumanidis, Ogawa and Sakoda (1989) and Kirkwood and Davenport (1991). Kubo et al. (1989) have made field observations. However, these studies considered only wind normal to the bridge axis. Also in most cases, the effects of free ends were taken into account only in a structural sense such as consideration of the mode shape and lower natural frequency of the structure. Apart from these, a full model test of a cable-stayed bridge under construction with wind angle of 30° was conducted by Zan (1987a). In Zan's study (1987a; Zan and Wardlaw, 1987), a correction of the lift coefficient in terms of a finite aspect ratio is suggested. This is similar to the approach for finite wings (Bisplinghoff, Ashley and Halfman, 1955). The experimental results of this study are re-plotted in Fig. 2.6 in comparison with the case in normal wind. The response in yawed wind exceeds the estimation obtained by taking representative wind velocity normal to the bridge. Also shown in Fig. 2.6 is a similar tendency observed by Irwin and Gamble (1985). Recently, Kirkwood (1991) has conducted an experiment that also studied the effect of the wind yaw angle on a simple model of a cable-stayed bridge under construction. The model had a relatively flat cross-section. The vertical model response in turbulent flow was found to become large when the wind yaw angle was approximately 70°.

2.5. Studies on Cantilevered Roofs

In the study of wind loads on cantilevered roof structures which have obviously an

unsupported free end, consideration of wind angle has been a normal procedure. Barnard (1981) conducted an experiment in turbulent boundary layer flow and reported the occurrence of strong leading-corner vortices under yawed wind which caused a large response particularly at the corners. This behaviour is pointed out to be somewhat parallel to that observed with slender delta wings. Because of this vortex effect, the maximum overall load on the roof was sometimes observed with a yaw angle of around 40° measured from normal to the free end. Also, the ratio of local pressure spectrum to the spectrum of fluctuating wind velocity became larger in the high frequency range, which suggests the existence of the vortex effect. Cook (1982) conducted an experiment for a similar structure under boundary layer flow. The largest overall bending moment of the cantilever beams which support the roof was observed with the wind normal to the free end (yaw angle 0°). However for a beam located close to the upwind corner, the largest moment was observed with 30° yaw angle.

Melbourne and Cheung (1988) studied the aeroelastic response of a cantilevered roof model in boundary layer turbulent flow with yaw angles. Response of beams which support the roof were measured, and the maximum response was obtained under wind normal to the free end for almost all beams. However, for the beam that was located at the leading edge, the magnitude of the response did not change up to a yaw angle of 70°. In an earlier study under turbulent wind from the free end direction by Melbourne (1977), an apparent tendency of intermittent displacements of the roof in upward direction was observed. These phenomena were attributed to the wake system developed behind the entire structure.

2.6. Concluding Remarks for Previous Studies

This brief literature review reveals that the understanding of bridge buffeting motions that has been accumulated allows us to make a reasonable prediction of full scale bridge response, by either experimental or analytical methods. However, most studies have restricted the wind direction only to the case when wind comes perpendicular to the bridge axis, and the effects of the change in wind direction have not been given much consideration. Although there are some

studies which have taken account of the wind directionality as stated in Section 2.4, neither clear explanations of the phenomena nor reliable methods for response prediction under yawed wind have been given.

However, as Davenport (1977) pointed out, it is vitally important to consider the wind directionality, if the wind climate data are to be incorporated into the analysis so that a realistic response prediction, such as expected annual peak response level or probability of exceeding certain response level for a given return period, is to be made. Actually, the inclusion of the wind directionality effects by using the local wind climate data and experimentally obtained bridge response under wind with different yaw angles make the peak torsional response prediction dramatically lower than the case without considering directional variation of wind climate (Davenport et al., 1980). It is obvious now that the consideration of the wind directionality is very important for the wind resistant design of bridges because it may significantly change the prediction of wind effects and thus lead to more reasonable design of structures.

The consideration of the wind directionality requires information about the bridge response under wind with yaw angles and the study on this subject, which has been more or less bypassed so far, is highly needed. Another interesting point is that structures having free ends, such as cable-stayed bridges under construction, seem to show larger response under yawed wind than completed bridges as discussed in Sections 1.3 and 2.4. Thus with this kind of structure, the response needs to be treated very carefully. This is one reason why cantilever supported models were used in the experimental phase of the present research.

Chapter 3. EXPERIMENTAL STUDY

3.1. Introduction

Experiments were conducted to investigate the effects of wind yaw angles using very simple models. The models have basically a flat plate cross-section and are cantilever supported. They were placed in turbulent flow and were expected to reveal only buffeting motion because a flat plate is usually prone to neither vortex induced oscillation nor single-degree-of-freedom flutter and the wind velocity tested was well below the critical wind velocity for coupled flutter. The aerodynamic interference of the flow with the model supporting mechanism is expected to be negligibly small for the flow from the free end direction. This was an advantage because the uncertain effects of the flow interference with the support do not have to be taken into account at least for these cases.

These models are regarded as an extremely simplified version of bridge decks representing cable-stayed bridges under construction. The models are, of course, too simple to have the results directly applicable to the actual cases. However, it was necessary to use a simple model, at least for the first step, to have a clear understanding of the effects of wind yaw angle, because the actual bridges involve many other factors which make the phenomena too complicated. The results of this investigation will obtain the basic knowledge with which more practical cases may be considered later.

Important parameters which affect the buffeting response of a cantilever supported model are listed below:

i) wind characteristics

- mean wind velocity and its distribution
- mean wind incidence to the structure
  - angle of attack (vertical)
  - wind yaw angle (horizontal)
- turbulence characteristics
  - spectrum
  - cross-correlation

  which are typically characterized by
  - intensities
  - scales

ii) structural characteristics

- geometrical shape
  - model width
  - model depth
  - model span length etc.
- mechanical characteristics
  - mass and mass moment of inertia
  - stiffness

    which is characterized by
    - natural frequencies
    - mode shapes
  - structural damping

The dependence of the buffeting response on these parameters can be more clearly expressed by introducing dimensionless parameters such as:

- reduced wind velocity:

  (wind velocity)/[(natural frequency)·(deck width)]

- density ratio:

  (density of the deck)/(density of the air)

- turbulence scale ratio:

  (scale of turbulence)/(deck width)

- depth to width ratio:

  (deck depth)/(deck width)

- span to width ratio:

  (deck span length)/(deck width)

The wind yaw angle is of course the main parameter for which effects are to be examined in this study. Some other parameters such as wind velocity, turbulence scale ratio, depth to width ratio and span to width ratio were also changed in the experiments to give a clear understanding about the effects of wind yaw angles. Some accompanying parameters such as turbulence intensity and turbulence power spectrum were changed at the same time. Some parameters such as the angle of attack and structural damping were not intended to be changed.

3.2. Instrumentation of the Experiments

3.2.1. Wind Tunnels

Two wind tunnels were used in the experiments. One is a closed circuit tunnel with 0.91 m × 0.91 m × 2.3 m closed test section at the Institute for Aerospace Research, National Research Council Canada. This wind tunnel will be referred to as the NRCC wind tunnel. The other is an open circuit tunnel with 1.68 m × 1.12 m × 12.2 m closed test section at the Department of Mechanical and Aerospace Engineering, Carleton University. This wind tunnel will be referred to as the Carleton wind tunnel. The choice of the tunnels was made according to their availability.

3.2.2. Turbulence Generating Devices

Most of the experiments were conducted under turbulent wind. Square mesh grids or spires with roughness blocks were put in the wind tunnel some distance upstream of the model position so that intense turbulence would be generated in the oncoming flow (Plates 3.1 and 3.2).

In the NRCC wind tunnel, three types of square mesh grids (Grids NI, NII and NIII) and a set of spires with roughness blocks were used. In the Carleton wind tunnel, two types of square mesh grids (Grids CI and CIII) were used. In this thesis, the flow behind grids will be referred to simply by these codes as Grid NI, Grid NII and so on. The flow behind spires with roughness blocks at the NRCC wind tunnel will be referred to as Shear Flow. Some experiments were also done in a flow with very low turbulence without any turbulence generating devices at the Carleton wind tunnel and this flow will be referred to as Smooth Flow in the following.

The grids were made of 11 mm thick plywood slats. The vertical slats were attached onto the horizontal slats constructing square mesh. Because the slats did not have indent, the plane of the vertical slats and that of the horizontal slats were 11 mm apart. This type of grid is sometimes called a biplane grid. The dimensions of the grids are given in Table 3.1. One can refer to the work by Vickery (1965) for the design of coarse grids for a desired turbulence. These square grids are expected to generate nearly uniform distribution of mean wind velocity at the model position with approximately homogeneous isotropic turbulence.

The spires were made of aluminium having a configuration shown in Fig. 3.1. Cubic roughness blocks were made of styrofoam with dimensions of 15 mm × 15 mm × 15 mm and attached on a 6 mm thick plywood plate in staggered positions with 61 mm intervals. The plywood plate was fixed on the wind tunnel floor behind the spires. The roughness blocks covered of 1.75 m from 0.20 m upstream of the model position. The spires together with the roughness blocks generate a thick boundary layer which can be used to simulate the planetary boundary layer. Irwin (1979) has done a study on the design of spires and roughness blocks for this purpose.

Table 3.1. Dimensions of the Grids

Grid	B (mm)	M (mm)	x/B
NI	50	200	38
CI			38
NII	25	100	40
NIII	10	40	62
CIII			72

where,
B: bar size
M: mesh size
x: grid to model distance

One thing to be perhaps mentioned concerning the flow condition is the existence of an object in the Carleton wind tunnel far upstream of the grid. It consists of a cylinder with a diameter of 20 cm and height of 60 cm located 7.5 m upstream of the model position and a plate of 100 cm wide × 120 cm long × 1.4 cm thick which was supported by 3.2 cm wide horizontal frames attached to the wind tunnel walls and was sitting horizontally on the cylinder. Another object of relatively small size was also on the plate. This object was a device for another project and it was decided to leave it in the wind tunnel because of its complexity of installation and because it was going to be used immediately after this experiment. Nevertheless, the uniformity of the flow around the model location was confirmed, and there seemed to be no problem to use the flow for the experiment as long as the flow characteristics were properly measured. For the measurement in a very low turbulent wind (Smooth Flow) at the Carleton wind tunnel, the model was located upstream of the object so that the flow around the model was not affected by the existence of the object.

3.2.3. Flow Measurement

The flow in the wind tunnel plays a role as the input to cause a variety of responses of the model. The flow characteristics, therefore, have to be known as much as possible in order to predict the output. However, the characteristics of turbulent flow can be defined only by statistically averaged values and they cannot be described as explicit functions of time and space coordinates in detail, because the various quantities in the flow show random variations with time and space coordinates (Hinze, 1975).

The measured statistical values in this study were: the intensities of turbulence which are the ratio of the r.m.s. values of fluctuating velocity components to the mean speed, the power spectra of turbulence which give the kinetic energy distribution of turbulence in the frequency domain, and the integral scales of turbulence which are typical lengths of energy containing eddies and are defined as integrals of the correlation coefficients over distance. Definitions of these terms are given in Section 2.3.5.

Under a horizontal smooth flow, no force in the vertical direction other than that due to the wake of the model itself acts on a model which has a symmetrical cross-section about the horizontal plane. However, for the case of turbulent flow, the vertical component (w-component) of the velocity makes the flow with a temporal angle of attack and random forces in vertical direction act on the model as discussed in Section 2.3.2. Because the model response was mainly in the vertical direction, the w-component has the dominant effect on the model response. Thus, measurement of the w-component of the flow became one of the most important objects. See Fig. 3.2 for the definition of coordinates for the flow.

A hot-film anemometer was used for the flow measurement. For the measurement of the vertical component of the velocity, a cross film probe that has a pair of films arranged in an "X" configuration at approximately ±45° to the flow direction was used. If the films of such "X" probes are in the x/z-plane, one film responds to (U+u)+w and the other to (U+u)−w. Linearized output was obtained through a measuring instrument for hot films (TSI Model 1054B with power

supply Model 1051-6). By adding or subtracting the adjusted output from each film of an "X" probe, the reading corresponding to U+u or w was taken. A sum and difference amplifier (TSI Model 1063) was used for this operation. This reading was used to evaluate the intensity and power spectrum of turbulence. The r.m.s. of the output from the hot film anemometer was measured by a voltmeter with true r.m.s. function (TSI Model 1076) or by a digital voltmeter (Hewlett Packard 3437A System Voltmeter) with a desktop computer (Hewlett Packard 9845B). Power spectra were taken by a spectrum analyzer (Hewlett Packard Structural Dynamics Analyzer 5423A). Two "X" probes were set at various distances apart and measurements at the two locations were taken simultaneously to obtain the spatial correlation of turbulence. The cross-correlations of the fluctuating velocity components at two locations were also measured by the spectrum analyzer. The measured cross-correlations were used to determine the integral scales of turbulence. A "U" probe which has a single film normal to the stream was also used to check the uniformity of the flow. One may refer to Bradshaw (1971) for the usage of the hot-wire (or hot-film) anemometers.

The flow measurement was done only at the model height. At different horizontal locations, the characteristics of the turbulence in the wind tunnel would change according to the distance from the grids or the spires. Therefore, in the cases where the model is set with wind yaw angles, the turbulence characteristics at the model change slightly depending on the span-wise location. So, the flow measurement was taken at several horizontal positions where the span of the model might be positioned.

3.2.4. Model Characteristics

The models used in the experiments can be separated into two groups. Models in each group were made of spring steel or aluminium respectively. Models made of spring steel were used in the first series of experiments conducted in April-June 1989 at the NRCC wind tunnel. They will be referred to as the steel models in the following. The steel model shapes were decided to cover a range of width and span length with comparable turbulence scale ratio to the

prototype case of cable-stayed bridges under construction. Steel model shapes are tabulated in Table 3.2(a) together with the model name. Dynamic characteristics of the models; i.e., the natural frequencies and the structural damping ratio, are also shown in the table. Based on the results of the first series of experiments, models made of aluminium were designed. Aluminium was chosen as the model material for the second group because of its relatively easy manufacturability. These models will be referred to as the aluminium models. More variety of model shapes were chosen for aluminium models including the change of depth. Aluminium model shapes together with the model name and dynamic characteristics are tabulated in Table 3.2(b). The aluminium models were used in the second series of experiments conducted in April-July 1990 mainly at the Carleton wind tunnel.

Table 3.2.(a) Characteristics of Steel Models

Model Name	Thick-ness (mm)	Length (mm)	Width (mm)	Natural Freq.		h_{s1} (%)
				1st	2nd	
SA	0.8	305.	6.4	7.1 Hz	44. Hz	0.37
SB			12.7			0.38
SC			25.4			0.35
SD		203.	6.4	15.9 Hz	98. Hz	0.47
SE			12.7			0.40
SF			25.4			0.30

Table 3.2.(b) Characteristics of Aluminium Models

Model Name	Thick-ness (mm)	Length (mm)	Width (mm)	Natural Freq. (Hz)			h_{s1} (%)
				1st	2nd	Tor.	
AC	0.8	305.	25.4	7.1	44.	-	0.45
AD	0.8			7.0	-	-	0.46
AE	1.6			13.6	-	-	0.16
AF	3.2			27.5	-	-	0.14
AF′	3.2			20.3	-	-	0.24
AG	6.4			16.0	-	-	0.23
AH	12.7			11.5	-	-	0.28
AI	25.4			8.3	-	-	0.20
AJ	0.8	203.	25.4	16.0	100.	-	0.33
AK		102.	25.4	65.	-	-	0.47
AL		305.	50.8	7.0	44.	-	0.45
AM		305.	102.	7.0	44.	40.	0.55
AN		305.	203.	7.1	45.	23.8	0.42
AO		305.	305.	6.9	41.	15.7	0.28
AP		203.	305.	16.4	104.	27.	0.19

where h_{s1} is the structural damping ratio for the first bending mode. The structural damping ratio for the first torsional mode is 0.10, 0.13, 0.19 and 0.18% for Model AM, AN, AO and AP respectively.

Models were cantilever supported in all cases. To avoid the excitation of the model due to the wind tunnel floor vibration, the models were supported directly on the building floor separated from the wind tunnel shell. For steel models, the model support was attached to a turntable (made of plexiglass, diameter of 378 mm, and thickness of 12.7 mm), which was loosely fit in the wind tunnel floor and supported from the building floor via a rotating

mechanism (Plates 3.1, 3.2 and 3.3). For aluminium models, the model support went through the wind tunnel floor and attached to a turntable which was supported from the building floor (Plates 3.4 and 3.5). In the second series of experiments, the turntable was located below the wind tunnel to reduce the size of the hole in the tunnel floor.

In this thesis, the term of "model location" is defined as the location at the rotation centre of the turntable at the height of the model. In other words, it is 152 mm from the model support in the direction of the model tip for steel models, and at the location of the model support for aluminium models. The model height from the wind tunnel floor was 100 mm and 140 mm for the steel and aluminium models respectively.

The model supporting mechanism was designed to support the model rigidly enough and to cause aerodynamic interference as little as possible. Therefore, the "clamping" part which holds the model in the wind tunnel was designed as small as possible. The clamping part has the same width as the model for aluminium models. A typical dimension of the clamping part for Model AC is given in Fig. 3.3. The shape of the clamping part should generally cause different effects on the aerodynamic interference. However, since this effect seems to be too complicated to handle precisely, the clamping part was designed with a simple rectangular section. In any case, as stated at the beginning of this chapter, the effect of the aerodynamic interference should be very small, if not entirely negligible, when the wind comes from the free end direction or its quadrant.

For thicker aluminium models having a thickness more than or equal to 3.2 mm (Models AF', AG, AH and AI), an aluminium piece having the designed thickness and width for the model was made 38.1 mm shorter than the model length and is connected to a small steel piece with thickness of 1.6 mm and the same width as the model. The small steel plate was connected to the model support and has the function of an elastic spring causing a model vibration with a comparable natural frequency with other models. Overall model length combining the aluminium piece and the steel plate was same as the designed model length. Side view of the steel piece and clamping part for thicker models is shown in Fig. 3.4.

3.2.5. Model Response Measurement

Model response was measured by strain gauges attached to the model at the location close to the support. A full Wheatstone bridge was made up by four strain gauges, two of which are attached on each surface of the model. The full bridge was connected to a control unit which also amplified the output by a factor of 1000. The amplified output was recorded by an analog data recorder (Racal Tape Recorder, STORE Model 7DS) and was also used for a real-time analysis. For models having a width more than 50.8 mm, two sets of full bridges were attached to the model at the same distance from the support but at a location close to each side of the model. By taking the sum and difference of the output from each full bridge, the vertical and torsional response of the model were expected to be obtained.

The strain gauge outputs were calibrated prior to the testing against the model tip deflection by applying a concentrated load at the model tip. However, the model vibrates with its natural mode shapes of vibration during the response measurement and the relationship between the strain at the strain gauge location and the tip deflection is different from that at the calibration. For the models with length of 305 mm, the theoretical calculation shows that the strain at the strain gauge location due to the dominant first mode of vertical bending vibration is 0.88 times that due to the static deflection by the concentrated load at the tip for the same tip deflection. Therefore, the calibration factor from the strain gauge output to the tip deflection obtained by the calibration was multiplied by 0.88 to get the actual tip deflection for the model response. This ratio becomes 0.89 and 0.93 for the models with length of 203 mm and 102 mm, respectively. For the torsional response, the ratio is 0.64 for both model length of 305 mm and 203 mm. For the thicker aluminium models with a steel piece as an elastic spring, no correction was made for the calibration factor because the model deflection shape can be assumed to be the same for both during the calibration and during the response measurement.

Three types of devices were used for the measurement of the model r.m.s. response. The first is a voltmeter with true r.m.s. function (TSI Model 1076) which was used for all cases. The

averaging time was chosen to be 10 or 100 sec although sometimes the measurement was still difficult because of the fluctuation of the reading. The second is a spectrum analyzer (Hewlett Packard Structural Dynamics Analyzer 5423A) which was used for most of the cases. This analyzer gives readings of the power spectrum and the variance from which the r.m.s. response is obtained. The bandwidth was taken so as to cover all major response peaks; typically from 0 to 25 Hz when only the first mode with natural frequency of approximately 7 Hz was dominant. The sampling time was about 60 sec. The third is a digital voltmeter (Hewlett Packard 3437A System Voltmeter) together with a dedicated desktop computer (Hewlett Packard 9845B) which was used for the measurement with the aluminium models. This combination gives peak and r.m.s. values of the response. The sampling rate was chosen as 100 points/sec for bending response and the sampling time was set to be as 100 sec. These choices were made as a compromise of the sampling rate which should be chosen to have enough points in a cycle and the sampling time which should be long enough to have a stable result, under a restriction of the maximum number of available sampling points by the digital voltmeter which was 9999. For a typical 7 Hz natural frequency of the model, 14 sampling points were in a cycle and the sampling time corresponds to close to 2 hours in the prototype time scale if the natural frequency of the prototype is taken as 0.1 Hz which is a fair approximation for a cable-stayed bridge under construction using the balanced cantilever method. The sampling time of 2 hours may seem to be long because the usual averaging time for the natural wind speed is between 5 minutes and 1 hour. However, it appeared to be a good choice in order to have more stable response. Although the measurement by the third device seemed to be most reliable and that by the first device least reliable, the three measurements agreed generally well all through the experiment. The measurements were carried out during the experiment, and also the time history of the model response was recorded on paper by a chart recorder throughout the experiments for the confirmation of the response. Low pass filters were also used during the measurement to eliminate possible high frequency noise by setting the cut-off frequency of 100 Hz for most cases.

The recorded data were mainly used for supplemental data reduction such as the check for the modal contribution to the overall response. Also, some of the torsional response data

were reduced using the recorded data with the digital voltmeter and the desktop computer. Sampling time of 100 sec with the rate of 356 points/sec were used for the torsional response.

For the measurement of the structural and aerodynamic damping, the free vibration decay method was used. Time histories of model free vibration decay in still air and also in very low turbulent flow (Smooth Flow) were obtained with a chart recorder. Measurement was taken later on the recorded paper to reduce the critical damping ratio for each case. The average of two or more measurements was taken for each case.

The noise in the output signal was usually negligibly small in magnitude. The ratio of the noise to the signal in terms of r.m.s was less than a few percent. For smaller output signals such as that for thicker models or that in very low turbulence, the ratio became higher. Nevertheless, it was not too large for most cases. The magnitude of the noise seemed to be stable, so the effect of the noise was removed by taking a representative value of r.m.s., $\sigma_r = (\sigma_m^2 - \sigma_n^2)^{1/2}$, where σ_m is the measured r.m.s. of the response and σ_n is the r.m.s. of the noise. The value of σ_r after this correction is used all through this thesis simply as the r.m.s. value of the response. However, there were a few cases where the noise was rather large. They were the response of the shorter steel models (Models SD, SE and SF), where the model natural frequency coincided with the vibration frequency of the wind tunnel. Although the turntable was structurally separated from the wind tunnel itself, the vibration of the wind tunnel seemed to be somehow transmitted to the model and caused an amplified vibration. The amount of this mechanically originated noise was measured by taking the signal from a covered model so that no wind can cause the vibration on the model while the wind tunnel was running. This noise was found to be very large for some cases and it was also unstable. Therefore, the model response with too large noise obtained for those shorter steel models were all regarded to be unreliable and they are not considered here. For other shorter steel model responses, the noise was removed and σ_r was used as mentioned above. In Appendix A where all the experimental results are given, the maximum value of a ratio σ_n/σ_m for each case is given to indicate the magnitude of the noise.

3.3. Flow Characteristics

Flow characteristics measured in the NRCC and Carleton wind tunnels are tabulated in Tables 3.3.

Although the distance between the grid and the model location was different for different wind tunnels, the configurations of the grids were the same for both wind tunnels. However, somewhat different flow characteristics were obtained. The reason for the difference is not clear but perhaps it is partly because of the existence of the object in the Carleton wind tunnel far upstream from the grid as is mentioned in Section 3.2.2.

Table 3.3.(a) Flow Characteristics, The NRCC Wind Tunnel

Item	Location	Grid NI	Grid NII	Grid NIII	Shear Flow
I_w (%)	A	11.8	9.0	6.4	14.7
	B	10.5	-	4.7	-
	C	10.8	-	6.1	-
	D	13.1	-	11.3	-
I_u (%)	A	17.0	10.0	7.5	9.9
	B	15.6	-	5.5	-
	C	14.5	-	6.9	-
	D	19.2	-	13.1	-
L_w^y (mm)	A	27.	-	10.	32.
	B	28.	-	12.	-
	D	24.	-	7.	-
L_w^x (mm)	A	29.	-	10.	42.
L_u^x (mm)	A	60.	35.	24.	89.

Table 3.3.(b) Flow Characteristics, The Carleton Wind Tunnel

Item	Location	Grid CI	Grid CIII
I_w (%)	A	10.6	6.2
	B	9.5	4.9
	C	10.7	6.4
	D	12.1	9.1
I_u (%)	A	15.5	8.0
	B	13.9	6.4
	C	15.0	7.9
	D	17.5	11.9
L_w^y (mm)	A	28.	10.
L_w^x (mm)	A	36.	14.
L_u^x (mm)	A	79.	24.
L_u^y (mm)	A	35.	12.

where

I_u, I_w: turbulence intensities
L_w^y, L_w^x, L_u^x, L_u^y: integral scales of turbulence
A: model location
B, C and D: locations 305 mm apart from A, see the figure below

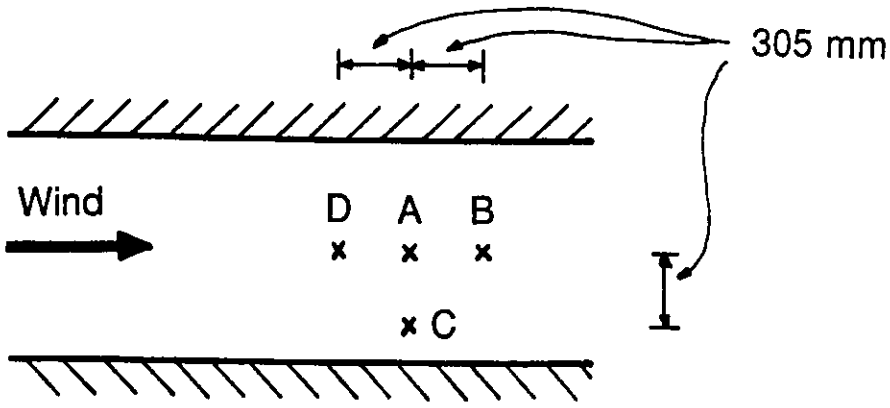

Power spectra of the fluctuating velocity component w measured at the model location are shown in Figs. 3.5. A log-log scale is used in the figures, and the ordinate is made dimensionless by using the variance of the fluctuating velocity and the frequency. The shape of the spectra agrees generally well with the von Kármán spectra mentioned in Chapter 2 with the given scales of turbulence.

3.4. Model Response Characteristics

All the model response seems to be typical buffeting motion which shows random change of amplitude with time. In the following, the discussion will be limited to the vertical bending response except in Section 3.4.2. All the experimental results are tabulated in Appendix A.

3.4.1. Effect of Model Width

The tendency of the model buffeting response with varied wind yaw angle was clearly affected by the model width. Response of models with different widths is shown in Figs. 3.6., where the ordinate is taken as the r.m.s. vertical bending response normalized by that of zero yaw angle case and the abscissa is the wind yaw angle β. The definition of the wind yaw angle β for the model is given in Fig. 3.2. From these figures, the tendency can be seen that the wider the model is, the larger the model response becomes with positive yaw angles, or when wind comes from the free end direction. This tendency is observed for both steel models (Fig. 3.6(a) and (b)) and aluminium models (Fig. 3.6(c) and (d)), and is more clearly seen with aluminium models where the model width was changed more extensively. This tendency was observed irrespective of flow conditions and wind velocities.

3.4.2. Effect of Model Length

The discussion above on the effect of model width was limited to the models with a length of 305 mm. However, if the effects of both scale of turbulence and Reynolds number are assumed to be negligible, the effect of model width should be regarded as the effect of the ratio of the model span length to the model width. In other words, with the assumption above, models with the same span to width ratio should respond in a same manner irrespective of the actual size of the model. Therefore, the change of model length is expected to cause a similar effect as the change of model width. However, as it can be seen from Fig. 3.7(a), the effect of model length is not obvious. The span to width ratio of Model AK is in-between those of Models AL and AM; nevertheless, the response of Model AK was significantly different from the response of Models AL and AM but similar to that of Model AC. The same is observed about Model AJ and shorter steel models.

The reason of the uncertainty regarding the effect of model length might be attributed to the aerodynamic interference by the model supporting system. When the wind comes from the free end direction, the effect of the aerodynamic interference on the approaching flow by the model supporting system should be very small. However, even in that case, it affects the flow shed from the model, and thus should somewhat change the aerodynamic forces acting on the model. The magnitude of this effect should be larger for the models with shorter span length, because the model supporting system was the same regardless of the model span length. Therefore, for shorter models, it may be reasoned that the effect of model span to width ratio was counteracted by the effect of the aerodynamic interference and thus significant difference of the responses was not observed. The evaluation of the effect of aerodynamic interference on the flow shed from the model is very difficult, so the discussion on the model response is limited only to the longer span length (305 mm) models.

On the other hand, for the wider models with different span lengths (Models AO and AP), the difference of the response against wind yaw angle was clearer (Fig.3.7(b)). The response with positive yaw angles became larger for the shorter span length model. The reason for the

different effect of model span length between narrow width models (Models AC, AJ, AK and steel models) and wider width models (Models AO and AP) is not certain.

3.4.3. Comparison with the "Cosine Rule"

In Figs. 3.6 and 3.7, a simple response prediction by the "cosine rule" is also shown with a broken line. The explanation of the cosine rule is given in Section 2.4. The predicted response by the cosine rule becomes proportional to cos β. It is clear that this simple cosine rule gives lower prediction than the actual model responses with positive yaw angles. If the average of the response magnitude at β and $-\beta$ is assumed to represent the response of a cable-stayed bridge under construction using balanced cantilever method with wind yaw angle β, the experimental results support the observations by the previous studies mentioned in Section 2.4 (Zan, 1987a; Irwin and Gamble, 1985), where the buffeting response of the full model of a cable-stayed bridge under construction does not decrease as rapidly as cos β with the increase of wind yaw angle β. This fact has an important interpretation that the simple response prediction by the cosine rule could be on the less conservative side, hence the response under yawed wind should be considered carefully for this type of structure.

3.4.4. Effect of Model Cross-Section

Most of the models used in the experiment had a rectangular cross-section. The exception was Model AD of which width and span length were the same with Model AC whereas the cross-section was made sharp-edged (Plate 3.6). As it can be seen from Fig. 3.8, response of both Models AC and AD shows essentially the same tendency for the change of wind yaw angles. This implies that the cross-sections of these models are close enough to a flat plate because the change of the edge shape did not affect the model response.

As mentioned in Section 3.2.4, thicker aluminium models (Models AG, AH and AI) had

a different model supporting mechanism from other models. To check the effect of the different model supporting mechanism, Model AF′ was made to have the same model dimensions as Model AF but with the model supporting mechanism for thicker models. Fig. 3.9 shows the response of Model AF and AF′. Both responses are much the same and thus the difference caused by the model clamping part is considered to be negligible.

Figs. 3.10 show the response of models with different thickness. For models with depth to width ratio up to 1/4 (Models AC, AE, AF and AG), the model response with positive yaw angles is slightly reduced for thicker models irrespective to the flow condition (Grid CI for Figs. 3.10(a) and (b), and Grid CIII for Figs. 3.10(c) and (d)). For thicker models with which depth to width ratio is 1/2 (Model AH) or 1 (Model AI), the response showed a peculiar tendency (Figs. 3.10(b) and (d)). This peculiar tendency even changed with different wind speed (see Section 3.4.5). This phenomenon might be related to the aerodynamic characteristics of the thicker model cross-section which is prone to a single-degree-of-freedom flutter. Affected largely by the self-excited aerodynamic forces, the tendency of the responses could be very complicated.

3.4.5. Effect of Wind Speed

The tendency of the model response against wind yaw angle did not change appreciably at different wind speed for flat plate aluminium models. For steel models, a slightly larger response for positive yaw angles was often observed at higher wind speed (Fig. 3.11(a)). Shorter length steel models (Models SD, SE and SF) more clearly showed slightly larger responses with positive yaw angles for higher wind speed (Fig. 3.11(b)). For thicker aluminium models (Models AH and AI), as shown in Fig. 3.11(c), the change of the wind speed caused considerable difference in the model response with wind yaw angle.

For some cases, the wind yaw angle was kept constant and the wind speed was changed. In Fig. 3.12(a), the ratio of the response at $\beta = 90°$ to that at $\beta = 0°$ seems to be unchanged. On the contrary, Fig. 3.12(b) shows that the ratio of the response at $\beta = 90°$ to $\beta = 0°$ became larger

when the wind speed was increased. Both Figs. 3.12(a) and (b) are the response of Model AC in fine grid turbulence but at different wind tunnels. For a wider model (Model AM), a larger ratio of the response at $\beta = 90°$ to that at $\beta = 0°$ was observed in coarse grid turbulence (Grid NI) with higher wind speed (Fig. 3.12(c)) but in fine grid turbulence (Grid NIII) the ratio did not change with wind speed (Fig. 3.12(d)). Figs. 3.12(e) and (f) show the cases for a thicker model (Model AH) with two flow conditions. Different tendencies against wind yaw angle for different wind velocities can be observed from these figures.

3.4.6. Effect of Flow Conditions

The effect of the flow conditions on the response with wind yaw angle is not very clear for most cases. However, for Model SC, the response becomes clearly larger with positive yaw angles in Grid NIII than in Grid NI (Fig. 3.13).

Although the intensities and scales of turbulence are not much different between Grid CI and NI or between Grid CIII and NIII, two wind tunnels sometimes gave different results. Figs. 3.14(a) and (b) show the response of Model AC with $\beta = 0°$. However, for $\beta = 90°$ with the same model, the response in two wind tunnels were not too different (Figs. 3.14(c) and (d)).

3.4.7. Spectra and Time Histories of the Response

Figs. 3.15 are typical spectra of the model response and Figs. 3.16 are time records of the corresponding response. The difference of the response characteristics between $\beta = 0°$ and $\beta = 90°$ is clear. The width of the spectrum for $\beta = 90°$ is narrower than that for $\beta = 0°$. From Figs. 3.16, it can be seen that the response amplitude changes more slowly for $\beta = 90°$ than the case of $\beta = 0°$. These different characteristics of the response can be explained by the difference of the aerodynamic damping. The change of the aerodynamic damping with wind yaw angle will be discussed in Section 3.5.

3.4.8. Torsional Response

For wider aluminium models (Models AM, AN, AO and AP), torsional response was also observed. The effect of model width seems to be similar to the case of vertical bending response (Figs. 3.17). That is, the wider the model is, the larger the model response becomes with positive yaw angles. However, the torsional response is much closer to the prediction by the cosine rule than the vertical bending response for the same model.

The response in coarse grid turbulence (Grid NI) shows that the ratio of the response at $\beta = \pm 45°$ to that at $\beta = 0°$ increased with higher wind speed and the ratio of the response at $\beta = 90°$ to $\beta = 0°$ did not change with the wind speed (Fig. 3.18(a)). Whereas the response in fine grid turbulence (Grid NIII) shows that the ratio of the response at $\beta = -45°$ to $\beta = 0°$ increased, the ratio at $\beta = +45°$ to $\beta = 0°$ did not change, and the ratio at $\beta = 90°$ to $\beta = 0°$ decreased with higher wind speed (Fig. 3.18(b)). The tendency of the decreasing ratio of the response at $\beta = 90°$ to that at $\beta = 0°$ with increasing wind speed was not observed for vertical responses.

3.4.9. Vibration Modes

Spectral analysis was carried out to identify the contribution of higher vibration modes. For most cases, the response energy consisted of the first mode. The exception was the vertical bending response in medium and fine grid turbulence at NRCC wind tunnel (Grid NII and NIII) where the second mode component became more significant and sometimes it was found to be comparable to the first mode contribution with relatively small wind yaw angle. This was particularly pronounced with the fine grid turbulence (Grid NIII) and with relatively high wind speed. Fig. 3.19 shows typical response spectra with large second mode contribution in fine grid turbulence at the NRCC wind tunnel.

Figs. 3.20(a)-(d) identify contribution of modal components under various flow conditions but with the same wind speed at the NRCC wind tunnel. The r.m.s. response of the first and

second mode components are given by $\sigma_1(\beta)$ and $\sigma_2(\beta)$, respectively, and the total is given by $\sigma(\beta)$, which corresponds to $[(\sigma_1)^2+(\sigma_2)^2]^{1/2}$ and everything is normalized by $\sigma(0)$. It is clearly observed that the contribution of the second mode was outstanding particularly in fine grid turbulence (Grid NIII). Fig. 3.20(e) shows a similar observation with Grid NIII and 30% lower wind speed. As it is obvious from the figure, the second mode contribution is less than the case of the higher wind speed. It is found that the lower the wind speed, the less the second mode contribution becomes, regardless of flow conditions. The large second mode contribution for the response was significant only at the NRCC wind tunnel, and not at the Carleton wind tunnel even in the fine grid turbulence (Grid CIII).

One thing perhaps to be mentioned is that the comparison between σ_1 and σ_2 is made in terms of the strain at the gauge location. If the comparison is made in terms of the tip vertical deflection, the contribution from the second mode should be considered to be approximately 21% of σ_2, because the same tip deflection by the second mode causes 4.8 times larger strain at the strain gauge location than the first mode.

3.4.10. Response in Smooth Flow

For Models AC, AL and AM, the responses were also measured in very low turbulent flow (Smooth Flow; $I_u = 0.8\%$, $I_w = 0.9\%$) at the Carleton wind tunnel. The main objective for the measurement in Smooth Flow was to confirm if the models show any tendency for instabilities such as flutter. Structures are usually more susceptible to instabilities in very low turbulent flow, and at the same time, the detection of instability phenomena could be easier. The response was very small compared with those in turbulent flows, but it still seemed to have a random nature and no instability phenomenon was observed in the wind speed range tested. The response in Smooth Flow is shown in Fig. 3.21. The relatively large response when the wind yaw angle was close to $-90°$ is probably caused by the wake generated behind the model supporting mechanism. The time history of this case showed random buffeting which is very similar to the case in turbulent flows. This suggests that the response is caused by the

fluctuations of the wake. The response against wind speed is shown in Figs. 3.22. A peculiar tendency of the response in lower speed range for Models AC and AL can be seen. The reason of this phenomenon is not clear, but it could be due to some sort of resonance between model movement and the wake behind the model. By conducting spectral analysis, it is found that the second mode contribution is large for small yaw angle and higher wind speed cases and it sometimes becomes even comparable to the first mode contribution. At the same time, a very low frequency component having its peak around 1 Hz is found to become very large (Fig. 3.23).

3.5. Aerodynamic Damping of Models

The aerodynamic damping is one of the most important factors when the buffeting response is calculated. Although the quasi-steady assumption allows to evaluate aerodynamic damping when the wind comes perpendicular to the model axis, the accuracy of this evaluation is doubtful. Furthermore, when the wind does not come perpendicular to the model axis, there is no means to theoretically evaluate the aerodynamic damping. Therefore, the aerodynamic damping was measured for some aluminium models (Models AC, AH, AL and AM) during the experiment.

The aerodynamic damping was measured with the following procedure. A hook was made of steel wire and it was attached to a string. The hook had a shape which could pull down the model tip when the string was pulled and could fall off from the model when the string was released. By using this hook and the string passing through a hole in the wind tunnel floor at the model support, the model can be set into free vibration from outside of the wind tunnel. The decaying time history of the vibration was recorded by a chart recorder, and the damping of the model was measured. At first, with no wind, the structural damping was measured. Then in a very low turbulent flow (Smooth Flow) with a specified wind speed, the model damping was measured for various wind yaw angles. The aerodynamic damping was then calculated by subtracting the structural damping from the damping obtained in Smooth Flow.

second mode components are given by $\sigma_1(\beta)$ and $\sigma_2(\beta)$, respectively, and the total is given by $\sigma(\beta)$, which corresponds to $[(\sigma_1)^2+(\sigma_2)^2]^{1/2}$ and everything is normalized by $\sigma(0)$. It is clearly observed that the contribution of the second mode was outstanding particularly in fine grid turbulence (Grid NIII). Fig. 3.20(e) shows a similar observation with Grid NIII and 30% lower wind speed. As it is obvious from the figure, the second mode contribution is less than the case of the higher wind speed. It is found that the lower the wind speed, the less the second mode contribution becomes, regardless of flow conditions. The large second mode contribution for the response was significant only at the NRCC wind tunnel, and not at the Carleton wind tunnel even in the fine grid turbulence (Grid CIII).

One thing perhaps to be mentioned is that the comparison between σ_1 and σ_2 is made in terms of the strain at the gauge location. If the comparison is made in terms of the tip vertical deflection, the contribution from the second mode should be considered to be approximately 21% of σ_2, because the same tip deflection by the second mode causes 4.8 times larger strain at the strain gauge location than the first mode.

3.4.10. Response in Smooth Flow

For Models AC, AL and AM, the responses were also measured in very low turbulent flow (Smooth Flow; $I_u = 0.8\%$, $I_w = 0.9\%$) at the Carleton wind tunnel. The main objective for the measurement in Smooth Flow was to confirm if the models show any tendency for instabilities such as flutter. Structures are usually more susceptible to instabilities in very low turbulent flow, and at the same time, the detection of instability phenomena could be easier. The response was very small compared with those in turbulent flows, but it still seemed to have a random nature and no instability phenomenon was observed in the wind speed range tested. The response in Smooth Flow is shown in Fig. 3.21. The relatively large response when the wind yaw angle was close to $-90°$ is probably caused by the wake generated behind the model supporting mechanism. The time history of this case showed random buffeting which is very similar to the case in turbulent flows. This suggests that the response is caused by the

fluctuations of the wake. The response against wind speed is shown in Figs. 3.22. A peculiar tendency of the response in lower speed range for Models AC and AL can be seen. The reason of this phenomenon is not clear, but it could be due to some sort of resonance between model movement and the wake behind the model. By conducting spectral analysis, it is found that the second mode contribution is large for small yaw angle and higher wind speed cases and it sometimes becomes even comparable to the first mode contribution. At the same time, a very low frequency component having its peak around 1 Hz is found to become very large (Fig. 3.23).

3.5. Aerodynamic Damping of Models

The aerodynamic damping is one of the most important factors when the buffeting response is calculated. Although the quasi-steady assumption allows to evaluate aerodynamic damping when the wind comes perpendicular to the model axis, the accuracy of this evaluation is doubtful. Furthermore, when the wind does not come perpendicular to the model axis, there is no means to theoretically evaluate the aerodynamic damping. Therefore, the aerodynamic damping was measured for some aluminium models (Models AC, AH, AL and AM) during the experiment.

The aerodynamic damping was measured with the following procedure. A hook was made of steel wire and it was attached to a string. The hook had a shape which could pull down the model tip when the string was pulled and could fall off from the model when the string was released. By using this hook and the string passing through a hole in the wind tunnel floor at the model support, the model can be set into free vibration from outside of the wind tunnel. The decaying time history of the vibration was recorded by a chart recorder, and the damping of the model was measured. At first, with no wind, the structural damping was measured. Then in a very low turbulent flow (Smooth Flow) with a specified wind speed, the model damping was measured for various wind yaw angles. The aerodynamic damping was then calculated by subtracting the structural damping from the damping obtained in Smooth Flow.

The aerodynamic damping may change if the flow condition is different. Because the response calculation is conducted for the model response in turbulent flow, it is more reasonable to measure the aerodynamic damping in turbulent flow. However, the measurement of the damping in turbulent flow is more complicated because the free vibration decay method cannot be used any more. Therefore, the damping was measured in Smooth Flow only and it was assumed that the aerodynamic damping in very low turbulence was a good representative of that in turbulent flow. All the results of the aerodynamic damping measurement are tabulated in Appendix B.

Figs. 3.24 show the change of the aerodynamic damping against wind yaw angle. The ordinate is the aerodynamic damping ratio $h_a(\beta)$. For flat plate models, the change of the aerodynamic damping is found almost proportional to cos β, except for the widest model (Model AM) particularly with negative yaw angles. The broken lines in the figures correspond to an approximation $h_{a0}\cdot\cos\beta$, which is used in the analysis in Chapter 4. For the thicker depth model (Model AH), the aerodynamic damping showed a very complicated tendency. The value of the aerodynamic damping for this model was very small because of the large mass ratio (ratio of the mass of the model to the mass of the air). This made the aerodynamic damping measurement a little more difficult for this case.

For Model AC, the aerodynamic damping was measured against wind speed for some wind yaw angles (Fig. 3.25). The aerodynamic damping seemed to change almost linearly with wind speed for the case of $\beta = -45°$ and 0°, but the case of $\beta = +45°$ showed some nonlinearity and the aerodynamic damping for $\beta = +90°$ case did not change very much with wind speed.

For the flat plate models with $\beta = 0°$, a prediction of the aerodynamic damping can be made by the quasi-steady approximation (eqn. 2.19). Table 3.4 shows the comparison between the measurement and the prediction where $dC_L/d\alpha$ for finite plate was used for the calculation. The experimental results are smaller than the prediction by the quasi-steady approximation.

Table 3.4. Comparison of the Experimental and Theoretical Aerodynamic Damping Ratio ($\beta = 0°$)

Model	U = 3.0 m/sec		U = 6.1 m/sec	
	Exp. (%)	Theo. (%)	Exp. (%)	Theo. (%)
AC	4.1	5.2	9.2	10.4
AL	2.7	4.4	6.2	8.7
AM	1.7	3.2	4.3	6.4

3.6. Concluding Remarks for the Experimental Study

The buffeting response of simplified cantilever models under wind with yaw angle was studied experimentally. A rather conspicuous and interesting tendency was observed. Among the factors that affect the model response tendencies, the effect of the model width was found to be prominent. The wider the model was, the larger the model response became under the wind from the free end direction compared with the response under the wind normal to the model axis. Sometimes, even larger response was observed under yawed winds than under normal wind. This particularly enhances the engineering importance of studying the response under wind with yaw angle, because the response under wind normal to the model axis, which is usually the case in wind tunnel tests, is not the critical case any more.

Also prediction by the cosine rule was found to give generally lower and less conservative values than the experimental results. This observation is consistent with the previous experimental studies of cable-stayed bridges under construction (Zan, 1987a; Irwin and Gamble, 1985). Since it is now apparent that the simple cosine rule does not apply for cantilever structures, a new approach for the prediction of the buffeting response under yawed wind is proposed in Chapter 4.

Chapter 4. THEORETICAL STUDY

4.1. Introduction

In order to explain the results of the experiments described in Chapter 3, the buffeting response of models under wind with yaw angle was calculated by modifying the conventional buffeting analysis. When a wind induced response of a structure is analytically obtained, the most critical part is often the assumption of the aerodynamic forces on the structure. If the structure has an aerodynamically bluff cross-sectional shape which causes flow separations, the practical way to evaluate the aerodynamic forces is to do wind tunnel test for the force measurement because the analytical method to predict the aerodynamic forces is still difficult with the current knowledge. On the other hand, if the structure has a streamlined cross-section, the aerodynamic forces can be calculated using the potential flow theory. This is the case of aerofoils under small angle of attack, and the studies of aerodynamic forces acting on aerofoils have been done extensively in aeronautics. Calculated aerodynamic forces generally agree well with the experimental results, and these theoretical methods together with experimental confirmation give us a large amount of knowledge about the aerodynamic forces acting on aerofoils.

In the present study, theoretical considerations were taken only for the models with flat plate sections. Aerodynamic forces acting on very thin flat plates are known to be similar to those on aerofoils, and the results obtained for aerofoils with symmetrical cross-sections could be used. By using a sophisticated computational method, calculations of the aerodynamic forces acting on an aerofoil in incompressible flow now seem to be a routine procedure which can be applied to any configurations and even in turbulent flow (Küchemann, 1978). This procedure could be used for the present case of flat plate models with wind yaw angles. However, this approach is not applicable to the structures with bluff cross-sections. The final objective that follows the current research is to clarify the effect of wind yaw angle on the buffeting response

of bridge decks in particular, which often have bluff cross-sections. This objective being kept in mind, the effect of wind yaw angle was evaluated with an analysis that was a modification of the conventional buffeting analysis, where the streamlined cross-section was not an essential requirement. The calculated results were compared with the experimental results and the validity of the analysis was examined. By accepting some approximations, the procedure of the analysis could apply to a structure with any cross-sectional shape, provided that some of the characteristics of the aerodynamic forces acting on the structure are measured. The description was given in Section 2.3 about the conventional buffeting analysis which was the base of the current analysis. The coordinates used in this chapter are defined in the same way as in Chapter 3 (Fig. 3.2).

4.2. Modified Buffeting Analysis

Similar to the conventional buffeting analysis, the strip theory approximation was adopted, where the generalized force was given by integrating the two-dimensional aerodynamic forces acting on each narrow "strip" sliced along the wind direction. On applying the strip theory approximation to the response under yawed wind, some considerations must have been taken other than that for the conventional buffeting analysis. Buffeting forces were calculated by assuming quasi-steady approximation as for the case of conventional buffeting analysis, whereas self-excited forces or aerodynamic damping were taken from the experimental results which seemed to be more reliable than the analytical evaluation. The procedure for the modified buffeting analysis will be given in the following, where the differences from the conventional buffeting analysis are described. The actual procedure given below will consider the cantilever supported flat plate models used in the experiment, thus the discussion will be limited to only vertical deflections and corresponding aerodynamic forces because the vertical response was found to be dominant in the experiment.

4.2.1. Consideration of Effective Wind Velocity for Cosine or Sine Direction

If the presence of the viscosity is neglected, the span-wise component of the flow can have no influence on the pressure distribution for an infinitely long plate. This can be explained, for example, in the following way (McCormick, 1979). If an infinitely long plate is assumed to be able to move freely in its longitudinal direction which goes through the wind tunnel walls normal to the flow, exposing a part of it to the flow in the wind tunnel. Then, with no viscosity, when the wind velocity in the wind tunnel, U′, and the angle of attack, α, are constant, the aerodynamic forces acting on the plate should be the same no matter how the plate is moving in its longitudinal direction with velocity V (Fig. 4.1(a)). If the relative wind velocity is considered, the situation in Fig. 4.1(a) is the same as in Fig. 4.2(b), which is a case with an infinite plate under a yawed wind. Therefore, the aerodynamic forces on an infinite plate depend only on the velocity component normal to the axis (U′, in Fig. 4.1(b)) and the velocity component parallel to the axis (V, in Fig. 4.1(b)) does not have any effect. For aeroplanes having swept wings, the relative wind velocity U_r corresponds to the speed of flight and $U' = U_r \cdot \cos \beta$ is assumed to be the effective wind velocity which actually generates the aerodynamic forces. This relationship for infinite aerofoils has been experimentally confirmed by Jacobs (1952).

Although the actual models were not infinitely long, the same logic as above is used in the present analysis. Thus effective wind velocity is taken as the velocity component perpendicular to the leading edge. Because the model plate has ends, there are two choices of leading edges, one is the side and the other is the end of the model. Then the corresponding effective wind velocity becomes $U_{eC} = U \cdot \cos \beta$ and $U_{eS} = U \cdot \sin \beta$. When U_{eC} is considered as the effective velocity, it will be called "cosine case", and when U_{eS} is considered it will be called "sine case" in the following description (Fig. 4.2). U_{eC} or U_{eS} is the effective wind velocity for each case. The response calculations were conducted for both cosine and sine cases with each wind yaw angle.

The choice of the cosine or sine case is as follows: the cosine case applies when $\beta = 0°$

and the sine case applies when $|\beta| = 90°$ because there is no flow component other than U_{ec} or U_{es} for these yaw angles. By extending this idea, one may reasonably assume that the cosine case applies if β is around 0° and the sine case applies if $|\beta|$ is close to 90°. For the angles in-between, further discussion will be made in Chapter 5.

4.2.2. Application of the Strip Theory Approximation

A somewhat modified strip theory approximation is applied to this modified buffeting analysis. As the usual strip theory approximation, aerodynamic forces acting on each "strip" sliced out parallel to the wind direction were calculated first, then the overall aerodynamic forces acting on the model were obtained by integrating them. However, it is apparent that two-dimensional aerodynamic forces cannot be used for the present case because the models are not sufficiently line-like against the effective wind velocity direction and they cannot be approximated as two-dimensional structures. This is particularly apparent when the sine case is considered. Therefore, aerodynamic forces for the strips were calculated based on the aerodynamic forces obtained for the plates having the same configurations as the models. The quasi-steady approximation was used for the calculation of the aerodynamic buffeting forces, so aerodynamic coefficients applicable to the finite plate having the same shape as the model were used. This is the same approach as the one by Zan (1987a). It should be noted that even for the same model, aerodynamic coefficients to be used are different for the cosine and sine cases, because the span and chord are reversed for each case. The effect of finite length of the models is considered with this procedure of calculating the aerodynamic forces acting on the strips using aerodynamic coefficients for the finite plate. However, it is still considering "quasi-two-dimensional" flow around the model, because calculating the aerodynamic forces based on the same aerodynamic coefficients for all the strips means neglecting the non-uniform aerodynamic force distribution in the direction normal to the effective wind velocity. The effect of the non-uniform aerodynamic force distribution may be included by using varied aerodynamic coefficients, however, as the first approximation, the same aerodynamic coefficients were used for all strips in the model.

To make the problem simpler, the aerodynamic forces acting on the parallelograms shown with broken line in Fig. 4.2 were assumed to be the same as those acting on the actual model. Then the strips were taken parallel to these assumed boundaries in the same direction as the wind, covering the entire model.

With the strip theory and quasi-steady approximation, the aerodynamic force in the vertical direction for the cosine case $dF_{z'C}(y',t)$ acting on a strip of area dS at the location of y′ and time t, with vertical fluctuating velocity w(y′,t), can be expressed as

$$\begin{aligned} dF_{z'C}(y',t) &= \frac{1}{2}\rho U_{eC}^2 (dS) C_{LC\alpha} \frac{w}{U_{eC}} \\ &= \frac{1}{2}\rho U (dS) C_{LC\alpha} \cos\beta \; w(y',t) \end{aligned} \tag{4.1}$$

For sine case,

$$dF_{z'S}(x',t) = \frac{1}{2}\rho U (dS) C_{LS\alpha} \sin\beta \; w(y',t) \tag{4.2}$$

where $dF_{z'C}(y',t)$ and $dF_{z'S}(x',t)$ are quasi-steady aerodynamic forces in vertical direction on the strip corresponding to cosine and sine case respectively; $C_{LC\alpha} = dC_{LC}/d\alpha$ and $C_{LS\alpha} = dC_{LS}/d\alpha$; C_{LC} and C_{LS} are the aerodynamic lift coefficients of the plate for the cosine and sine case, or in other words, for the wind with $\beta = 0°$ and $\beta = 90°$ respectively; α is the angle of attack; x′, y′ and z′ are coordinates for the model taken in the model width, span-wise and vertical direction respectively (Fig. 3.2) and t is time. Here, C_L is assumed to be zero for $\alpha = 0°$ and also the drag force is neglected because a flat plate cross-section is considered.

4.2.3. Calculation of Generalized Buffeting Forces on a Strip

Modal analysis was applied as in the case of conventional buffeting analysis. In order to calculate the generalized force contributing to the specific structural mode, the information of

the mode shape is necessary.

For the cosine case, the model deflection was assumed to be the same everywhere inside a strip having the same value as that at the location where the resultant lift force acts. Then the generalized force for the r-*th* mode acting on a strip $dF_{z'Cr}$ defined by eqn. (4.3) is obtained in the same way as the conventional buffeting analysis:

$$dF_{z'Cr}(y') = dF_{z'C}\,\phi_r(y') \tag{4.3}$$

where $\phi_r(y')$ is the r-*th* mode shape of the model at the location where the resultant lift force acts.

For the sine case, the deflectional shape of a strip is basically the same as the mode shape of the model and can be integrated as the generalized force acting on the strip as

$$dF_{z'Sr}(x',t) = \frac{1}{2}\rho U(db)\sin\beta\; w(x',t)\int_0^{l_s} C_{LS\alpha}(s)\,\phi_r(s)\,ds \tag{4.4}$$

where db is the width of the strip; l_s is the length of the strip; $C_{LS\alpha}(s)$ expresses the lift force distribution along the strip; $\phi_r(s)$ is the r-*th* mode shape along the strip which is similar to $\phi_r(y')$ and s is the coordinate along the strip with the origin at the leading edge. The distribution of $C_{LS\alpha}(s)$ with s slightly changes according to the angle of attack, the aspect ratio of the plate and the location of the strip, but the same distribution shown in Fig. 4.3 taken from McCormick (1979, p. 87) was used all through the present calculation as an approximation. The area between $C_{LS\alpha}(s)$ and the horizontal axis is equal to $C_{LS\alpha}$.

4.2.4. Calculation of Overall Generalized Buffeting Forces

As the conventional buffeting analysis, the overall generalized aerodynamic force was determined by the integration of the generalized forces acting on the strips together with the mode shapes of the model.

For the cosine case, the resultant lift force on a strip is acting at the quarter chord point from the leading edge, so the integration should be taken on the line connecting these points in the parallelogram. The spectral analysis is to be carried out as the conventional buffeting analysis and the spectral density of the overall generalized force $S_{Fz'Cr}$ is, then,

$$S_{Fz'Cr}(f) = (\frac{1}{2}\rho U b C_{LC\alpha}\cos\beta)^2 \int_{e}^{l+e}\int_{e}^{l+e} S_{ww}(f,y',y'')\phi_r(y')\phi_r(y'')\,dy'\,dy'' \tag{4.5}$$

where S_{ww} is the cross-spectrum between w's at y′ and y″; l is the length of the model and e = (b/4)·tan β where b is the width of the model. In the region where y′ or y″ becomes more than l, the value of ϕ_r is assumed to be equal to $\phi_r(l)$.

For the sine case, the corresponding spectral density is

$$S_{Fz'Sr}(f) = (\frac{1}{2}\rho U \sin\beta \int_{0}^{l} C_{LS\alpha}(s)\phi_r(s)\,ds)^2 \int_{0}^{b}\int_{0}^{b} S_{ww}(f,x',x'')\,dx'\,dx'' \tag{4.6}$$

Sometimes the two-dimensional aerodynamic admittance is considered in the buffeting analysis, which takes into account of the non-uniformity of the flow field around the strip. In this analysis, the aerodynamic admittance is assumed to be unity as the first approximation.

4.2.5. Aerodynamic Damping

So far, only the buffeting force components were considered. There is actually the self-excited aerodynamic force due to the movement of the model as explained in Section 2.3.1. For the present analysis, the contribution of the self-excited force can be included by adding the aerodynamic damping to the damping term of the equation of motion as in Section 2.3.3. For the buffeting analysis, the damping term has a large effect on the response prediction. In order to reduce the uncertainty in the analysis, aerodynamic damping ratio for the first mode based on the experiment was used in the analysis. This means that the unsteady effect with the natural

frequency of the first mode is considered for the self-excited force. The aerodynamic damping ratio, h_a, was measured in very low turbulent flow under various wind yaw angles. The results are given in Section 3.5, and it was found that the change of the aerodynamic damping with wind yaw angle could be approximated by the following relationship:

$$h_a = h_{a0} \cos\beta \tag{4.7}$$

This approximation was used for the present analysis, and actual values of h_{a0} used in the response calculation for Models AC, AL and AM are given in Table 4.1. For the evaluation of the aerodynamic damping under wind velocities "in-between", interpolated values from Table 4.1 were used. The total damping ratio h_T then becomes, as eqn. (2.20),

$$h_T = h_s + h_a \tag{4.8}$$

where h_s is the structural damping ratio. The damping ratio was measured only for the first mode vibration, so it is applicable to the first mode only. This does not seem to pose much of a problem since the response observed in the experiment was dominantly in the first mode, and the calculation can be done assuming only the first mode contribution with enough accuracy. For the cases where the second mode contribution was to be calculated, the damping ratio for the second mode was assumed to be the same as that for the first mode.

Table 4.1. Values of h_{a0} (%)

Model	U = 3.0 m/sec	U = 6.1 m/sec
AC	4.0	9.4
AL	2.6	6.6
AM	2.0	5.0

4.2.6. Model Response Power Spectrum

Using the expressions above, the response power spectrum S_{qr} in terms of the generalized coordinate for the r-*th* mode can be obtained by, as shown in eqn. (2.24),

$$S_{qr}(f) = \frac{S_{Fz'r}(f)|H_r(f)|^2}{\omega_r^4 M_r^2} \tag{4.9}$$

where $S_{Fz'r}(f)$ is $S_{Fz'Cr}(f)$ or $S_{Fz'Sr}(f)$ depending on the case; $|H_r(f)|^2$ is the mechanical admittance given by eqn. (2.25); ω_r is the natural circular frequency of the r-*th* mode and M_r is the generalized mass of the mode (eqn. (2.16)).

Variance of the response is obtained by integration

$$\sigma_{qr}^2 = \int_0^\infty S_{qr}(f)\,df \tag{4.10}$$

where σ_{qr}^2 is the variance of the generalized coordinate q_r. The r.m.s. is the square root of variance. Therefore, by following the procedure stated above, the r.m.s. response of the model is obtained.

4.2.7. Evaluation of Aerodynamic Lift Coefficients and Other Parameters

For a rectangular thin flat plate, the aerodynamic lift coefficient depends on the aspect ratio AR. The aspect ratio is defined as the ratio of span to chord length for a rectangular plate. Therefore, even for the same plate, the aspect ratio is different for the cosine and the sine case. AR = *l*/b for the cosine case and AR = b/*l* for the sine case, where *l* and b are the model span length and the width respectively.

The lift slope $C_{L\alpha} = dC_L/d\alpha$ for the rectangular thin plate of AR larger than 2 is available

from a literature (ESDU, 1977) which tabulates calculated lift slope for wings with various aspect ratio. For the cosine case where AR = *l*/b is equal to or greater than 3, the lift slope $C_{LC\alpha}$ is obtained in this way.

On the other hand, for the sine case where AR = b/*l* is smaller than or equal to 1/3, more considerations are needed to evaluate the lift slope $C_{LS\alpha}$. The linear theory shows that for a delta wing having small aspect ratio (Bisplinghoff, Ashley and Halfman, 1955):

$$C_{L\alpha:l} = \frac{\pi}{2} AR \tag{4.11}$$

Here the aspect ratio AR for a delta wing is defined as AR = l^2/S where *l* is the wing span length and S is the wing area. This definition of the aspect ratio is consistent with the definition given for the rectangular flat plate at the beginning of this section. Eqn. (4.11) was used to approximate $C_{LS\alpha:l}$ which is the lift slope of the rectangular plate model for the sine case with linear theory. This approximation generally agrees well with the more accurate theoretical calculation (Schlichting and Truckenbrodt, 1979, p. 167).

Furthermore, for a small aspect ratio rectangular plate (AR less than 2, say), effects of some additional lift generated by the vortices formed along the sides of the plate become evident and not negligible. This additional lift becomes more significant for both larger angle of attack and smaller aspect ratio. This effect causes nonlinear change of C_L with the angle of attack. Fig. 4.4 shows an example of the change of measured lift coefficient against angle of attack α for a rectangular plate with AR = 0.5 (Gersten, 1961). The lift slope based on the linear theory $C_{L\alpha:l}$ corresponds to the slope at $\alpha = 0°$, which apparently gives lower estimation than the "effective" lift slope. In order to account this nonlinear effect for the small aspect ratio rectangular plate, equivalent lift slopes were evaluated based on the measured lift coefficients. If measured lift coefficients which change nonlinearly with angle of attack are denoted by $C_{L:meas}(\alpha)$, the average lift slope between zero and peak angle of attack α_{peak} is expressed by

$$C_{L\alpha:n} = [C_{L:meas}(\alpha_{peak}) - C_{L:meas}(0)]/\alpha_{peak} = C_{L:meas}(\alpha_{peak})/\alpha_{peak} \quad (4.12)$$

The peak angle of attack was taken as w_{peak}/U, where w_{peak} is a possible maximum of w calculated by assuming Gaussian distribution of w. $C_{L\alpha:n}$ given by eqn. (4.12) is assumed to be the equivalent lift slope considering effects of nonlinear aerodynamic lift. $C_{L:meas}$ was taken and interpolated from the results of Winter (1936) who did extensive measurements of aerodynamic coefficients for small aspect ratio plates.

For the sine case, both lift slopes of $C_{LS\alpha:l}$ and $C_{LS\alpha:n}$ which correspond to eqns. (4.11) and (4.12) respectively are used in the calculation for comparison. Actual lift slopes used in the calculation are given in Table 4.2. For the sine case, the calculation results using $C_{LS\alpha:l}$ will be referred to as "linear" and the results using $C_{LS\alpha:n}$ will be referred to as "nonlinear" in the following.

Table 4.2. Lift Slope Used in the Analysis

Model	Cosine Case	Sine Case		
		"Linear"	"Nonlinear" $C_{LS\alpha:n}$	
	$C_{LC\alpha}$	$C_{LS\alpha:l}$	Grid CI	Grid CIII
AC	5.0	0.13	0.87	0.68
AL	4.2	0.26	1.15	0.96
AM	3.1	0.52	1.46	1.20

For both $C_{LC\alpha}$ and $C_{LS\alpha}$, their values change according to the location of the strip. In the present analysis, constant value of $C_{LC\alpha}$ or $C_{LS\alpha}$ is used for all the strips regardless of the location as mentioned in Section 4.2.2.

As the case of conventional buffeting analysis in Section 2.3.5, the turbulence used in the experiment was assumed to be isotropic, and the expression of the cross-spectrum for the w-component based on the von Kármán spectrum was used in the analysis.

4.3. Results of the Analysis

The results of the calculation based on the proposed modified buffeting analysis is shown in Figs. 4.5 and 4.6 together with the experimental results. The calculation results of both cosine and sine cases are shown in each figure, and for the sine case, the results of both "linear" and "nonlinear" which correspond respectively to the results using $C_{LS\alpha:l}$ and $C_{LS\alpha:n}$ are shown. The ordinate is the r.m.s. vertical deflection at the tip and is made dimensionless by dividing by the model width. For the calculation, only the first mode is considered because the higher mode contribution to the result has been found to be negligibly small.

The abscissa for Figs. 4.5 gives the wind yaw angle β. These figures show the calculation results of Models AC, AL and AM under different flow conditions (Grid CI and CIII) and wind speeds (U = 3.0 and 6.1 m/sec). The comparison with the experimental results at the Carleton wind tunnel shows that

(1) The results of the cosine case at $\beta = 0°$ are generally comparable to the experimental results except for the case in fine grid turbulence (Grid CIII) with wind speed of 6.1 m/sec.

(2) Experimental results at $\beta = 90°$ are found between "nonlinear" and "linear" results of the sine case.

(3) The change of the model response with wind yaw angle is generally well reproduced by the calculation results if the cosine case was chosen for small $|\beta|$ and proper values between "nonlinear" and "linear" of the sine case were chosen for β close to 90°. However in the intermediate yaw angle range where the cosine case and sine case intersect ($50° \le \beta \le 80°$), while the experimental results show a smooth transition, the

calculation results cannot avoid a sharp bend or jump because the transition is made as a matter of the choice between them.

For the comparison among the calculated results, the ratio of the calculated r.m.s. response of "nonlinear" sine case at $\beta = 90°$, $\sigma(90°)$, to the calculated response of cosine case at $\beta = 0°$, $\sigma(0°)$, is defined as $R = \sigma(90°)/\sigma(0°)$, and is used as an index which expresses the tendency of the calculated responses with wind yaw angle in the following. R indicates how large the response with positive yaw angles compared with zero yaw angle case. Values of R are tabulated in Table 4.3.

Table 4.3. Values of $R = \sigma(90°)/\sigma(0°)$

Model	Grid CI		Grid CIII	
	U=3.0 m/s	U=6.1 m/s	U=3.0 m/s	U=6.1 m/s
AC	1.32	2.04	1.68	2.95
AL	1.64	2.55	1.95	3.40
AM	2.24	3.41	2.15	3.47

From the table, it can be seen that

(1) The wider the model width is, the larger R becomes.

(2) R is larger for responses in higher wind speed. This tendency is more enhanced in fine grid turbulence (Grid CIII).

(3) For narrower width models (Models AC and AL), R is larger for responses in fine grid turbulence (Grid CIII). This tendency is stronger for the narrowest model (Model AC), but is not clear for the widest width model (Model AM).

The abscissa in Figs. 4.6 shows the wind speed. These figures show the calculation results of Models AC, AL and AM under different flow conditions (Grid CI and NI or CIII and NIII) and wind yaw angles (β = 0° and 90°). For the case of β = 0° where wind comes normal to the model axis, only the cosine case is to be considered and the calculation is actually the same as the conventional buffeting analysis. For β = 90° case where wind comes from the free end direction, only the sine case is to be considered. The experimental results are also shown in the figures. Both experimental results in the NRCC and Carleton wind tunnel are plotted in the figures. The comparison of the calculation results with the experimental results shows that

(1) Calculation results of the response in the NRCC and Carleton wind tunnels based on the flow characteristics indicated by measured turbulence are not very different from each other but the calculation results for the NRCC wind tunnel are slightly larger than those for the Carleton wind tunnel. However, the experimental results for different wind tunnels sometimes showed quite different responses as stated in Section 3.4.6.

(2) For the response of β = 0° (cosine case), the calculation results generally compare well with the experimental results if the results in a wind tunnel which shows smaller values than those in the other wind tunnel are chosen.

(3) For the response of β = 90° (sine case), the experimental results are between "nonlinear" and "linear" results of the analysis.

Chapter 5. DISCUSSION

5.1. Comparison of the Experimental and Analytical Results

In this chapter, overall discussion will be given on the results of the present research. Because the analysis considered only the vertical bending response, the discussion will be naturally restricted to the vertical motion, except in Section 5.8. The comparison of the experimental and analytical results can be summarized as follows:

(1) For the models with a flat plate cross-section, the most evident tendency of the experimental results is the fact that the wider the model is, the larger the response becomes with positive yaw angles compared with zero yaw angle case (Section 3.4.1). The analytical calculation showed the same tendency (Section 4.3). In other words, the experimental and analytical results agree in this most conspicuous tendency which mostly determines the response characteristics regarding wind yaw angles.

(2) Concerning the wind speed, analytical results showed that the higher the wind speed, the larger the response becomes with positive yaw angles. This tendency was not confirmed by the experimental results with aluminium models, but better observed with steel models (Section 3.4.5). Nevertheless, the tendency observed in the experiment was much weaker than indicated by the analysis.

(3) With narrower models (Models AC and AL), analytical results showed that the response with positive yaw angles should be larger for the fine grid turbulence (Grid CIII) than the coarse grid turbulence (Grid CI). In the experiment, this tendency was not clearly seen for most cases, but a few cases showed agreement with it (Section 3.4.6).

(4) The analytical results showed that there should not be much differences between the

response in the NRCC and Carleton wind tunnels. However, the experimental results sometimes showed quite different tendencies particularly at higher wind speed.

(5) Analytical results for the $\beta = 0°$ case generally showed a good quantitative agreement if they were compared with the smaller experimental response of the two different wind tunnels. For $\beta = 90°$ case, the experimental results come between the "nonlinear" and "linear" sine case calculation results.

(6) In the analysis, the cosine and sine cases were chosen according to the wind yaw angle which characterized the change of response prediction with wind yaw angle. The overall analytical results seem to agree very well with the experimental results, if the choice of the cosine and sine cases are properly made and an appropriate value between "nonlinear" and "linear" boundary for the sine case is taken. However there is an intermediate range ($50° \leq \beta \leq 80°$) where the choice of the cosine or sine cases cannot express the experimental response perfectly as stated in Section 4.3.

(7) In the experiment, the response in the second mode occasionally became dominant especially in fine grid turbulence at the NRCC wind tunnel (Grid NIII) as stated in Section 3.4.9. However, the second mode contribution was always negligible compared with the first mode in the calculation.

Discussion will be given in the following sections, which give possible explanations and means for improvements of the analysis which may reduce the discrepancies stated above.

5.2. Applicability of the Quasi-Steady Approximation

In the analytical calculation conducted in Chapter 4, the aerodynamic admittance was assumed as unity. This means that the quasi-steady approximation was assumed to be completely

applicable for the buffeting force. If the unsteadiness of the flow around the cross-section is to be counted, an appropriate aerodynamic admittance should be used in the analysis as stated in Section 2.3.6. For aerofoils, the aerodynamic admittance between the w-component of velocity and the fluctuating lift force was theoretically derived by Sears (1941), which is often referred to as the Sears function (Fig. 5.1). If this theoretical aerodynamic admittance is introduced in the calculation, the result becomes 15 to 60% less for the cosine case ($\beta = 0°$) and 40 to 75% less for the sine case ($\beta = 90°$). Examples of the results using the Sears function are compared with the previous results in Figs. 5.2. Because the Sears function is rapidly decreasing from unity with increase of reduced frequency fB/U, the reduction of the response prediction is generally larger for the sine case where the chord length B is taken as the model span length l divided by sin β, which is larger than B for the cosine case which is model width b divided by cos β.

For two-dimensional cases, the validity of the Sears function is well accepted. Also the fluctuating lift of aerofoils under a flow with two-dimensionally fluctuating w-component experimentally supports it (for example, Jancauskas and Melbourne, 1986). However, if the Sears function is to be used in the present analysis, the calculation results sometimes give considerably lower prediction than the experimental results as stated above.

5.3. Applicability of the Strip Theory Approximation

In the analysis, the strip theory approximation was used, where the aerodynamic force acting on a span-wise section or a "strip" are assumed to be determined by the two-dimensional flow that has the same angle of attack at the strip. In other words, the effects of the flow around the neighbour strips are neglected with this approximation.

The strip theory assumption is usually thought to be applicable if the body under consideration is slender enough that the flow over the body can be assumed to be two-dimensional. However, if the approaching flow is turbulent, the flow over the body is three-

dimensional because turbulent flow itself has a three-dimensional structure. The aerodynamic force acting on a strip is not determined solely by the flow around the strip, but the flow over neighbour span-wise locations also effects the aerodynamic force on the strip. For example, the measurement of the fluctuating lift force on a narrow section (which can be thought as a strip) of an aerofoil in a turbulent flow shows the considerable effect of the flow over the neighbour sections, and actually the flow over the neighbour sections generates the lift force on the strip (Lamson, 1948). The angles of attack at the neighbour sections are less correlated to the one at the strip, and the lift forces acting on the strip generated by the flow over neighbour sections are also less correlated. The correlation becomes less and less if the flow considered is further and further away from the strip. Lamson put two plates parallel to the mean flow direction very close to the strip in order to separate the effect of the flow outside of the plate to the lift forces on the strip and obtain nearly two-dimensional flow around the strip (Fig. 5.3). In that case, the measured aerodynamic admittance became close to the Sears function which is a theoretical aerodynamic admittance for two-dimensional flow. However, when the plates were removed, the measured aerodynamic admittance became much lower, or the magnitude of the fluctuating lift on the strip became smaller. This is attributed to less correlation of the lift force generated by flow over the neighbour sections. Thus, this experimental result clearly shows that the flow over the neighbour sections actually generates the aerodynamic force on the strip, and if the body is in turbulent flow, the aerodynamic force acting on the strip is quite different from those in two-dimensional flow having same angle of attack at the strip even if the body has two-dimensional shape with infinite span length.

Therefore the applicability of the strip theory approximation is questionable in turbulent flow. However, the buffeting analysis based on the strip theory approximation may still give a reasonable prediction, because while the actual amplitude of the fluctuating aerodynamic force is smaller than the estimation by the strip theory approximation, the actual correlation of the aerodynamic force acting on different strips should be larger than the correlation of the fluctuating wind velocity component which is assumed to be the correlation of the aerodynamic force with the strip theory approximation. For example in eqn. 2.24, the term $1/2 \cdot \rho \cdot B \cdot U \cdot dC_l/d\alpha$ should be smaller in the actual case because of the effect from the less correlated aerodynamic

force produced by the flow over neighbour sections. On the other hand, the term representing correlation of the lift force should be larger than $S_{ww}(y,y',f)$, and thus the overall prediction of $S_{qr}(f)$ could be a fair approximation. Jackson et al. (1973) compared the analytical results based on the strip theory approximation and more accurate three-dimensional theory for an infinite aerofoil in turbulent flow. The accuracy of the three-dimensional theory was confirmed by an experiment. The comparison showed that the results based on the strip theory approximation give somewhat larger values than those by the three-dimensional theory. The comparison was made for the case of $L_x^v/B = 0.41$, but they concluded the discrepancy would reduce for larger L_x^v/B.

5.4. Evaluation of Turbulence Characteristics

In the analysis, the widely used von Kármán spectrum of turbulence was assumed. Then the expression of eqn. (2.27) is obtained for the power spectrum of w-component. If this power spectrum is plotted in dimensionless form $fS_w(f)/\sigma_w^2$ as in Figs. 3.5, the spectrum has a shape as shown in Fig. 5.4 which gives its peak at $fL_z^w/U = 0.212$. General characteristics of turbulence can be described as follows (Hinze, 1975, p. 221): Eddies having wave numbers ($2\pi f/U$) around this peak value correspond to so-called energy-containing eddies which consist the main part of the kinetic energy of turbulence. The larger eddies with smaller wave numbers than the peak produce smaller and smaller eddies through inertial interaction, thereby transferring energy to the smaller eddies. These larger eddies are the ones initially generated by mechanical disturbances such as grids, and thus their characteristics are dependent on the conditions of formation. On the other hand, eddies having larger wave numbers than energy-containing eddies are generated by the transferred energy from larger eddies. This larger wave number range is called the universal equilibrium range, because there is a continuous energy flux from larger eddies to smaller ones with small dissipation of the energy by viscosity, thus a statistical equilibrium exists. The characteristics of eddies in this range can be assumed to depend only on the energy dissipation and kinematic viscosity of the fluid. This state of equilibrium is called "universal" because the state is independent of the external conditions and is always close to isotropic at least locally even if global structure of the flow is not isotropic.

For some case of bridge buffeting, the natural frequencies of bridge are in the frequency range of universal equilibrium. Because the eddies in this equilibrium range are independent of the conditions of their formation, their characteristics are stable and power spectra in this frequency range generally agree well with theoretical expressions such as the von Kármán spectra. On the other hand, lower natural frequencies of bridge can be in the range of energy-containing eddies because of a smaller scale of turbulence or a higher wind speed. For the present experiment, due to the restriction of the model manufacturability and the availability of the wind speed range in wind tunnels, the natural frequencies of the models were generally less than $0.212 \cdot U/L_z^w$, which means the eddies that excite the model are subjected to the external conditions which generate turbulence and consequently are not very stable. Actually, there is a considerable difference in the slope of the curve at the left of the spectral peak between Grid NIII and CIII (Fig. 3.5(c) and (e)). This is thought to be a reason for the difference in observed model response at different wind tunnels as stated in Section 5.1 (4) and the second mode response appearance which was observed only at the NRCC wind tunnel (Section 5.1 (7)). The applicability of the von Kármán spectrum for this particular analysis is therefore questionable. However, the measured spectra are not very reliable in the lower frequency range because there are not many data points. No definite data being available for the spectra in the lower frequency range, the von Kármán spectrum was used in the analysis which at least gave a standard measure of the response. Another advantage of using the von Kármán spectrum is that a theoretical expression of the cross-spectrum based on it is available, which can be used consistently with the von Kármán spectrum.

As can be seen from Section 3.3, the turbulence used in the experiments is not isotropic. As stated above, the eddies that excited the models could have been affected by this non-isotropy because they are in lower-than-the-peak frequency range. Turbulence characteristics used in the analysis are thus questionable because they are derived by assuming isotropy. Perhaps more turbulence characteristics including the cross-spectra should have been obtained experimentally and used in the analysis. However, it would require a long averaging time in order to obtain reliable data for lower frequency region. A further measurement was not attempted in this study.

Overall, uncertainty of the turbulence characteristics seems to have made the quantitative comparison of the experimental and analytical results more difficult. However, a refinement of the analysis in this standpoint is not essential to achieve the main objective of the present study which is to clarify the effect of wind yaw angle on the buffeting response.

5.5. Estimation of Sine Case Response

The calculation results of "nonlinear" sine case gave generally higher values than experimental results as stated in Section 5.1 (5). If "nonlinear" sine case results are seen in relation to cosine case results in Figs. 4.5, the response of sine case also tends to be higher than the experimental results. Discussions on this point will be given in this section.

One uncertain point in the calculation of "nonlinear" sine case is the evaluation of $C_{LS\alpha:n}$ which is an equivalent lift slope considering the nonlinearity of the lift force and defined as an average lift slope between zero and peak angle of attack as explained in Section 4.2.7. Another reasonable way to evaluate the equivalent lift slope $C_{LS\alpha:n}$ is to take the slope of measured lift coefficient at representative angle of attack corresponding to σ_w/U, for example. This way of evaluation was also tried and it was found that it gave similar value as $C_{LS\alpha:n}$ used in the calculation. Because two ways of evaluation gave similar results, the evaluation of $C_{LS\alpha:n}$ was considered to be a good approximation.

Another point to be considered is the aerodynamic admittance which was assumed to be unity in the calculation. As discussed in Section 5.2, an aerodynamic admittance such as the Sears function may be used in the analysis, and in that case, the reduction of the calculation results will be larger for sine case than for cosine case. Therefore, the introduction of the aerodynamic admittance reduces the difference of the response with wind yaw angle between experiment and analysis.

Also in the analysis, the distribution of the lift force along a strip was assumed to have

the shape shown in Fig. 4.3 and to be unchanged throughout. However, for small aspect ratio plates which correspond to the sine case, the distribution of lift force could be considerably different. For this case, the additional lift force is generated by the vortices formed along the sides of the plate, as stated in Section 4.2.7. The position of the resultant lift force under this additional lift force was evaluated by experimental lift and moment coefficients collected by Gersten (1961). It was found that the resultant lift force seems to work further back on the section than the case of Fig. 4.3 where the resultant lift applies at the quarter-chord distance from the leading edge. Therefore, for the $\beta = 90°$ case, the first mode generalized force acting on the model is actually smaller than the calculated using the lift distribution shown in Fig. 4.3. In other words, the consideration of the actual lift force distribution for the sine case will reduce the predicted response, thus the agreement will be improved. However, since there are no data for the lift distribution for small aspect ratio plates available, the distribution was assumed to be unchanged throughout the analysis. Furthermore, strictly speaking, the lift force distribution changes according to the span-wise location of the section and the angle of attack. However, it is too complicated to consider all of these effects in this study since its objective is to find out the basic characteristics of buffeting response in yawed wind.

In the experiment, the characteristics of the flow changed depending on the distance from the grids. However in the analysis, flow characteristics at the model support location were used for the calculation, and the possible variation of the flow characteristics was not considered. The variation of the flow characteristics could influence the results significantly particularly when $|\beta|$ is close to 90° which corresponds to the sine case, because the model span is almost parallel to the flow direction and thus the flow characteristics should vary most significantly along the model span. If the location considered is closer to the grids, turbulence intensities become larger and scales of turbulence become smaller, as can be seen from Table 3.3. The larger turbulence intensity causes a larger response whereas the smaller scale of turbulence causes a smaller response. Therefore, the variation of two characteristics has opposite effects on the response amplitude and they may somewhat cancel each other. Response prediction for the $\beta = 90°$ case by the calculation of the sine case using the flow characteristics at the model free end location showed a slightly larger value than that using the flow characteristics at the model support, but

the wider the model is, the smaller the difference becomes. For Model AM, the predicted responses using the different flow characteristics become almost the same.

5.6. Choice of Cosine and Sine Case for the Intermediate Range of Yaw Angle

As stated in Section 5.1 (6), there was a range where neither cosine case nor sine case could reproduce the experimental results with varied wind yaw angles very well. This is an intermediate range in which cosine and sine cases intersect. While the experimental results showed smooth transition in this yaw angle range, the analytical results could not show the same tendency because it was assumed to be a matter of the choice between cosine and sine cases.

In this intermediate range, an attempt can be made to consider the contribution of both cosine and sine cases together. In order to do so, a possible procedure is as follows: First, the wind velocity is resolved into two components which correspond to effective wind velocity for cosine and sine cases (U_{eC} and U_{eS}). When the wind velocity is resolved, the fluctuating velocity component w is also to be resolved into two components w_C and w_S, each of which corresponds to cosine and sine cases. In order to satisfy the geometrical condition, the relation

$$w_C + w_S = w \tag{5.1}$$

must hold. Then, the contribution of cosine and sine cases should be calculated based on the corresponding resolved wind velocity components. If the contribution from cosine and sine cases can be assumed to be linearly superposed, a simple addition of the two contributions would give the overall response. Furthermore, fluctuating velocity component w and r.m.s. bending response have a linear relationship as can be seen from eqns. (2.24), (2.27) and (2.39). Therefore, the overall r.m.s. response σ can be expressed as

$$\sigma = K_C w_C + K_S w_S \tag{5.2}$$

where K_C and K_S are functions of the flow and model characteristics, but under a given condition they can be considered as constants. Now, the "best" resolution of the fluctuating velocity component w into w_C and w_S that minimize the discrepancy stated in Section 5.1 (6) needs to be considered. However, if eqn. (5.2) is considered under the condition of eqn. (5.1), it can be seen that the overall r.m.s. response σ can only take the values between $K_C \cdot w$ and $K_S \cdot w$, because w_C and w_S cannot take the opposite sign to w. Since $K_C \cdot w$ and $K_S \cdot w$ correspond to the cosine and sine case respectively, the most likely overall response is merely the larger result of cosine or sine cases.

It may be natural to assume that the contributions from cosine and sine cases cannot be linearly superposed, because there are always flow separations along the sides of the model when β is not 0°. Then, instead of eqn. (5.2), a nonlinear relationship such as

$$\sigma^2 = (K_C w_C)^2 + (K_S w_S)^2 \tag{5.3}$$

should hold. With this kind of relationship, the overall response σ can have more similar results to the experimental results. However, there is not enough knowledge of what kind of nonlinear relationship actually exists among the overall response, cosine and sine cases. Hence, in the present analysis, the results of cosine and sine cases are shown as they are.

5.7. Extent of Flow Field Regulation

Another factor which can be considered is the extent of flow field regulation caused by the model vibration. The movement of the model causes a periodical fluctuation over the flow field covering the model. Because this fluctuation is caused by the model movement, the extent of the regularity of the fluctuation should be affected by the amplitude and mode shape of the model vibration. If this regularity is strong, the correlation of the aerodynamic forces acting on the span-wise model sections would become higher, and the model response would become larger. Concerning the mode shape, one could expect that this flow regulation effect is larger when the mode shape is uniform than when it is not uniform. Also one could expect that the

movement of the leading edge plays the principal role on the regulation effect.

When the wind yaw angle is changed, the leading edge of the model against the wind also changes its position. For a cantilever model, the mode shape of the leading edge is uniform for the free end; non-uniform for the sides of the model; and zero for the fixed end. Together with the fact that the model amplitude is usually largest at the free end, the extent of the flow field regulation per unit length of the leading edge should be largest when the wind is coming from the free end direction. This effect may be estimated by the product of the effective wind speed (U_{ec} for the sides and U_{es} for the free end) and the integration of the amplitude along the leading edge. If the overall extent of the flow regulation is assumed to be the addition of the contribution from the possible two leading edges, this effect is expected to become largest under the wind with $\beta = 40°$ for model AM, for example. Therefore, this effect might explain some of the discrepancy between the experimental and the analytical results in the intermediate range of yaw angle. However, because there is no certain way to evaluate this effect, it was not considered in the present analysis.

5.8. Further Discussions

So far in this chapter, discussions were restricted to the vertical bending response of models with flat plate cross-sections. In the actual bridge buffeting, some other conditions may also need to be considered. Torsional response which may even be coupled with lateral motion and also the response with aerodynamically bluff cross-sections are probably the important aspects to be considered.

Both of these aspects were examined in the experiment to some extent, however the theoretical approach for these cases was not tried in the present study. One reason is the lack of reliable aerodynamic damping data for these cases. The aerodynamic damping is a dominant factor in prediction of the response, but a theoretical evaluation of the aerodynamic damping under yawed wind is very difficult. Thus a semi-experimental approach was used in the modified

buffeting analysis in Chapter 4. For torsional response, measurement of the aerodynamic damping is also difficult, and therefore reliable response predictions are very hard to obtain. For vertical motion, the aerodynamic damping was approximated to be proportional to cos β. However, probably this is not the case for torsional motions. For vertical motions, movement of the cross-sections sliced out in the wind direction is quite different with different yaw angles, namely, a pure translational motion with $\beta = 0°$ and a motion having the mode shape with $\beta = 90°$. Perhaps this change of characteristics of motion made a large change of aerodynamic damping almost proportional to cos β. On the other hand, the movement of the cross-section is not so different for torsional motions with different yaw angles. Therefore, the change of the aerodynamic damping might not be as large as the case of vertical motions. This implies that the torsional response for large yaw angle is smaller than the vertical bending response, if the relative value to zero yaw angle case is compared. This agrees with the observations in Section 3.4.8. Also, an uncertainty of the aerodynamic damping is another reason for the discrepancy between experimental and theoretical results on the appearance of the second mode, because aerodynamic damping for the first mode was assumed to be the same for the second mode in the analysis.

For bluff cross-section models, the aerodynamic damping was experimentally measured. However, values of the aerodynamic damping became very small because of the relative massiveness of the models, and the result of the measurement is not too reliable. Even if reliable aerodynamic damping is obtained, there is another difficulty for the analysis of bluff cross-section models because the aerodynamic force is not known. Nevertheless, if the aerodynamic force coefficients and the aerodynamic force distribution for both $\beta = 0°$ and 90° are experimentally obtained, it is possible to apply the procedure of the modified buffeting analysis in Chapter 4. For bluff cross-section models, flow separations are always expected, and thus the assumption of taking effective wind velocity as the normal component to the corresponding leading edge may not hold as the case of the flat plate models, though the same assumption can be still the first approximation.

Also for bluff cross-section models, the applicability of the linear summation of self-

excited and buffeting aerodynamic forces still remains to be examined. For the buffeting response of bluff cross-section models, another interesting point to be considered is the inclusion of the random aerodynamic force due to the wake behind the cross-section. As Kumarasena, Ehsan and Scanlan (1989) pointed out, a bluff body forms a wake behind it and the wake would generate random aerodynamic force on the body to some extent. However, this is a highly nonlinear phenomenon including the interaction of the wake with turbulence in the oncoming flow and the unsteady flow due to body motion, and further studies are definitely required.

The modified buffeting analysis proposed in the present study is by no means perfect. The direction for possible improvements have been discussed in this chapter. However, it is either difficult or it makes the result obscure if these aspects are included in the analysis because many uncertain points still exist. The objective of the present study is to clarify the effect of wind yaw angle on the buffeting response. In order to achieve this objective, the important thing is to examine the fundamental factors at first. Thus, uncertain factors are avoided, and reasonable and well accepted assumptions only are used in the present analysis. Nevertheless, by considering these fundamental aspects, the principal effects of wind yaw angle are well explained. Because the procedure of the analysis is straightforward, the interpretation of the result is comprehensible. The objective of the study is considered to be achieved by the proposed modified buffeting analysis.

Chapter 6. CONCLUSIONS

6.1. Conclusions

The understanding of the bridge behaviour under wind with yaw angle is necessary if the bridge response is considered under the actual wind condition because the wind direction is almost constantly changing. However, although the studies on the wind-induced bridge response have accumulated considerable amount of knowledge on the subject, the effect of the wind directionality has not been studied very much. This is because the wind normal to the bridge axis has been thought to be the most dangerous wind direction which causes the largest bridge response. Nevertheless, this is just a hypothetical critical case and the wind directionality should be considered in a more realistic and reasonable design. Furthermore, the wind normal to the bridge may not be the most dangerous for structures that have unsupported free ends. Examples of these structures are the cable-stayed bridges under construction using the balanced cantilever method and the cantilevered roof structures. Some previous experimental studies on cable-stayed bridges under construction have shown that the response under yawed wind does not decrease as expected. Nevertheless, not much attention has been given to this phenomenon and more study has been required to explain it.

With the background stated above, the effect of wind yaw angle on the buffeting response of simple cantilever models in turbulent flow was extensively examined in the present study. The models can be thought as a very simple version of a cable-stayed bridge under construction. The following findings were obtained from the experimental study.

For the flat plate cross-section models,

(1) The change of the vertical bending response magnitude with various wind yaw angles was very much affected by the model width. The wider the model is, the larger the response

becomes under the wind from the free end direction. For wider models, even larger response was observed under wind from the free end direction than the wind normal to the model axis.

(2) The simple response prediction under yawed wind by taking response as proportional to cos β, where β is the wind yaw angle taken from normal to the model axis, generally underestimated the actual model response particularly for the wind from the free end direction. For the torsional response, this simple prediction gave relatively close values to the experimental results compared with the case of vertical bending response.

(3) The turbulence characteristics and the wind speed had some effects on the response but they were not as conspicuous or consistent as the effect of the model width.

(4) The aerodynamic damping of the first bending mode was found to be very sensitive to the wind direction. Its variation was almost proportional to cos β.

For the thicker cross-section models,

(5) The vertical bending response under wind from the free end direction became slightly smaller for the thicker models. The thicker models having depth to width ratio more than 1/4 showed peculiar response against varied wind yaw angles.

In order to explain these findings, the conventional buffeting analysis was modified so that it can predict the response under yawed wind. This modified buffeting analysis was applied to the vertical bending response of the flat plate cross-section cantilever models. The modification was made in the following ways.

(1) The mean wind velocity component normal to the leading edge of the model was taken as the effective wind velocity. Corresponding to the choice of the leading edge under

yawed wind, the calculation was separately done for the cosine and sine cases.

(2) The strip theory approximation was adopted where the strips were taken parallel to the actual wind direction. For the sine case, the generalized buffeting force acting on a strip was calculated by considering the mode shape of the strip and the buffeting force distribution.

(3) The buffeting force was calculated assuming the quasi-steady approximation. The lift force coefficient of the finite plate having the aspect ratio corresponding to the cosine or sine case was used for each case. For the sine case, the effect of the nonlinear change of the lift force with the angle of attack was included in the analysis.

(4) Based on the experiment, the variation of the aerodynamic damping with wind yaw angle was approximated to be proportional to cos β.

Although there were some discrepancies between the analytical and experimental results, the overall agreement of the results is satisfactory because the analysis can reproduce the response characteristics such as the conspicuous effect by the model width. The quantitative agreement may be improved if more clearly defined turbulence is used in the experiment, but this is not essential to the understanding for the effect of the wind yaw angle.

6.2. Recommendations for Further Study

Application of the modified buffeting analysis to a cable-stayed bridge under construction is a immediate extension of the current study. If the bridge cross-section is aerodynamically similar to a flat plate, the analysis can be directly applied by considering the mode shapes of the structure. Consideration of non-isotropic turbulence is another possible extension for the analysis. Because the atmospheric turbulence is non-isotropic, it would be useful to include it in the

analysis. In that case, the imaginary part of the cross-spectra of the turbulence may also play an important role on the response.

It would be interesting if the modified buffeting analysis is applied to the torsional response and the response of a structure with aerodynamically bluff cross-section under yawed wind. The same procedure can be also used in these cases, but the evaluation of the aerodynamic damping under yawed wind will be difficult. Further study for the determination of the aerodynamic damping under yawed wind is needed so that it can be obtained without conducting a full model experiment. The response prediction for the intermediate yaw angle range where neither the cosine nor sine case predict the response very well is also an interesting subject. For the practical purpose, however, the prediction of the response in this range may be made by connecting cosine and sine cases with a smooth curve.

Further research is still needed for the conventional buffeting analysis itself on the subjects such as the validity of the strip theory approximation, the interaction of the self-excited and buffeting forces and the effect of the wake behind the bluff bridge section. The modified buffeting analysis does not give any answers to these subjects, but it extends the limitation of the conventional buffeting analysis by considering the response of cantilever structures under yawed wind for the first time. This must be another step for a more realistic design which takes account of the wind directionality.

REFERENCES

Arzoumanidis, S.G., Ogawa, K. and Sakoda, H., "Wind Tunnel Testing of the Karnali River Bridge", Proc. ASCE Structures Congress 1989, San Francisco, pp. 59-72, August 1989.

Barnard, R.H., "Wind Loads on Cantilevered Roof Structures", J. Wind Engineering and Industrial Aerodynamics, Vol. 8, Nos. 1-2, pp. 21-30, July 1981.

Blake, W.K., Mechanics of Flow-Induced Sound and Vibration, Vol. II: Complex Flow-Structure Interactions, Academic Press, Orlando, Florida, 1986.

Bradshaw, P., An Introduction to Turbulence and Its Measurement, Pergamon Press, Oxford, U.K., 1971.

Bisplinghoff, R.L., Ashley, H. and Halfman, R.L., Aeroelasticity, Addison-Wesley, Cambridge, Massachusetts, 1955.

Cook, N.J., "Reduction of Wind Loads on a Grandstand Roof", J. Wind Engineering and Industrial Aerodynamics, Vol. 10, No. 3, pp. 373-380, December 1982.

Davenport, A.G., "The Response of Slender Line-Like Structures to a Gusty Wind", Proc. ICE, Vol. 23, pp. 389-408, 1962a.

Davenport, A.G., "Buffeting of a Suspension Bridge by Storm Winds", J. Structural Division, Proc. ASCE Vol. 88, No. ST3, pp. 233-268, June 1962b.

Davenport, A.G., "The Use of Taut Strip Models in the Prediction of the Response of Long Span Bridges to Turbulent Wind", Proc. IUTAM/IAHR Symp. on Flow-Induced Structural Vibrations, Karlsluhe, Germany, August 1972, Flow-Induced Structural Vibrations, E. Naudascher, ed., Springer-Verlag, Berlin, pp. 373-381, 1974.

Davenport, A.G., "The Prediction of Risk under Wind Loading", Proc. 2nd Int. Conf. on Structural Safety and Reliability, Munich, Germany, pp. 511-538, September 1977.

Davenport, A.G., Isyumov, N., Fader, D.J. and Bowen, C.F.P., "A Study of Wind Action on a Suspension Bridge During Erection and on Completion: The Narrows Bridge", Halifax, Nova Scotia, Canada, BLWT-3-69, University of Western Ontario, May 1969a.

Davenport, A.G., Isyumov, N., Fader, D.J. and Bowen, P., "An Aeroelastic Study of the Northumberland Straits Bridge -- Cantilevered Concrete Design", BLWT-4-69, University of Western Ontario, May 1969b.

Davenport, A.G., Isyumov, N., Rothman, H. and Tanaka, H., "Wind Induced Response of

Suspension Bridges - Wind Tunnel Model and Full Scale Observations", Proc. 5th Int. Conf. on Wind Engineering, Fort Collins, Colorado, July 1979, J. E. Cermak, ed., Pergamon Press, Oxford, U.K., Vol. 2, pp. 807-824, 1980.

Davenport, A.G., Isyumov, N. and Tanaka, H., "A Study of Wind Action for the Bronx-Whitestone Suspension Bridge, New York, N.Y.", BLWT-SS3-76, University of Western Ontario, June 1976.

Davenport, A.G. and King, J.P.C., "The Incorporation of Dynamic Wind Loads into the Design Specifications for Long Span Bridges", Proc. ASCE Fall Convention & Structure Congress, New Orleans, Louisiana, pp. 1-30, October 1982.

Davenport, A.G. and King, J.P.C., "The Influence of Topography on the Dynamic Wind Loading of Long Span Bridges", J. Wind Engineering and Industrial Aerodynamics, Vol. 36, Nos. 1-3, Part 2, pp. 1373-1382, October 1990.

Dowell, E.H. (ed.), Curtiss, H.C. Jr., Scanlan, R.H. and Sisto, F., A Modern Course in Aeroelasticity, 2nd Ed., Kluwer Academic publishers, Netherlands, 1989.

Eringen, A.C., "Response of Beams and Plates to Random Loads", J. Applied Mechanics, Vol 20, pp. 46-52, March 1957.

ESDU, "Lift-Curve Slope and Aerodynamic Centre Position of Wings in Invicid Subsonic Flow", Engineering Sciences Data, Item No. 70011, Engineering Sciences Data Unit, London, July 1977.

Farquharson, F.B. (ed.), Vincent, G.S., von Kármán, Th. and Dunn, L.G., "Aerodynamic Stability of Suspension Bridges", University of Washington Engineering Experiment Station Bulletin No.116, Parts I-V, Seattle, 1950-54.

Ferraro, V. and Irwin, P.A., "Recent Experiences with Aeroelastic Wind Tunnel Studies of Cable-Stayed Bridges", Proc. Canada-Japan Workshop on Bridge Aerodynamics, National Research Council Canada, National Aeronautics Establishment, Ottawa, pp. 227-238, September 1989.

Gamble, S.L. and Irwin, P.A., "The Action of Wind on a Cable Stayed Bridge During Construction", Proc. 5th US National Conf. on Wind Engineering, Lubbock, Texas, pp. 4A 33-39, November 1985.

Gersten, K., "Calculation of Non-Linear Aerodynamic Stability Derivatives of Aeroplanes", Advisory Group for Aeronautical Research and Development, Report 342, April 1961. Also published as, "Nichtlineare Tragflächentheorie insbesondere für Tragflügel mit kleinem Seitenverhältnis", Ingenieur-Archiv, Vol. 30, pp. 431-452, 1961, which seems to have correct numbers for figures.

Harris, R.I., "The Nature of the Wind", Proc. Seminar held at ICE, London, June 1970, The

Modern Design of Wind-Sensitive Structures, Construction Industry Research and Information Association, London, pp. 29-55, 1971.

Hinze, J.O., Turbulence, 2nd ed, McGraw-Hill, New York, 1975.

Holmes, J.D., "Prediction of the Response of a Cable Stayed Bridge to Turbulence", Proc. 4th International Conf. on Wind Effects on Buildings and Structures, Heathrow, U.K., September 1975, K. J. Eaton, ed., Cambridge University Press, Cambridge, U.K., pp. 187-197, 1977.

Horlock, J.H., "Fluctuating Lift Forces on Aerofoils Moving Through Transverse and Chordwise Gusts", Trans. ASME, Vol. 90, Ser. D, No.4, pp. 494-500, December 1968.

Irwin, H.P.A.H., "Wind Tunnel and Analytical Investigations of the Response of Lions' Gate Bridge to a Turbulent Wind", National Research Council Canada, NAE-LTR-LA-210, June 1977.

Irwin, H.P.A.H., "Design and Use of Spires for Natural Wind Simulation", National Research Council Canada, NAE-LTR-LA-233, August 1979.

Irwin, P.A., "Wind Buffeting of Cable-Stayed Bridge During Construction", Proc. ASCE Structures Congress 1987, Orlando, Florida, pp. 164-177, August 1987a.

Irwin, P.A., "Prediction and Control of the Wind Response of Long-Span Bridges with Plate Girder Decks", Proc. ASCE Structure Congress 1987, Orlando, Florida, pp. 268-280, August 1987b.

Irwin, P.A. and Gamble, S.L., "Wind tunnel Tests for the Annacis Island Bridge, Vancouver, British Columbia", Report No.48515031 submitted to CBA Buckland and Taylor, Morrison Hershfield Ltd., December 1985.

Irwin, H.P.A.H. and Schuyler, G.D., "Experiments on a Full Aeroelastic Model of Lions' Gate Bridge in Smooth and Turbulent Flow", National Research Council Canada, NAE-LTR-LA-206, October 1977.

Jackson, R., Graham, J.M.R. and Maull, D.J., "The Lift on a Wing in a Turbulent Flow", The Aeronautical Quartery, Vol. 24, Part 3., pp. 155-166, August 1973.

Jacobs, von W., "Experimentelle Untersuchungen am schiebenden Flügel", Ingenieur-Archiv, Vol. 20, pp. 418-426, 1952.

Jancauskas, E.D. and Melbourne, W.H., "The Aerodynamic Admittance of Two-Dimensional Rectangular Section Cylinders in Smooth Flow", J. Wind Engineering and Industrial Aerodynamics, Vol. 23, Nos. 1-3, pp. 395-408, July 1986.

Khalil, M.S. and Bush, L.H., "Vancouver's Skytrain Cable-Stayed Bridge -- Dynamic Behaviour",

Proc. ASCE Structure Congress 1987, Orlando, Florida, pp. 357-372, August 1987.

Kirkwood, K.F.R., "Aspects of Aerodynamics of Cable-Stayed Bridge Deck During Construction", Master of Science Thesis, University of Western Ontario, November, 1991.

Kirkwood, K. and Davenport, A.G., "Aerodynamics of Cable-Stayed Bridge Decks During Construction", Proc. 1991 CSCE Annual Conf., Vol. 2, pp. 82-91, May 1991.

Kubo, Y., Watanabe, A., Kuga, N., Tokuyama, S., Kato, K. and Morimoto, M., "Field Observation of Aerodynamic Responses of a PC Cable-Stayed Bridge During Its Erection", Proc. ASCE Structures Congress 1989, San Francisco, pp. 628-637, August 1989.

Küchemann, D., The Aerodynamic Design of Aircraft, Pergamon Press, Oxford, U.K., 1978.

Kumarasena, T., Ehsan, F. and Scanlan, R.H., "Buffeting Response Computations for an Existing Bridge", Proc. Canada-Japan Workshop on Bridge Aerodynamics, National Research Council Canada, National Aeronautics Establishment, Ottawa, pp. 217-226, September 1989.

Lamson, P., "Measurements of Lift Fluctuations due to Turbulence", National Advisory Committee for Aeronautics, Technical Note 3880, March 1957.

Lepage, M.F. and Irwin, P.A., "A Technique for Combining Historical Wind Data with Wind Tunnel Tests to Predict Extreme Wind Loads", Proc. 5th US National Conf. on Wind Engineering, Lubbock, Texas, pp. 2B 71-78, November 1985.

Liepmann, H.W., "On the Application of Statistical Concepts to the Buffeting Problem", J. Aeronautical Sciences, Vol. 19, No. 12, pp. 793-800 and 822, December 1952.

Matsumoto, M. and Prenninger, P.H.W., "Consideration of Higher Vortex-Exited Modes in Reliability Analyses of Bridge Structures", J. Wind Engineering and Industrial Aerodynamics, Vol. 32, Nos. 1-2, pp. 171-180, September 1989.

McCormick, B.W., Aerodynamics, Aeronautics, and Flight Mechanics, John Wiley & Sons, New York, p. 281, 1979.

Melbourne, W.H., "Cross-Wind Response of Structures to Wind action", Proc. 4th Int. Conf. on Wind Effects on Buildings and Structures, Heathrow, U.K., September 1975, K. J. Eaton, ed., Cambridge University Press, Cambridge, U.K., pp. 343-358, 1977.

Melbourne, W.H., "Model and Full Scale Response to Wind Action of the Cable Stayed Box Girder West Gate Bridge", Proc. IAHR/IUTAM Symp. on Practical Experiences with Flow-Induced Vibrations, Karlsruhe, Germany, September 1979, Practical Experiences with Flow-Induced Vibrations, E. Naudascher and D. Rockwell, eds., Springer-Verlag, Berlin, pp. 625-632, 1980.

Melbourne, W.H. and Cheung, J.C.K., "Reducing the Wind Loading on Large Cantilevered Roofs", Proc. 7th Int. Conf. on Wind Engineering, Part 1, Aachen, Germany, July 1987, J. Wind Engineering and Industrial Aerodynamics, Vol. 28, Nos. 1-3, pp.401-410, August 1988.

Okauchi, I., Ito, M. and Miyata, T., Wind Resistant Structures (Taifu-Kozo, in Japanese), Maruzen, Tokyo, p. 177, May 1977.

Roberts, J.B. and Surry, D., "Coherence of Grid-Generated Turbulence", J. Engineering Mechanics Division, Proc. ASCE, Vol. 99, No. EM6, pp. 1227-1245, December 1973.

Scanlan, R.H., "The Action of Flexible Bridges under Wind, II: Buffeting Theory", J. Sound and Vibration, Vol. 60, No. 2, pp.201-211, 1978.

Scanlan, R.H., "On The State of Stability Considerations for Suspended-Span Bridges under Wind", Proc. Symp. on Practical Experiences with Flow-Induced Vibrations, IAHR/IUTAM, Karlsruhe, Germany, September 1979, Practical Experiences with Flow-Induced Vibrations, E. Naudascher and D. Rockwell, eds., Springer-Verlag, Berlin, pp. 595-618, 1980.

Scanlan, R.H., "Aeroelastic Simulation of Bridges", J. Structural Engineering, Vol. 109, No. 12, pp. 2829-2837, December 1983.

Scanlan, R.H., "Role of Indicial Functions in Buffeting Analysis of Bridges", J. Structural Engineering, Vol. 110, No. 7, ASCE, pp. 1433-1446, July 1984.

Scanlan, R.H., "Interpreting Aeroelastic Models of Cable-Stayed Bridges", J. Engineering Mechanics, Vol. 113, No. 4, ASCE, pp. 555-575, April 1987.

Scanlan, R.H. and Gade, R.H., "Motion of Suspended Bridge Spans under Gusty Wind", J. Structural Division, Proc. ASCE, Vol. 103, No. ST9, pp. 1867-1883, September 1977.

Scanlan, R.H. and Tomko, J.J., "Airfoil and Bridge Deck Flutter Derivatives", J. Engineering Mechanics Division, Proc. ASCE, Vol. 97, No. EM6, pp. 1717-1737, December 1971.

Schlichting, H. and Truckenbrodt, E., Aerodynamics of the Airplane, McGraw-Hill, New York, 1979.

Scruton, C., "Experiments on the Aerodynamic Stability of Suspension Bridges", National Physical Laboratory, NPL Aero Report 185 and 199, 1951.

Scruton, C., "An Experimental Investigation of the Aerodynamic Stability of Suspension Bridges with special reference to the Proposed Severn Bridge", Proc. ICE, Vol. 1, Part 1, pp. 189-222, 1952.

Sears, W.R., "Some Aspects of Non-Stationary Airfoil Theory and Its Practical Application", J.

Aeronautical Sciences, Vol. 8, No.3, pp. 104-108, January 1941.

Simiu, E. and Scanlan, R.H., Wind Effects on Structures, 2nd. Ed., John Wiley & Sons, New York, 1985.

Soo, H.S.-W. and Scanlan, R.H., "Calculation of the Wind Buffeting of the Lions' Gate Bridge and Comparison with Model Studies", Proc. 6th Int. Conf. on Wind Engineering, Gold Coast, Australia, March 1983, J. Wind Engineering and Industrial Aerodynamics, Vol. 14, Nos. 1-3, pp. 201-210, December 1983.

Tanaka, H., "On Wind Tunnel Testing of Taut Strip Bridge Models", Proc. 3rd US-Japan Workshop on Bridge Engineering, Tsukuba, Japan, pp. 318-323, May 1987.

Tanaka, H., "Similitude and Modelling in Wind Tunnel Testing of Bridges", Preprint of Int. Colloquium on Bluff Body Aerodynamics and Its Applications, Kyoto, Japan, J. Wind Engineering, No. 37, Japan Association for Wind Engineering, pp. 429-446, October 1988.

Tanaka, H. and Davenport, A.G., "Response of Taut Strip Models to Turbulent Wind", J. Engineering Mechanics, Proc. ASCE, Vol. 108, No. EM1, pp. 33-49, February 1982.

Tanaka, H. and Davenport, A.G., "Wind-Induced Response of Golden Gate Bridge", J. Engineering Mechanics, Vol. 109, No. 1, ASCE, pp. 296-312, February 1983.

Vickery, B.J., "On the Flow behind a Coarse Grid and Its Use as a Model of Atmospheric Turbulence in Studies Related to Wind Loads on Buildings", National Physical Laboratory Aerodynamics Division, NPL Aero Report 1143, March 1965.

Vincent, G.S., "Golden Gate Bridge Vibration Studies", J. Structural Division, Proc. ASCE, Vol. 84, No. ST6, Paper 1817, October 1958.

Wardlaw, R.L., "Sectional versus Full Model Wind Tunnel Testing of Bridge Road Decks", DME/NAE Quarterly Bulletin No. 1978 (4), National Research Council Canada, National Aeronautical Establishment, pp. 25-47, January 1979.

Wardlaw, R.L., Tanaka, H. and Utsunomiya, H., "Wind Tunnel Experiments on the Effect of Turbulence on the Aerodynamic Behaviour of Bridge Road Decks", Proc. 6th Int. Conf. on Wind Engineering, Gold Coast, Australia, March 1983, J. Wind Engineering and Industrial Aerodynamics, Vol. 14, Nos. 1-3, pp. 247-257, December 1983.

Winter, H., "Flow Phenomena on Plates and Airfoils of Short Span", National Advisory Committee for Aeronautics, Technical Memorandum No. 798, July 1936.

Xiang, H., Xie, J. and Lin, Z., "Aerodynamic Study on a Proposed Cable-Stayed Bridge in Shanghai, China", Proc. 7th Int. Conf. on Wind Engineering, Part 2, Aachen, Germany, July

1987, J. Wind Engineering and Industrial Aerodynamics, Vol. 29, Nos. 1-3, pp. 419-427, August 1988.

Xie, J., Savage, M.G. and Tanaka, H., "Identification of the Aerodynamic Admittance Functions for Bridge Road Decks", Proc. 2nd Asia-Pacific Symp. on Wind Engineering, Beijing, June 1989, Recent Advances in Wind Engineering, T. F. Sun, ed., International Academic Pub., Pergamon Press, Oxford, U.K., Vol.2, pp. 618-628, 1989.

Xie, J., Tanaka, H., Wardlaw, R.L. and Savage, M.G., "Buffeting Analysis of Long Span Bridges to Turbulent Wind with Yaw Angle", J. Wind Engineering and Industrial Aerodynamics, Vol. 37, No. 1, pp. 65-77, February 1991.

Xie, J. and Xiang, H.F., "State-space Method for 3D Flutter Analysis of Bridge Structures", Proc. Asia Pacific Symp. on Wind Engineering, Roorkee, India, pp. 269-276, December 1985.

Zan, S.J., "The Effect of Mass, Wind Angle and Erection Technique on the Aeroelastic Behaviour of a Cable-Stayed Bridge Model", National Research Council Canada, NAE-AN-46, September 1987a.

Zan, S.J., "Wind Tunnel Investigation of the Wind-Induced Response of the Roosevelt Lake Steel Arch Bridge Using an Aeroelastic Model", National Research Council Canada, NAE-LTR-LA-306, October 1987b.

Zan, S.J. and Wardlaw, R.L., "Wind Buffeting of Long Span Bridges with Reference to Erection Phase Behaviour", Proc. ASCE Structure Congress 1987, Orlando, Florida, pp. 432-448, August 1987.

Zan, S.J., Yamada, H. and Tanaka, H., "The Influence of Turbulence and Deck Section Geometry on the Aeroelastic Behaviour of a Cable-Stayed Bridge Model", National Research Council Canada, NAE-AN-40, August 1986.

FIGURES

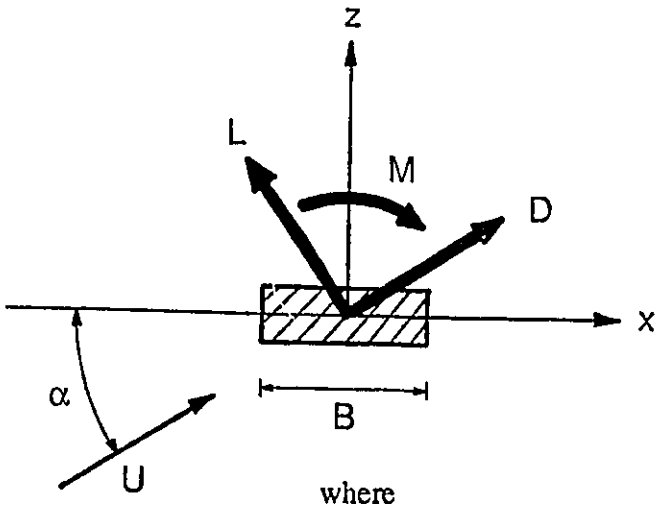

where

U: wind speed
D: aerodynamic drag force
L: aerodynamic lift force
M: aerodynamic pitching moment
x: horizontal coordinate
z: vertical coordinate
α: angle of attack

and aerodynamic forces are defined as

$$D = 0.5\rho BU^2C_D$$

$$L = 0.5\rho BU^2C_L$$

$$M = 0.5\rho B^2U^2C_M$$

where, D, L and M are taken per unit length, and

C_D: drag coefficient
C_L: lift coefficient
C_M: moment coefficient
B: typical dimension of the section

Fig. 2.1. Aerodynamic Forces and Coefficients

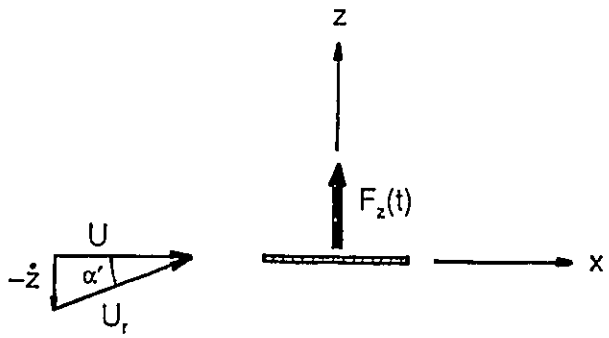

where

$F_z(t)$: quasi-steady aerodynamic force in vertical direction
U_r: relative wind velocity
α′: instantaneous angle of attack

Fig. 2.2. Quasi-Steady Aerodynamic Force by Vertical Body Motion

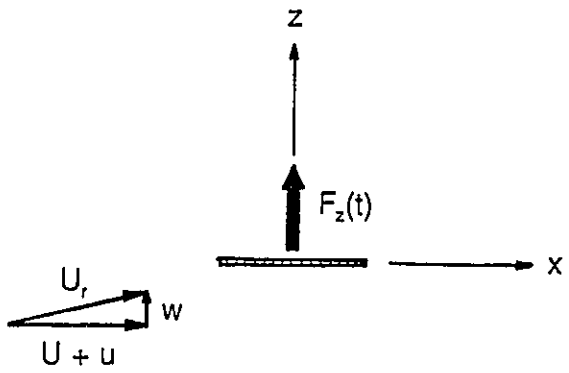

where

u: fluctuating wind velocity component in horizontal direction
w: fluctuating wind velocity component in vertical direction

Fig. 2.3. Quasi-Steady Aerodynamic Force by Fluctuating Wind Velocity

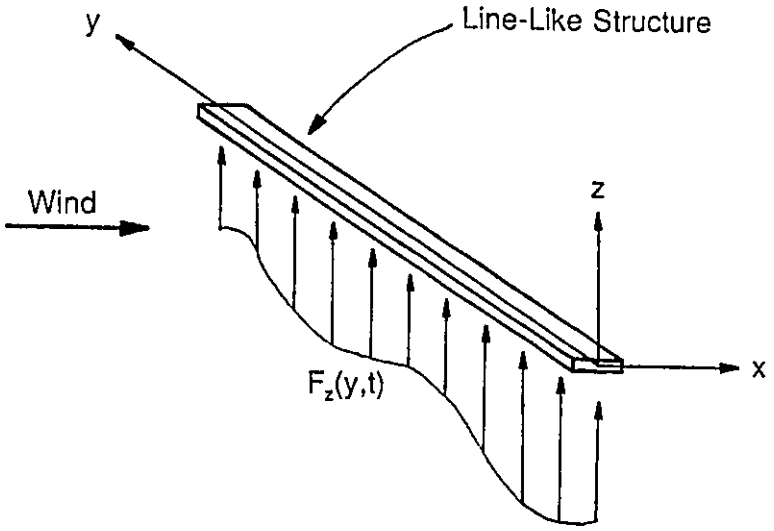

Fig. 2.4. Line-Like Structure under Wind Loading

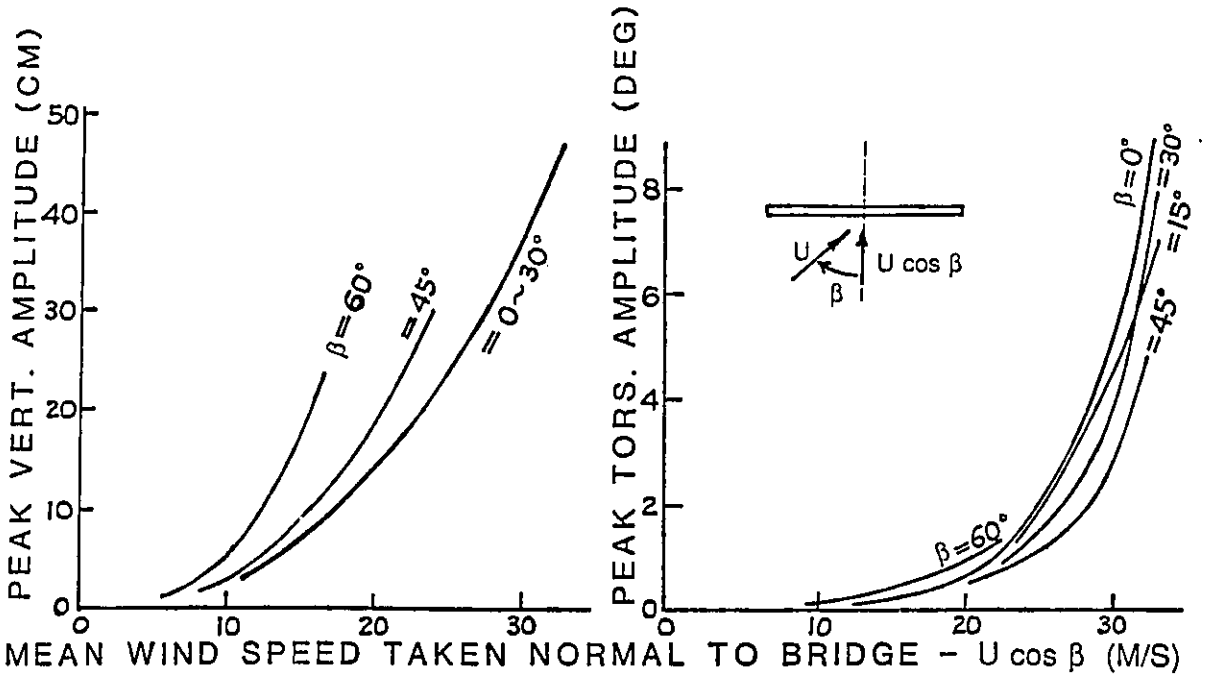

Fig. 2.5. Taut Strip Model Response under Yawed Wind
(Davenport, Isyumov and Tanaka, 1976)

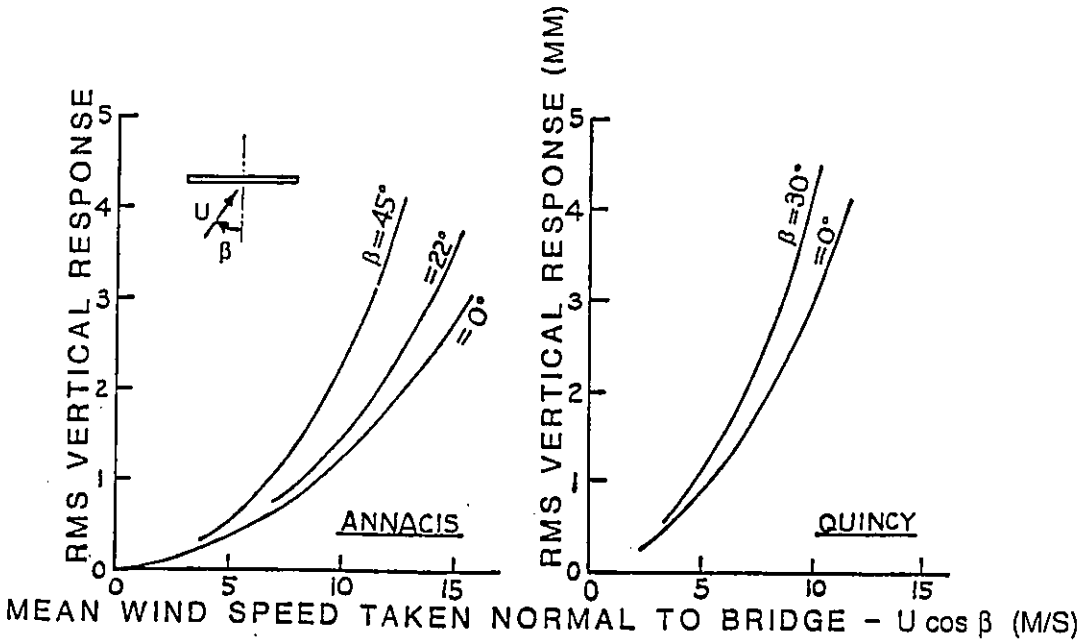

Fig. 2.6. Full Model Response of Cable-Stayed Bridge under Construction in Yawed Wind
(Irwin and Gamble, 1985; Zan, 1987a)

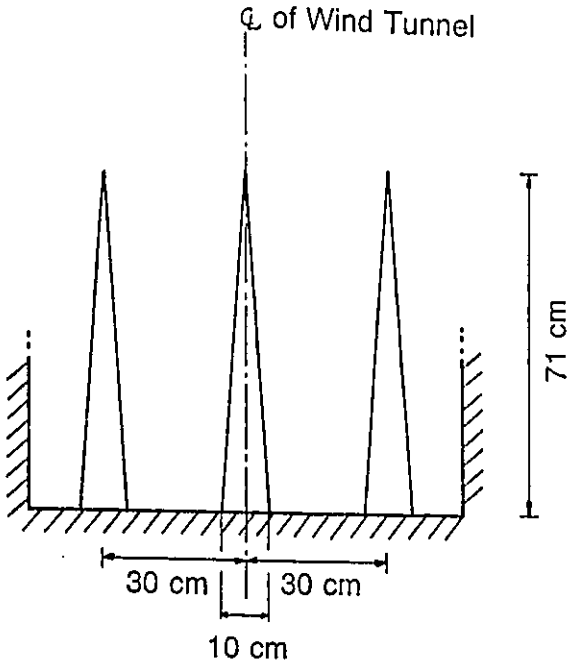

Fig. 3.1. Dimensions of the Spires

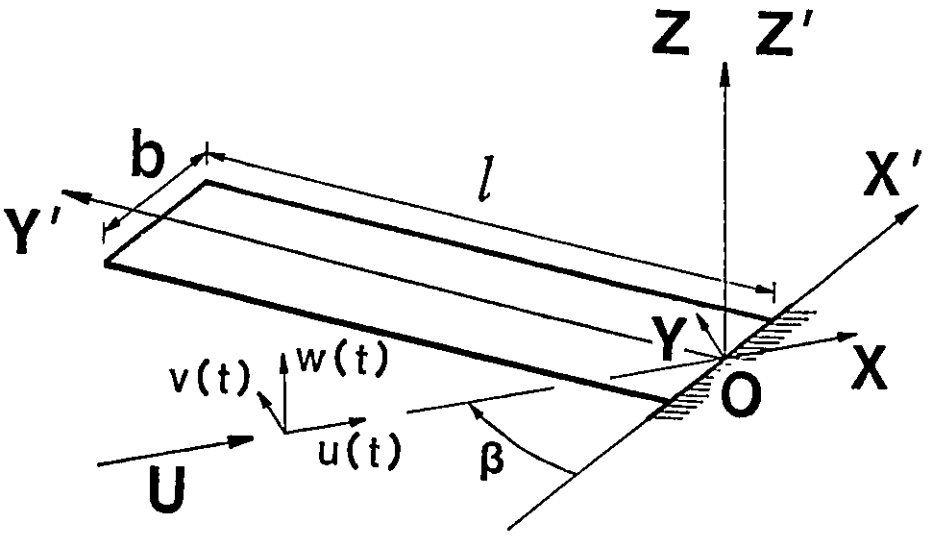

Fig. 3.2. Coordinates

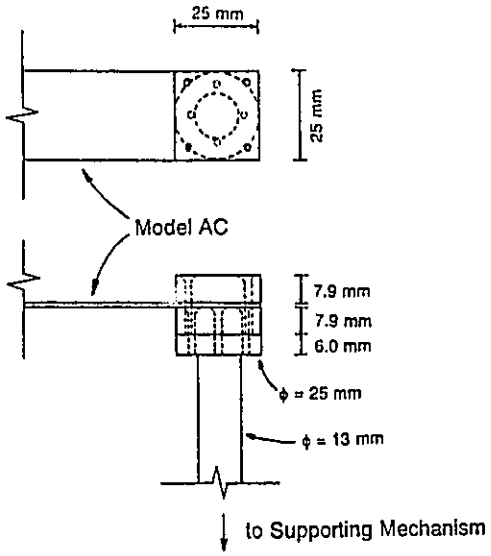

Fig. 3.3. Clamping Part of Model AC

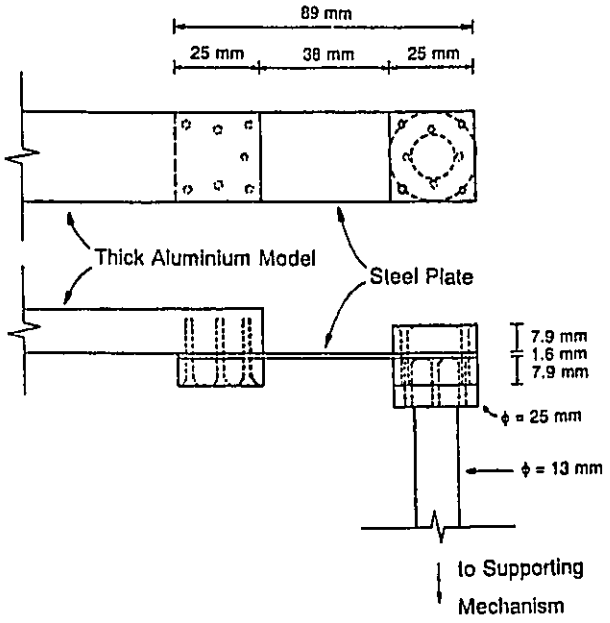

Fig. 3.4. Clamping Part of Thicker Models

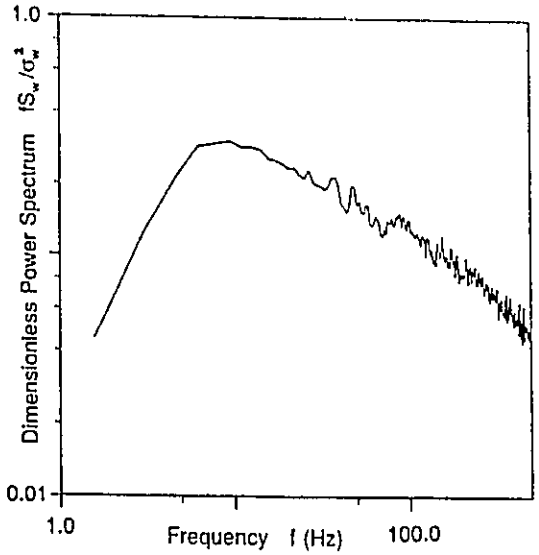

(a) Grid NI, U = 3.0 m/s

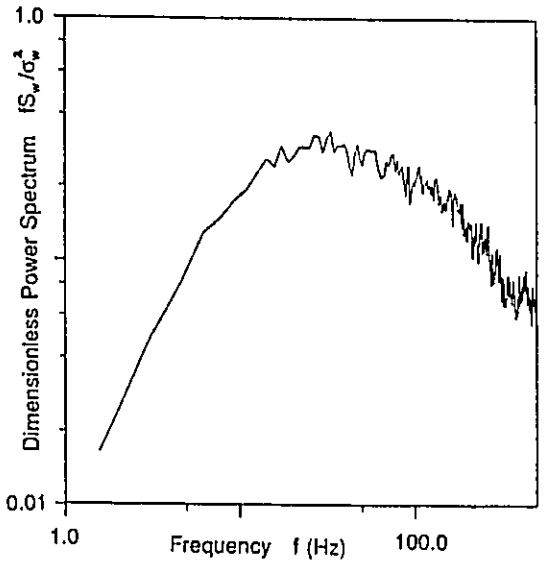

(b) Grid NII, U = 3.7 m/s

Fig. 3.5. Dimensionless Power Spectra of w-Component

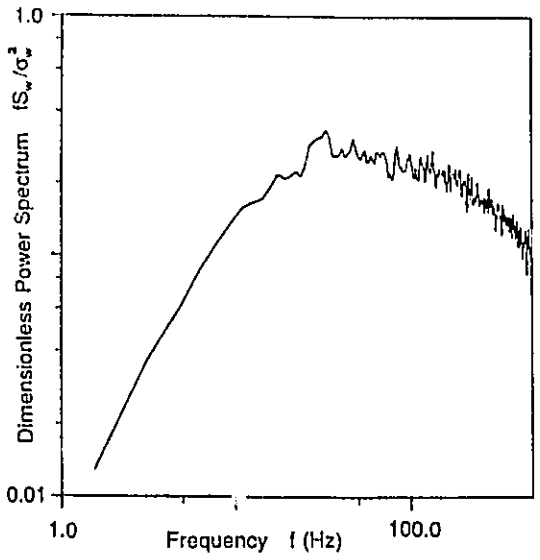

(c) Grid NIII, U = 3.0 m/s

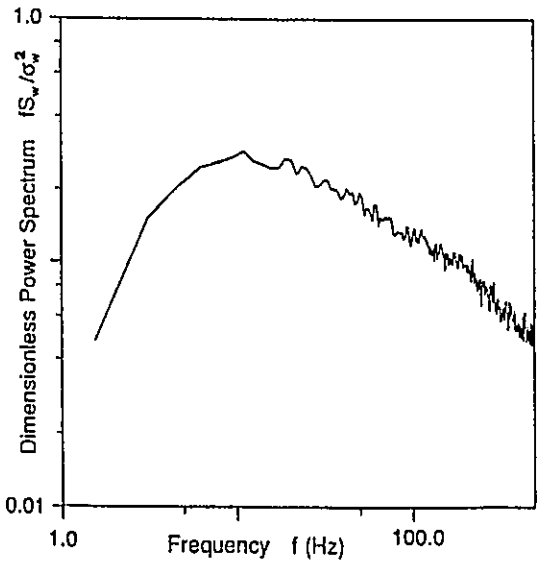

(d) Grid CI, U = 3.0 m/s

Fig. 3.5. Dimensionless Power Spectra of w-Component (Continued)

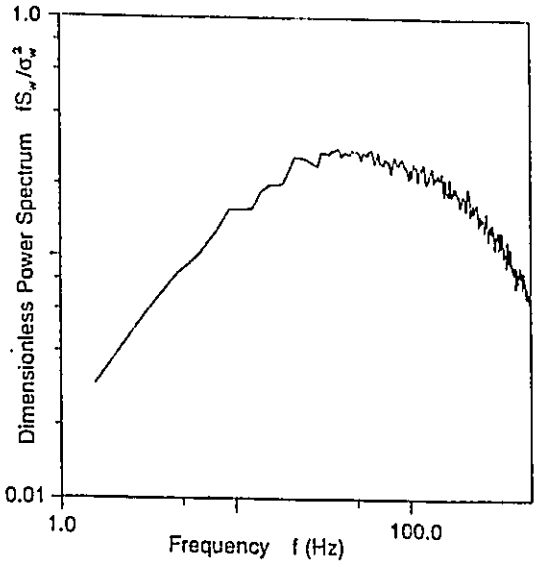

(e) Grid CIII, U = 3.0 m/s

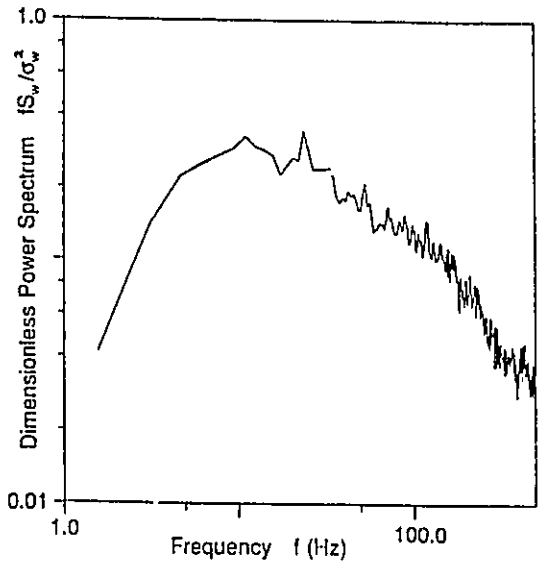

(f) Shear Flow, U = 3.7 m/s

Fig. 3.5. Dimensionless Power Spectra of w-Component (Continued)

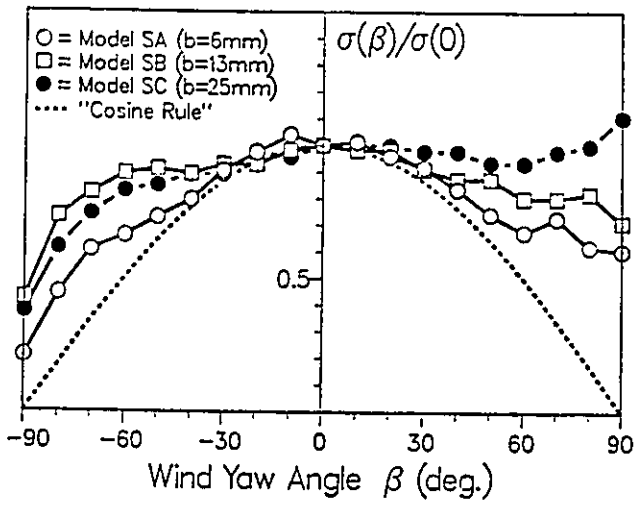

(a) l = 305 mm, Grid NIII, U = 6.4 m/s

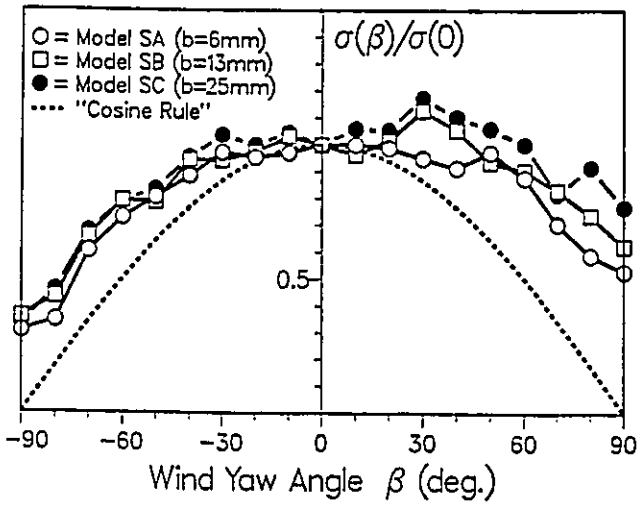

(b) l = 305 mm, Shear Flow, U = 6.4 m/s

Fig. 3.6. Effect of Model Width

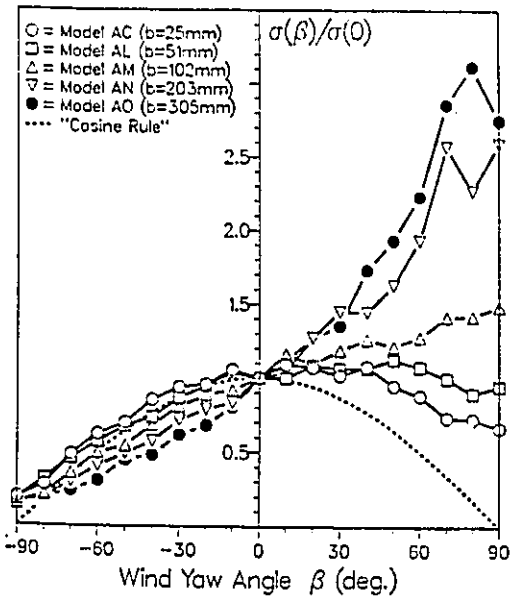

(c) l = 305 mm, Grid CI, U = 3.0 m/s

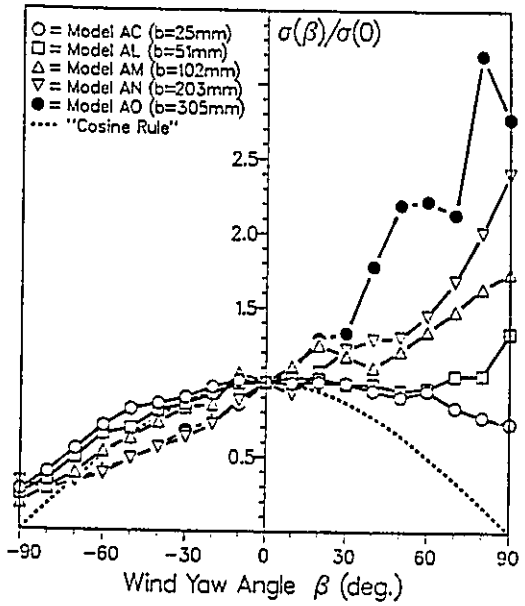

(d) l = 305 mm, Grid CIII, U = 3.0 m/s

Fig. 3.6. Effect of Model Width (Continued)

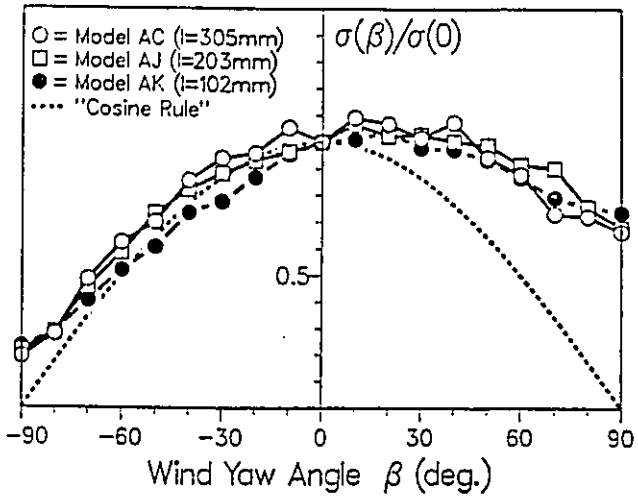

(a) b = 25.4 mm, Grid CI, U = 3.0, 7.0 and 9.1 m/s for Model AC, AJ and AK respectively

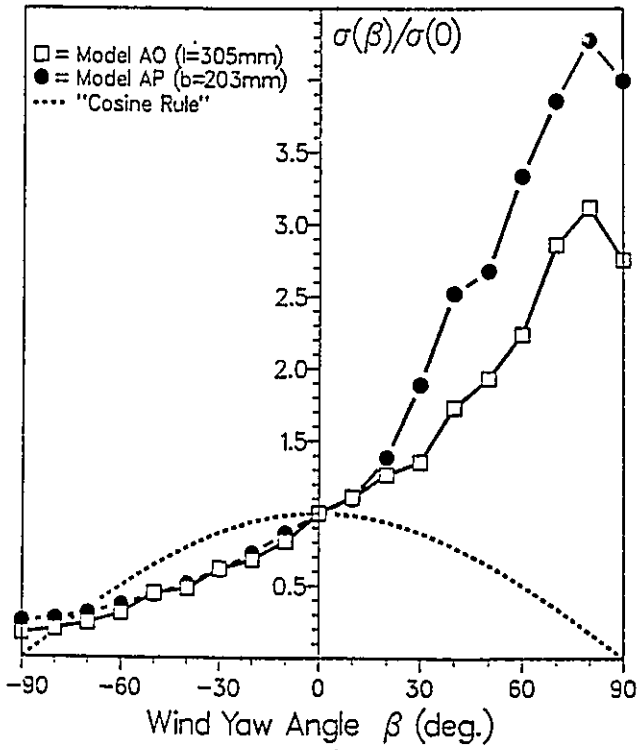

(b) b = 305 mm, Grid CI, U = 3.0 and 7.0 m/s for Model AO and AP respectively

Fig. 3.7. Effect of Model Length

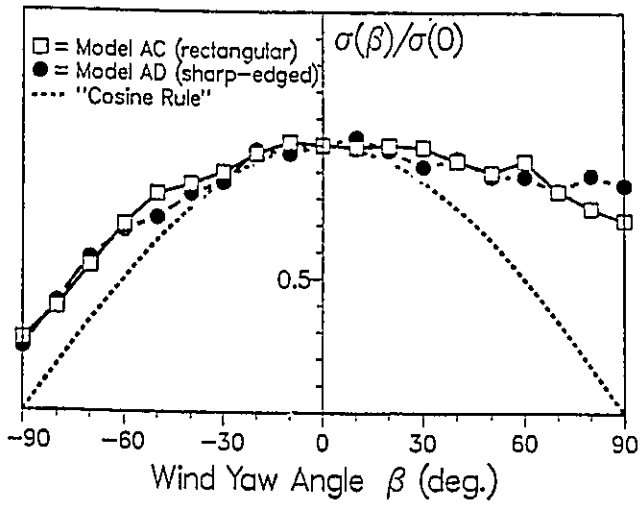

Fig. 3.8. Sharp-Edged vs. Rectangular Cross-Section Model Response, Grid CIII, U=3.0 m/s

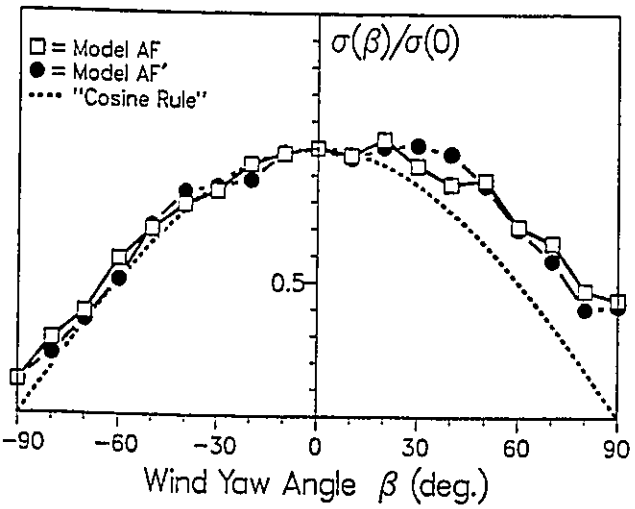

Fig. 3.9. Model Response with Different Clamping Part, Grid CI,
U = 11.9 and 8.8 m/s for Model AF and AF' respectively

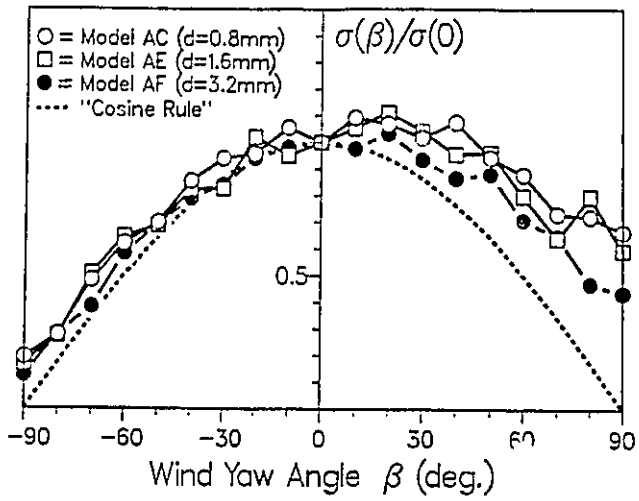

(a) b = 25.4 mm, Grid CI, U = 3.0, 5.8 and 11.9 m/s
for Model AC, AE and AF respectively

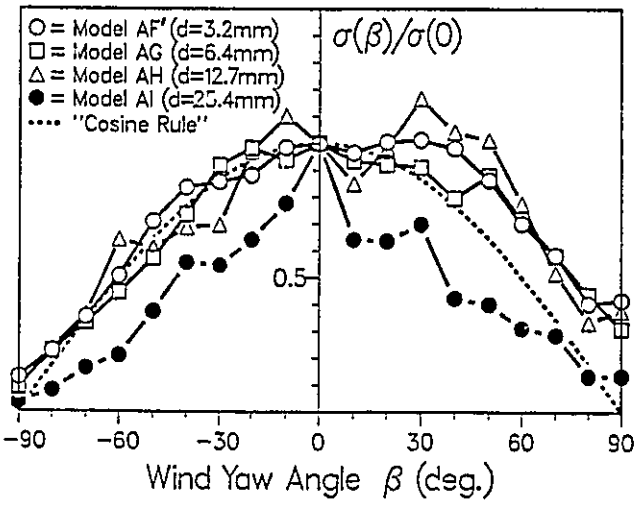

(b) b = 25.4 mm, Grid CI, U = 8.8, 7.0, 4.9 and 3.7 m/s
for Model AF', AG, AH and AI respectively

Fig. 3.10. Effect of Model Thickness

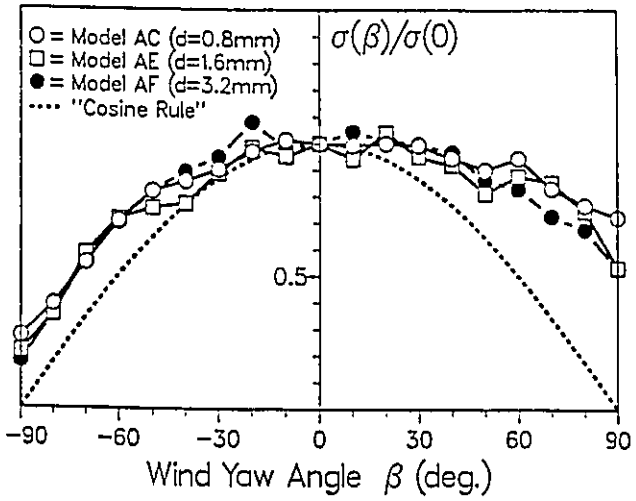

(c) b = 25.4 mm, Grid CIII, U = 3.0, 5.8 and 11.9 m/s for Model AC, AE and AF respectively

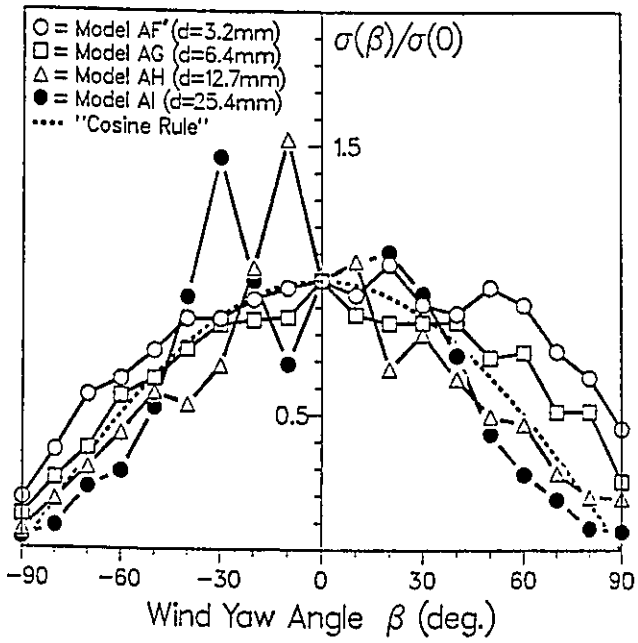

(d) b = 25.4 mm, Grid CIII, U = 8.8, 7.0, 4.9 and 3.7 m/s for Model AF', AG, AH and AI respectively

Fig. 3.10. Effect of Model Thickness (Continued)

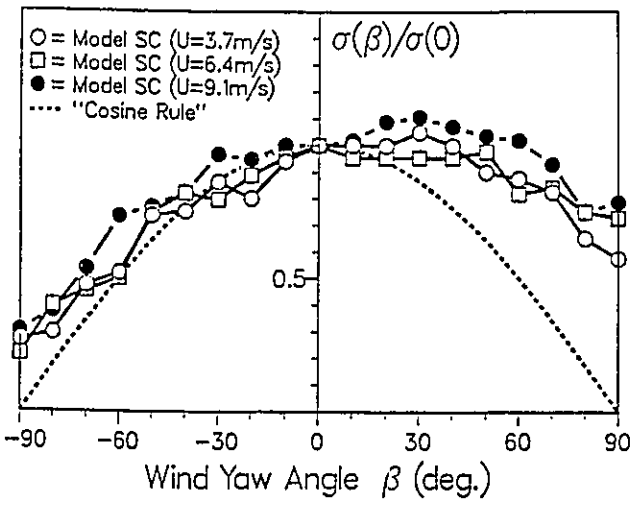

(a) l = 305 mm, d = 0.8 mm, Grid NI

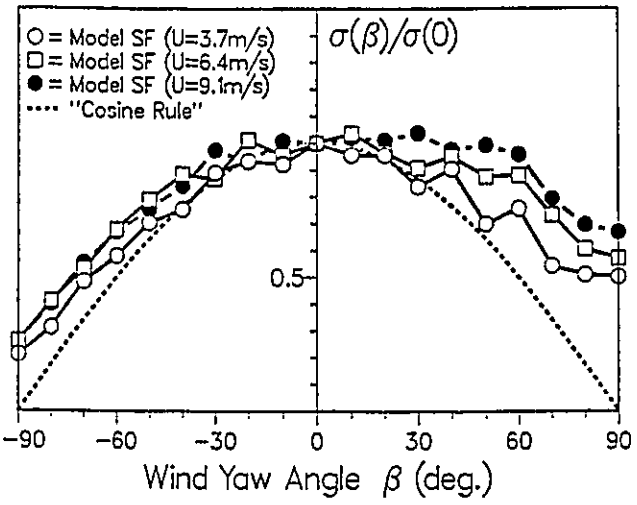

(b) l = 203 mm, d = 0.8 mm, Shear Flow

Fig. 3.11. Effect of Wind Speed

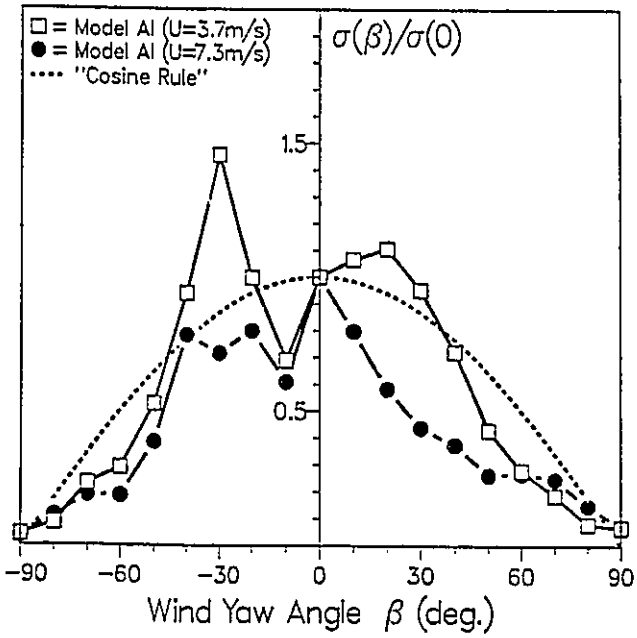

(c) l = 305 mm, d = 25.4 mm, Grid CIII

Fig. 3.11. Effect of Wind Speed (Continued)

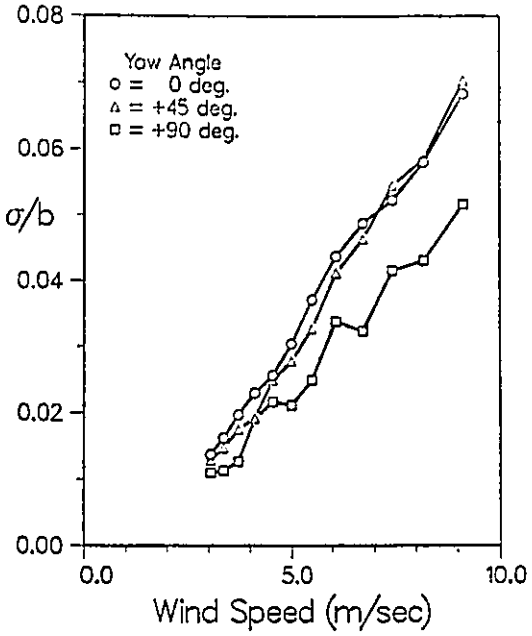

(a) Model AC, b = 25.4 mm, d = 0.8 mm, Grid CIII

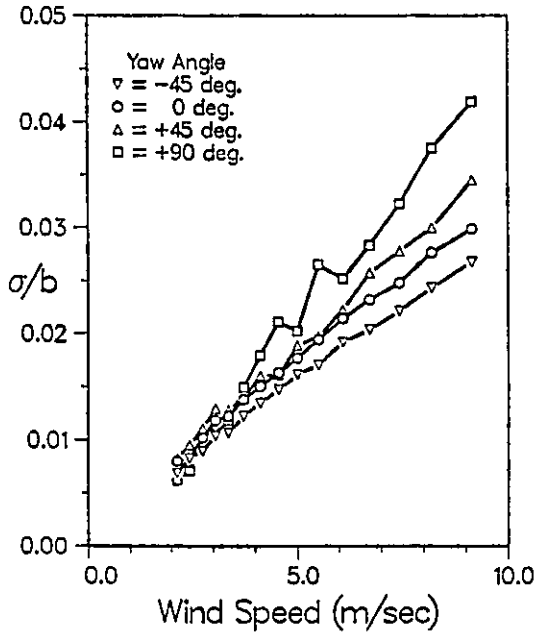

(b) Model AC, b = 25.4 mm, d = 0.8 mm, Grid NIII

Fig. 3.12. Model Response vs. Wind Speed

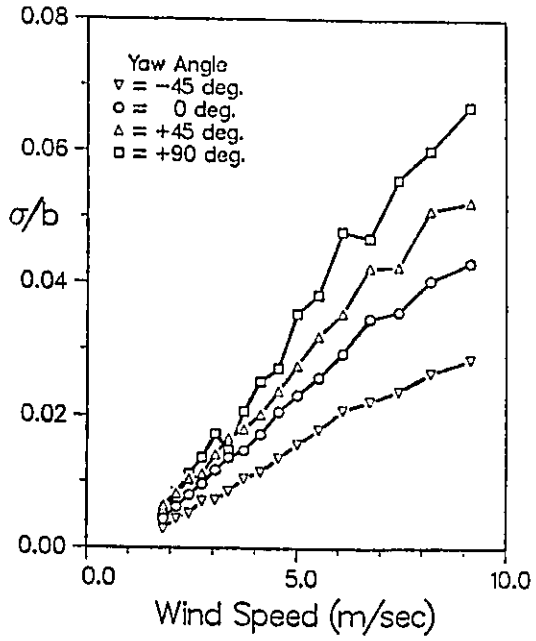

(c) Model AM, b = 102 mm, d = 0.8 mm, Grid NI

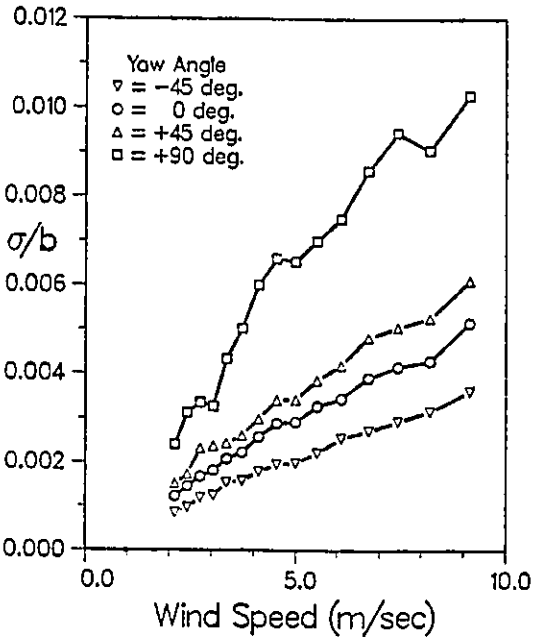

(d) Model AM, b = 102 mm, d = 0.8 mm, Grid NIII

Fig. 3.12. Model Response vs. Wind Speed (Continued)

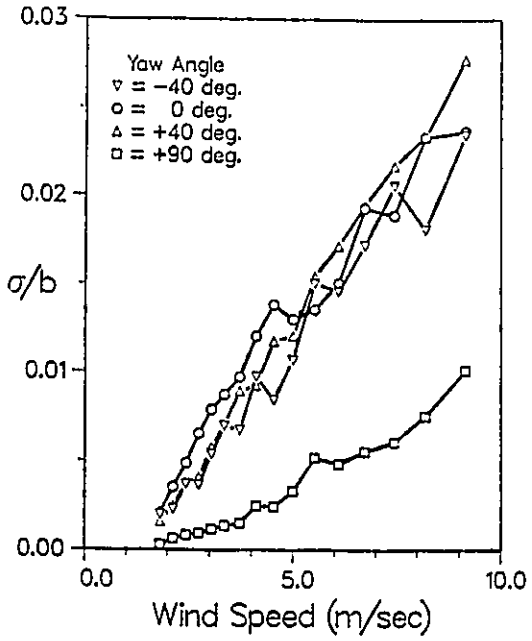

(e) Model AH, b = 25.4 mm, d = 12.7 mm, Grid NI

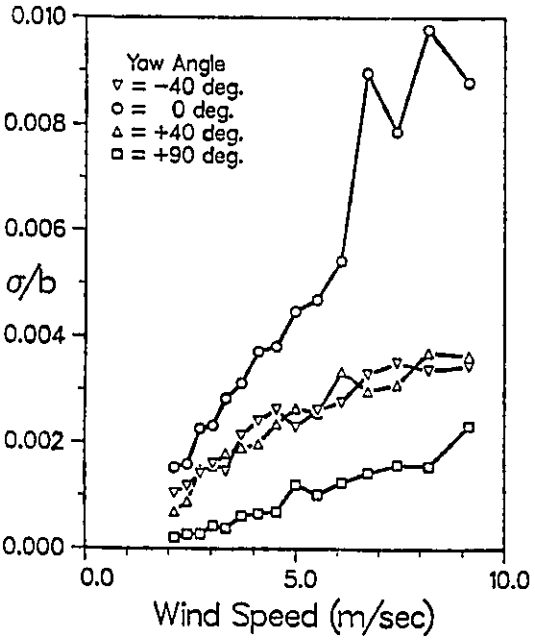

(f) Model AH, b = 25.4 mm, d = 12.7 mm, Grid NIII

Fig. 3.12. Model Response vs. Wind Speed (Continued)

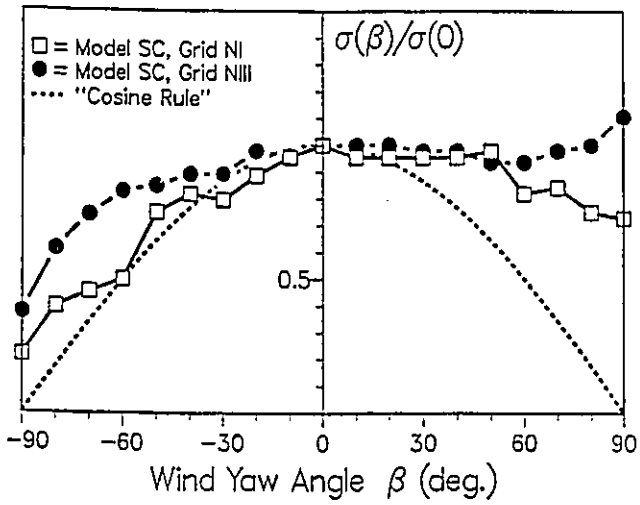

Fig. 3.13. Effect of Flow Condition, U = 6.4 m/s

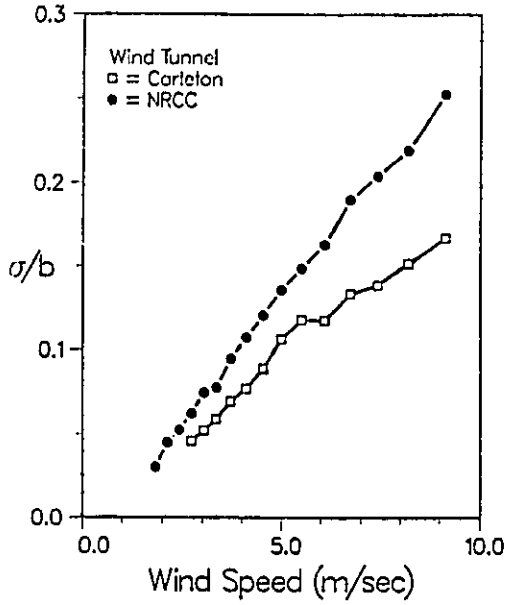

(a) β = 0°, Grid NI and CI

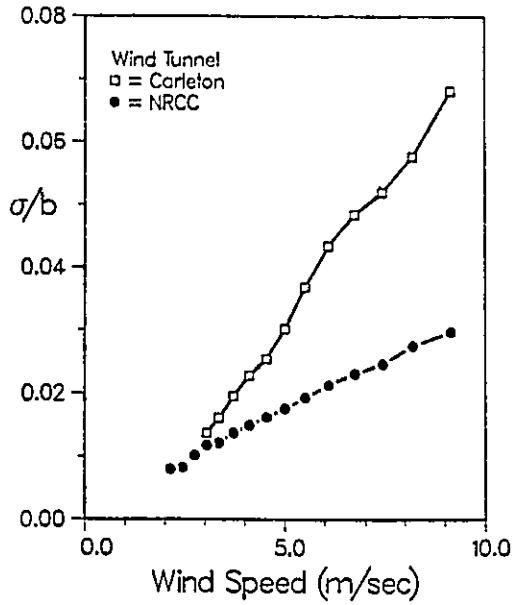

(b) β = 0°, Grid NIII and CIII

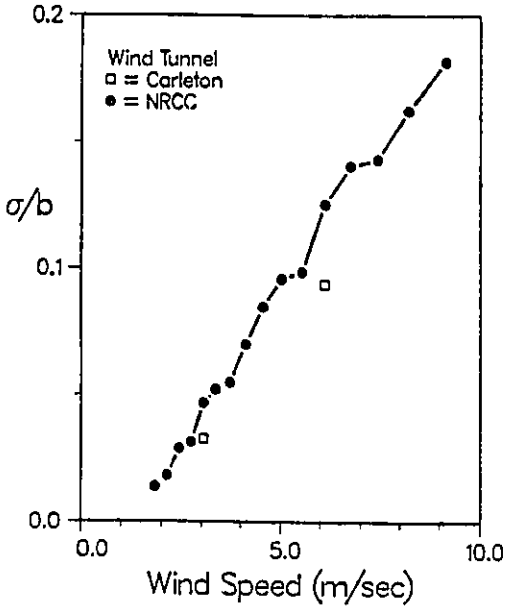

(c) β = 90°, Grid NI and CI

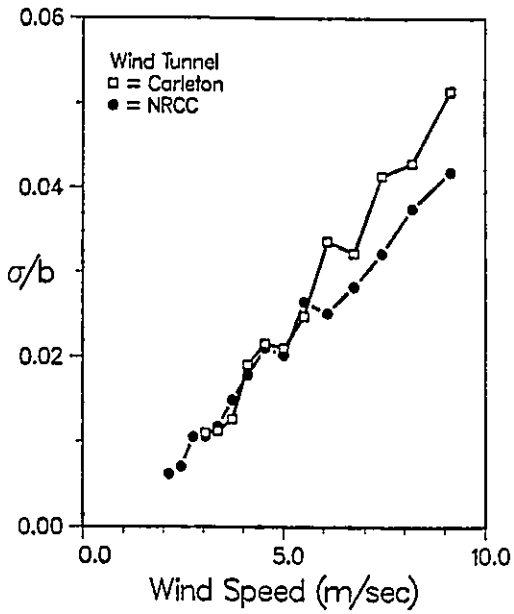

(d) β = 90°, Grid NIII and CIII

Fig. 3.14. Model Response in Different Wind Tunnel, Model AC

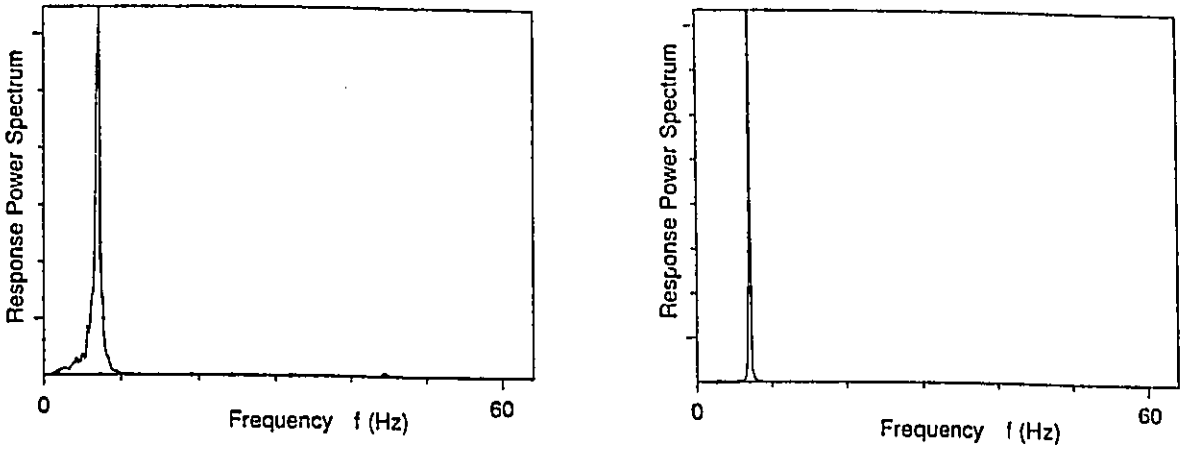

(a) $\beta = 0°$ (b) $\beta = 90°$

Fig. 3.15. Response Spectra, Model AC, Grid NI, U = 3.0 m/s

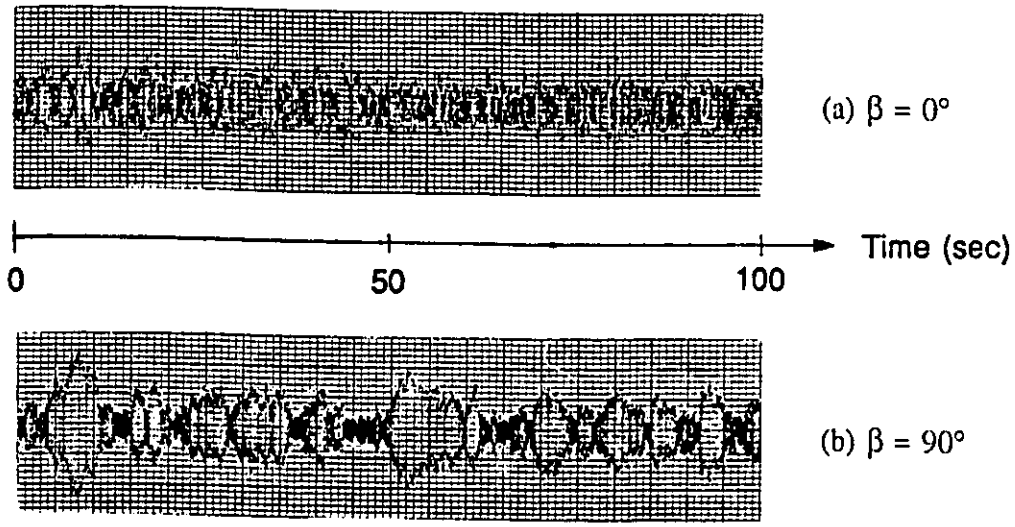

Fig. 3.16. Response Time History, Model AC, Grid NI, U = 3.0 m/s

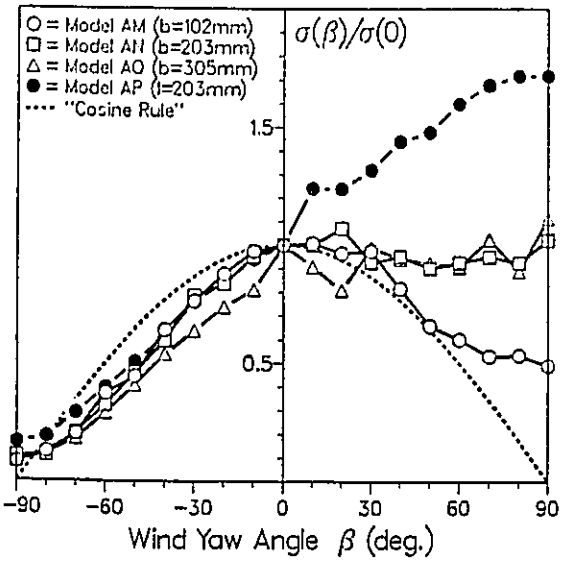

(a) Grid CI, U = 3.0 m/s for Model AM, AN and AO and 7.0 m/s for Model AP

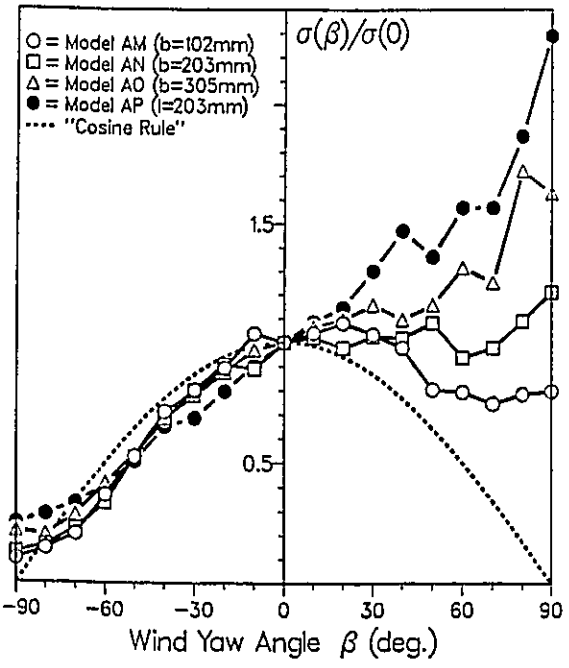

(b) Grid CIII, U = 3.0 m/s for Model AM, AN and AO and 7.0 m/s for Model AP

Fig. 3.17. Torsional Response of Different Width Models

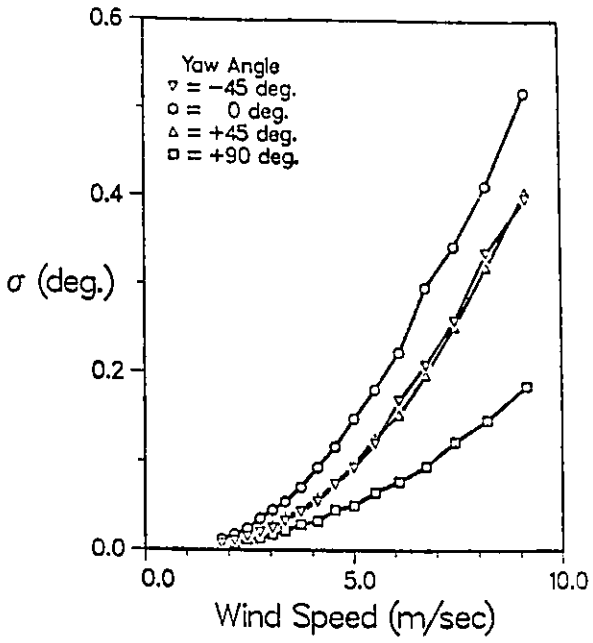

(a) Grid NI

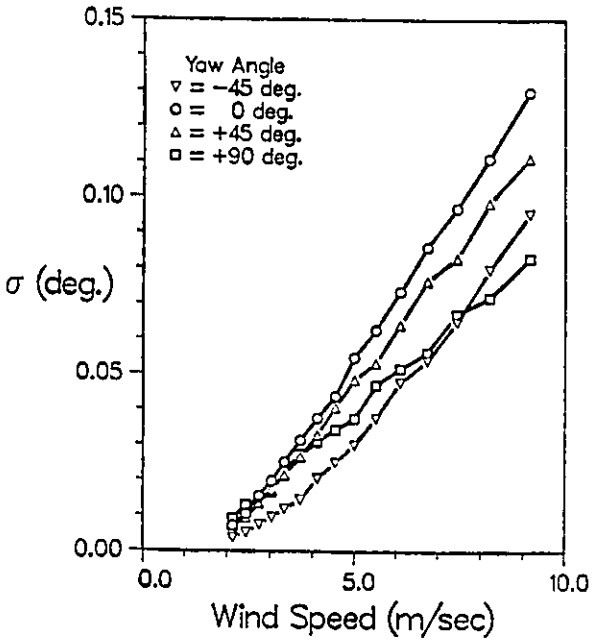

(b) Grid NIII

Fig. 3.18. Torsional Model Response vs. Wind Speed, Model AM

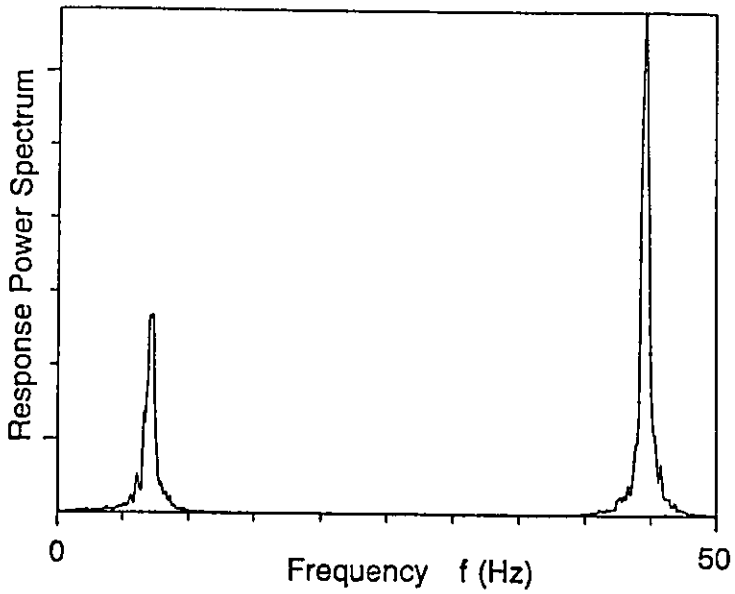

Fig. 3.19. Response Spectrum with Large Second Mode Contribution, Model SC, Grid NIII, $\beta = 0°$, U = 9.1 m/s

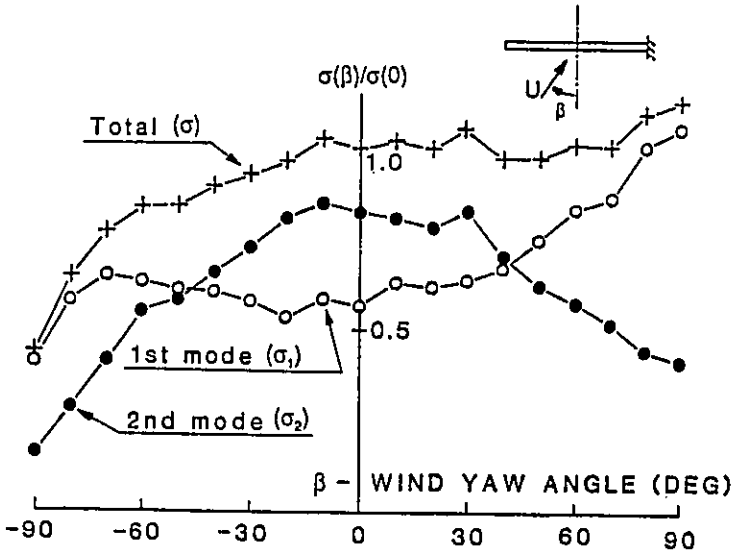

(a) Grid NIII, U = 9.1 m/s

Fig. 3.20. First and Second Mode Contribution, Model SC

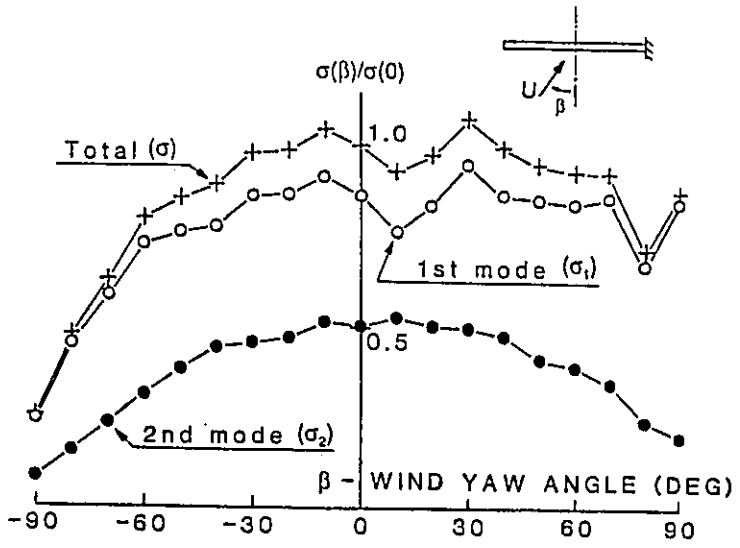

(b) Grid NII, U = 9.1 m/s

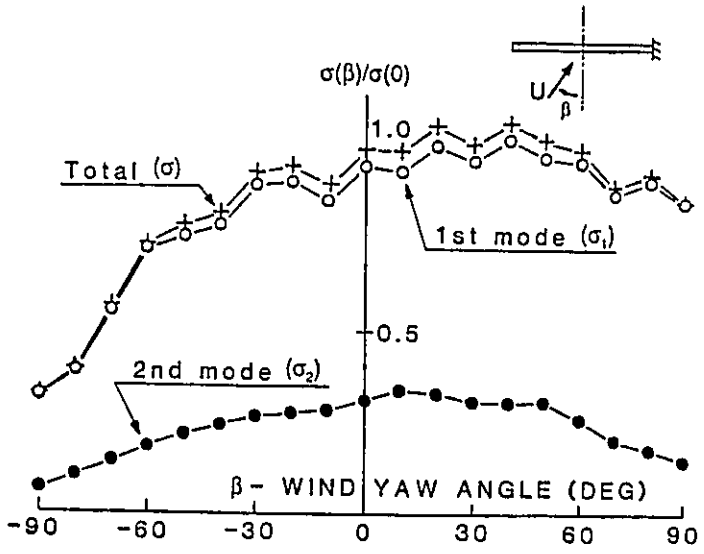

(c) Grid NI, U = 9.1 m/s

Fig. 3.20. First and Second Mode Contribution, Model SC (Continued)

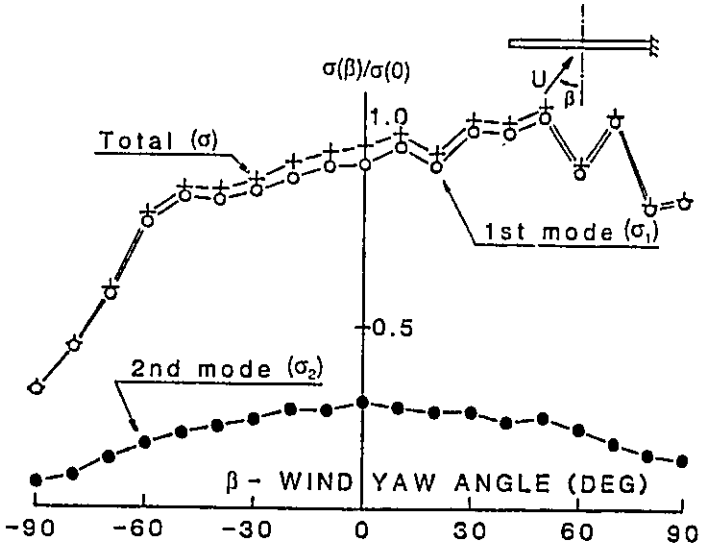

(d) Shear Flow, U = 9.1 m/s

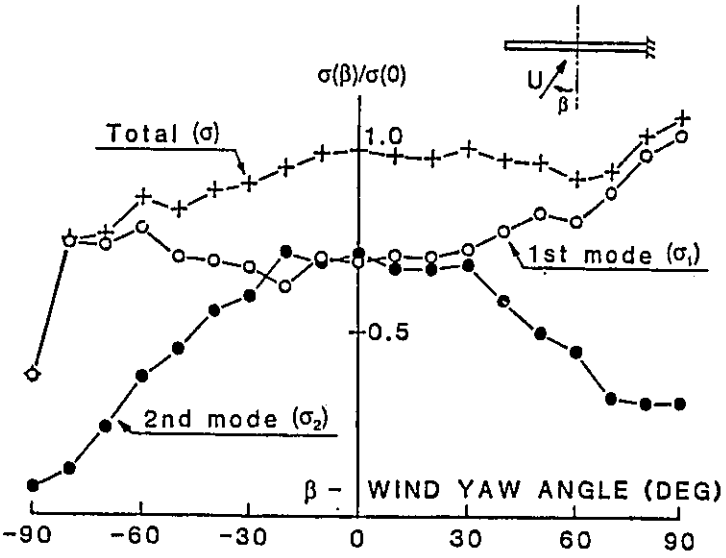

(e) Grid NIII, U = 6.4 m/s

Fig. 3.20. First and Second Mode Contribution, Model SC (Continued)

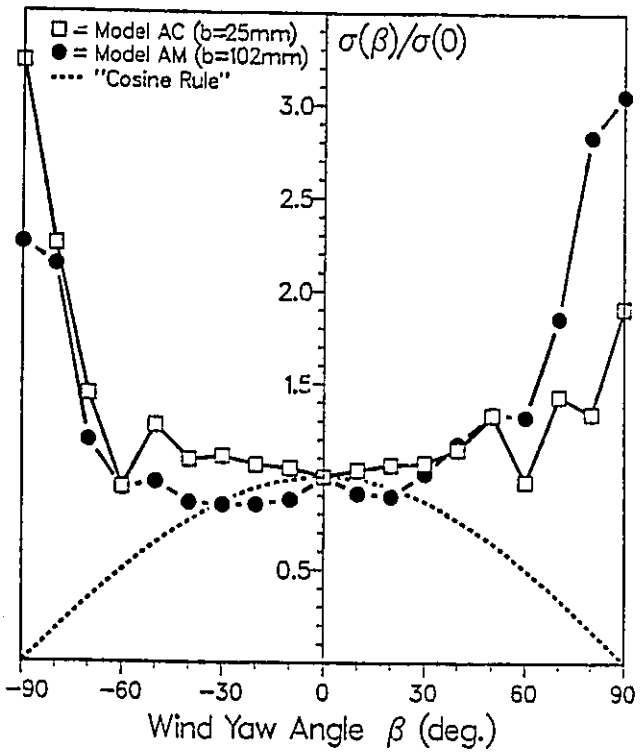

Fig. 3.21. Model Response in Very Low Turbulent Flow, U = 3.0 m/s

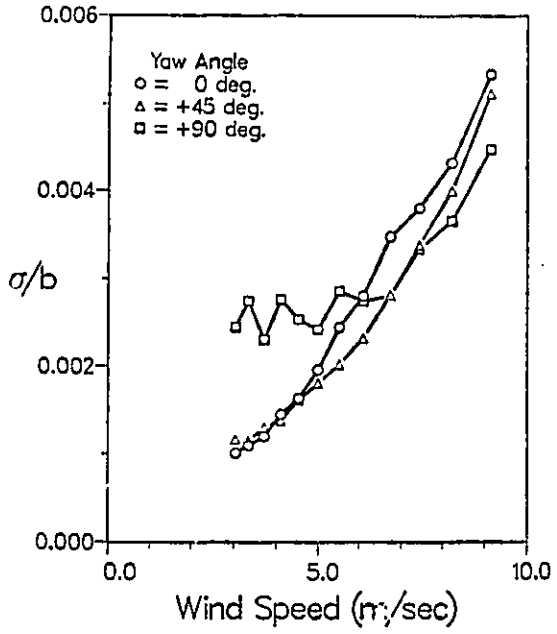

(a) Model AC, b = 25.4 mm

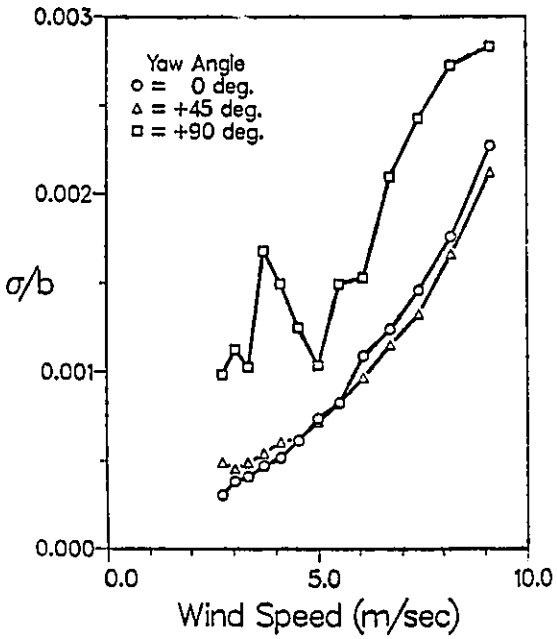

(b) Model AL, b = 50.8 mm

Fig. 3.22. Model Response in Very Low Turbulent Flow vs. Wind Speed

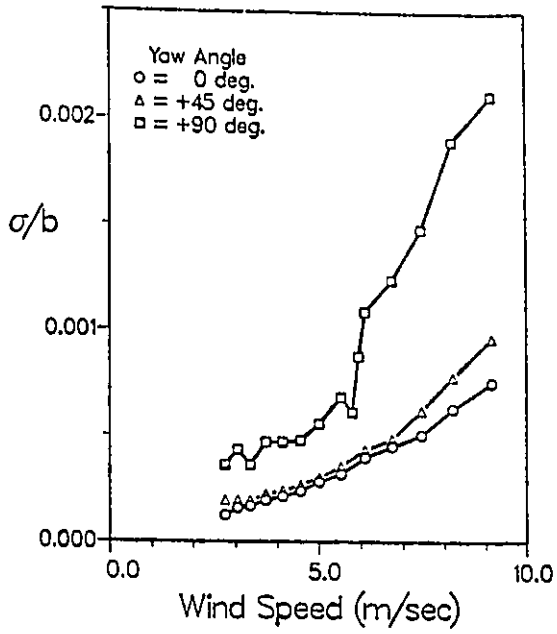

(c) Model AM, b = 102 mm

Fig. 3.22. Model Response in Very Low Turbulent Flow vs. Wind Speed (Continued)

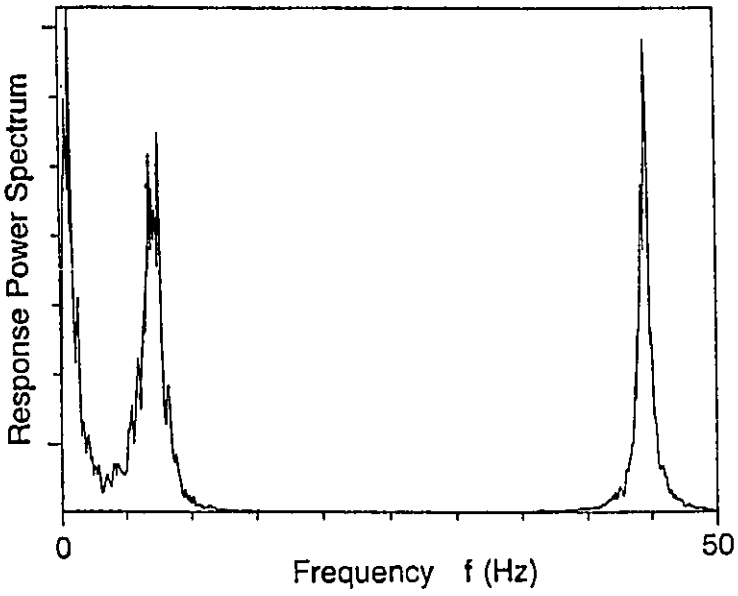

Fig. 3.23. Power Spectrum of Model Response in Very Low Turbulent Flow, Model AC, $\beta = 0°$, U = 6.1 m/s

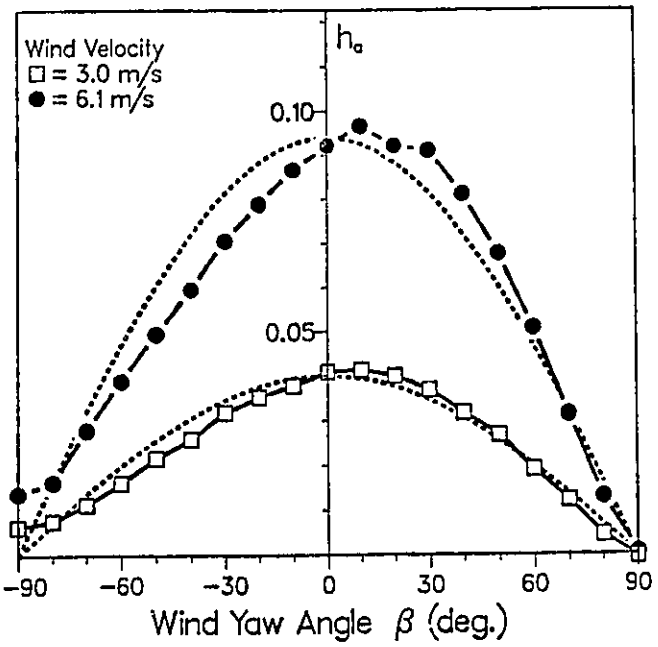

(a) Model AC, b = 25.4 mm, d = 0.8 mm

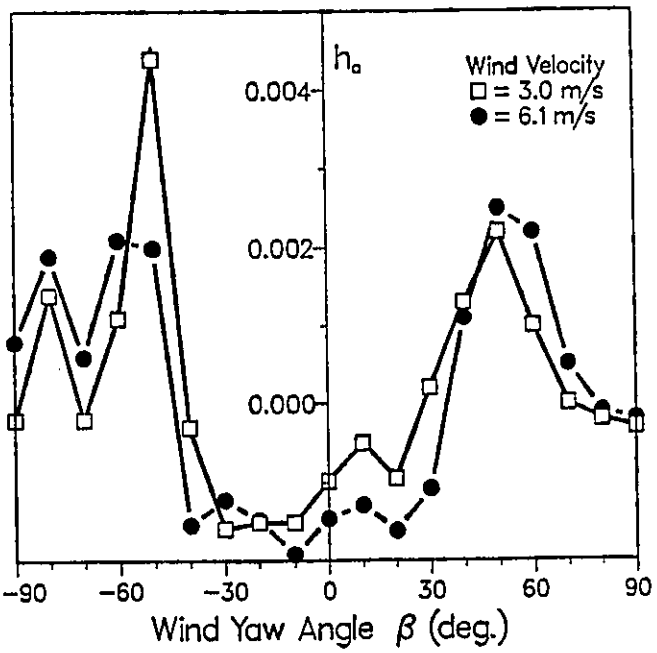

(b) Model AH, b = 25.4 mm, d = 12.7 mm

Fig. 3.24. Aerodynamic Damping vs. Wind Yaw Angle

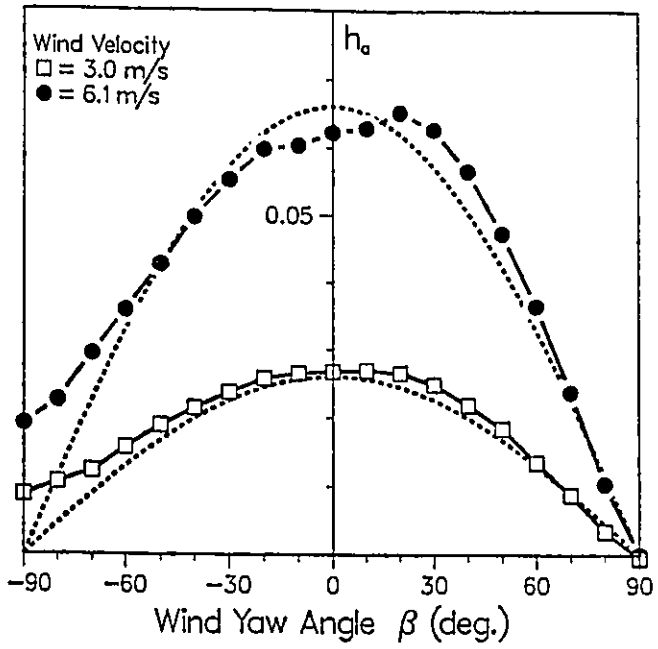

(c) Model AL, b = 50.8 mm, d = 0.8 mm

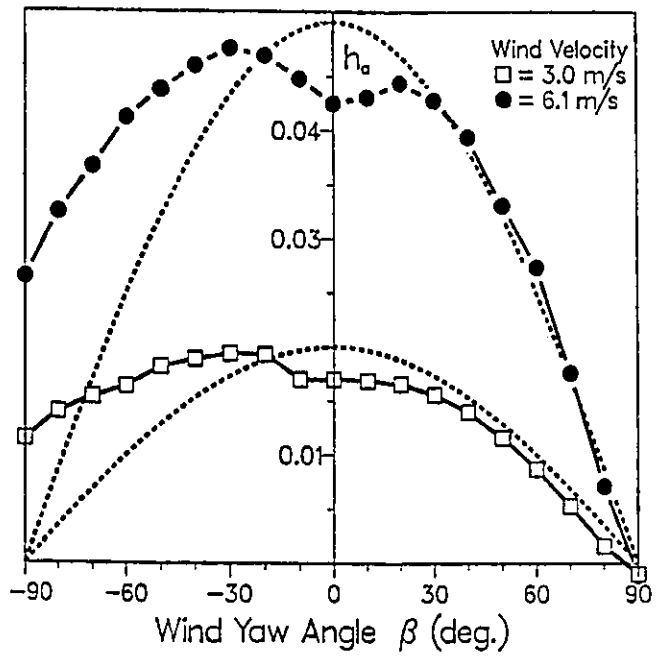

(d) Model AM, b = 102 mm, d = 0.8 mm

Fig. 3.24. Aerodynamic Damping vs. Wind Yaw Angle (Continued)

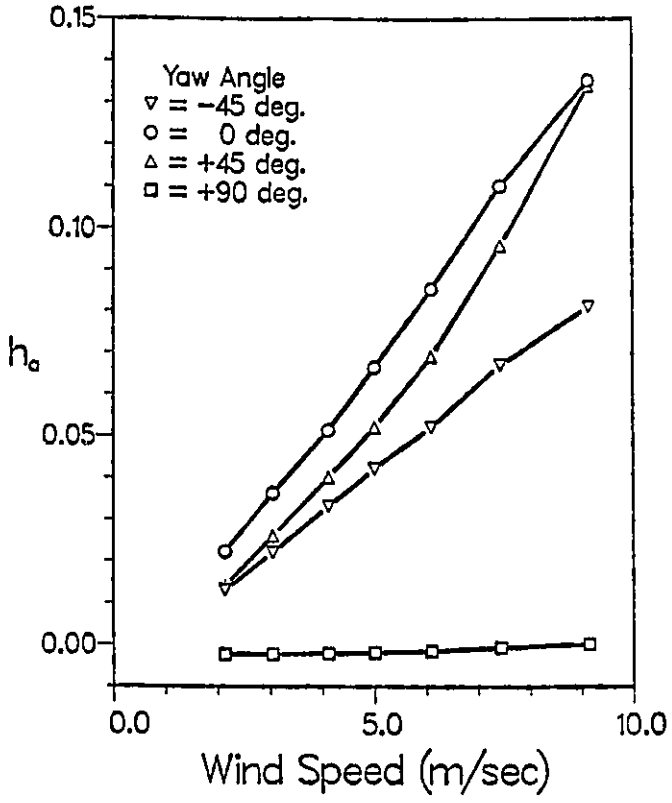

Fig. 3.25. Aerodynamic Damping vs. Wind Speed, Model AC

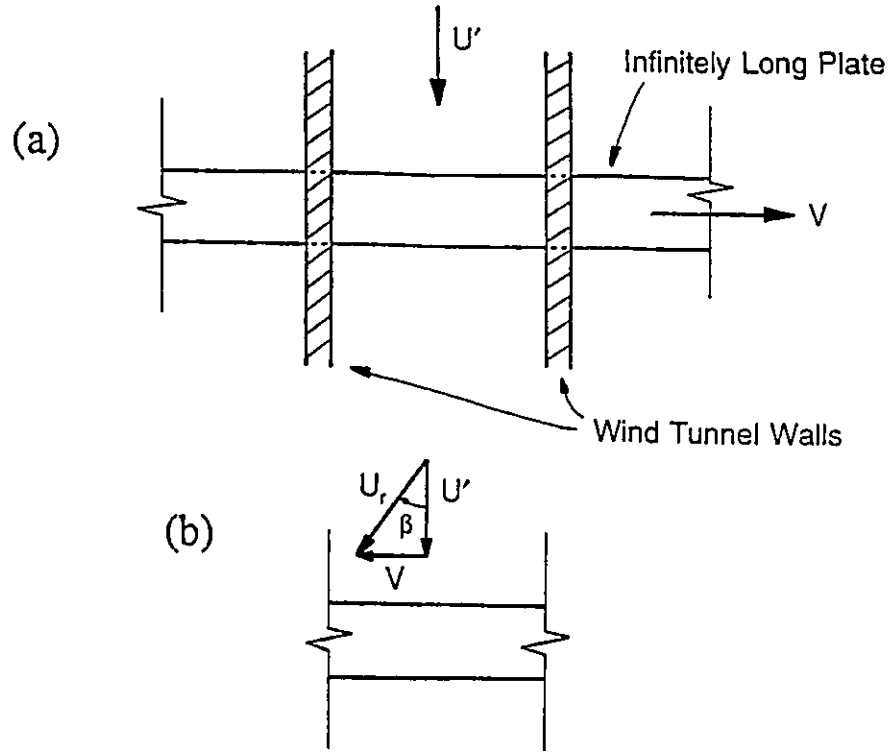

Fig. 4.1. Infinitely Long Plate Moving in Longitudinal Direction

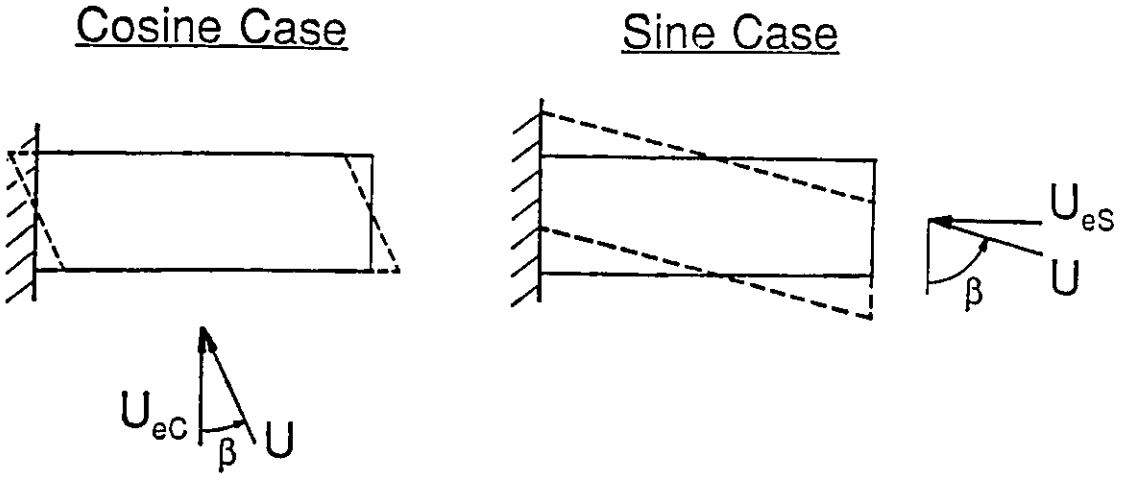

Fig. 4.2. Cosine and Sine Case

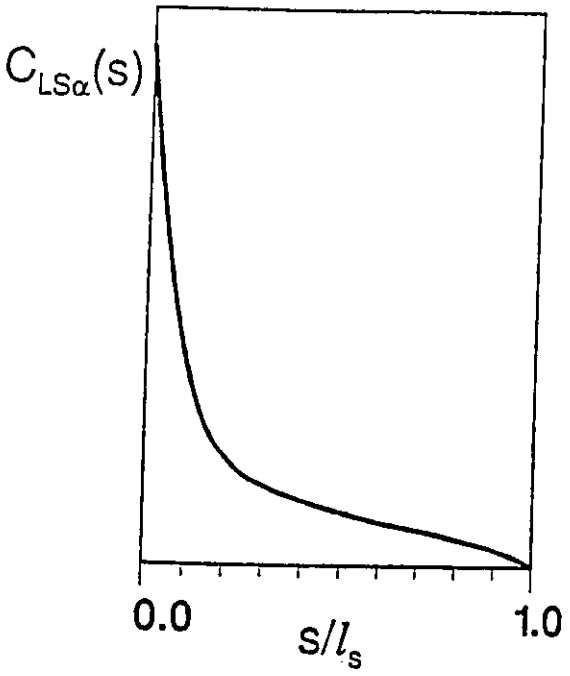

Fig. 4.3. Shape of $C_{LS\alpha}(s)$

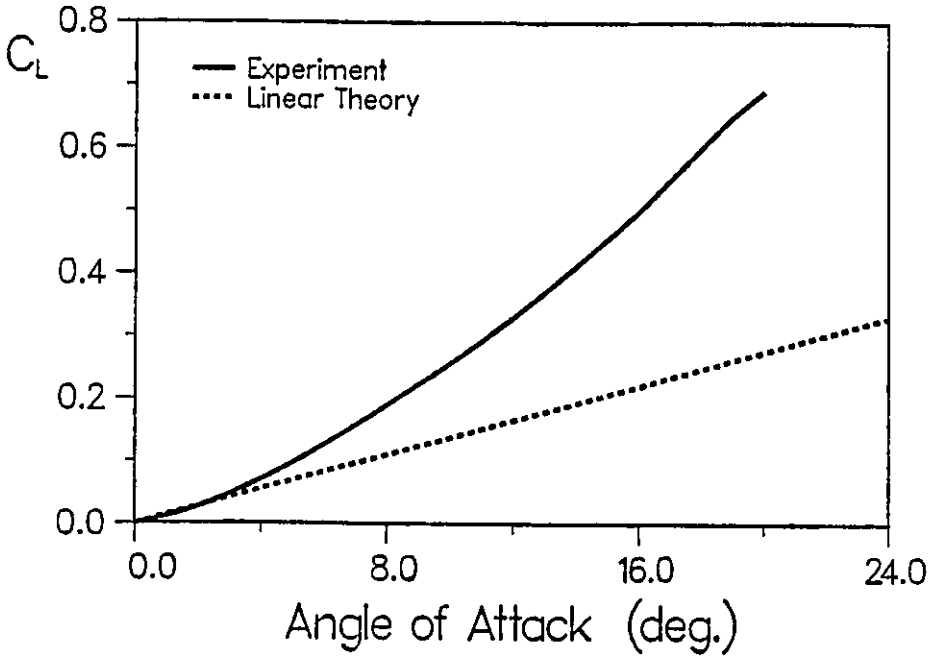

Fig. 4.4. Lift Coefficient for Small Aspect Ratio Plate, AR = 0.5 (Gersten, 1961)

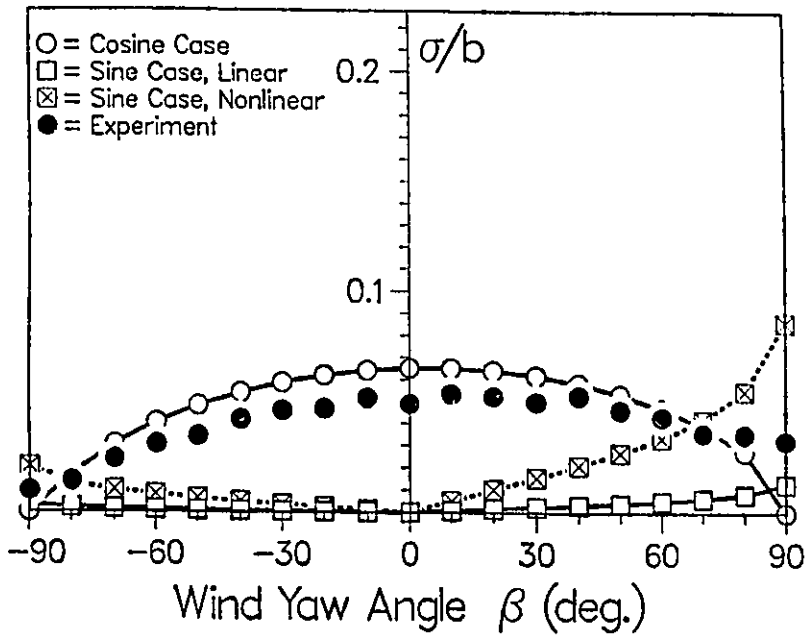

(a) Model AC, b = 25.4 mm, Grid CI, U = 3.0 m/s

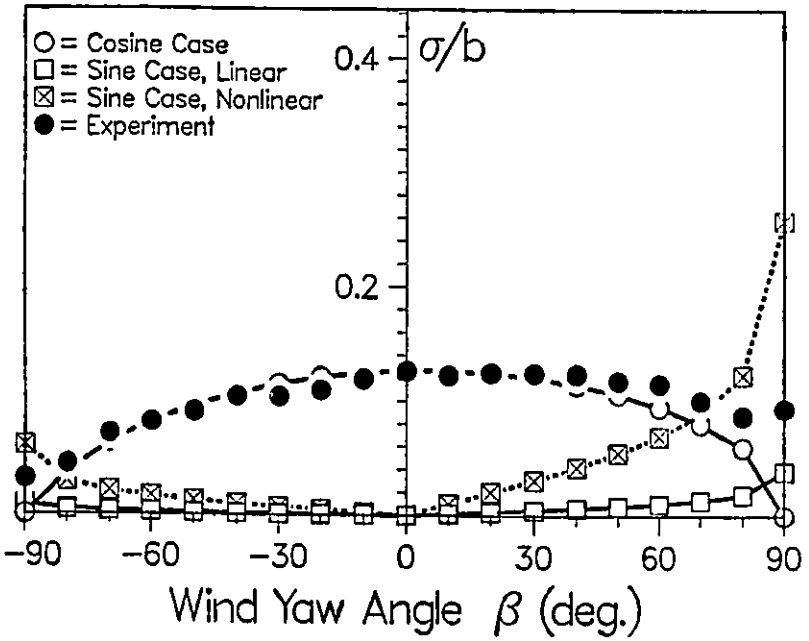

(b) Model AC, b = 25.4 mm, Grid CI, U = 6.1 m/s

Fig. 4.5. Results of Modified Buffeting Analysis

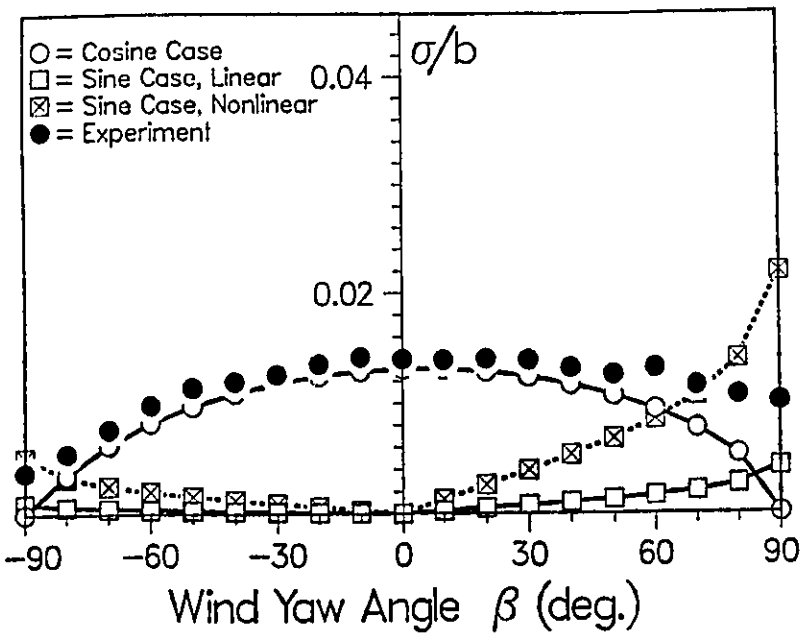

(c) Model AC, b = 25.4 mm, Grid CIII, U = 3.0 m/s

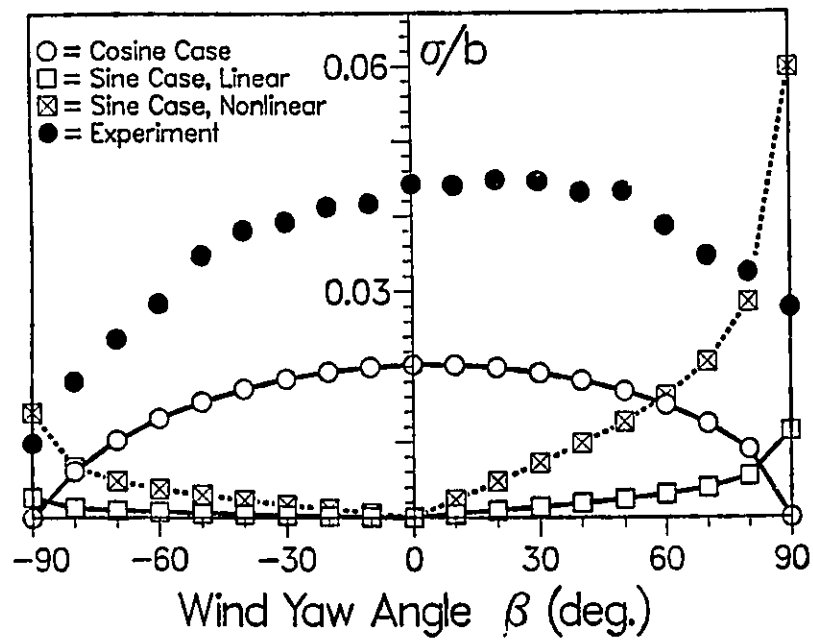

(d) Model AC, b = 25.4 mm, Grid CIII, U = 6.1 m/s

Fig. 4.5. Results of Modified Buffeting Analysis (Continued)

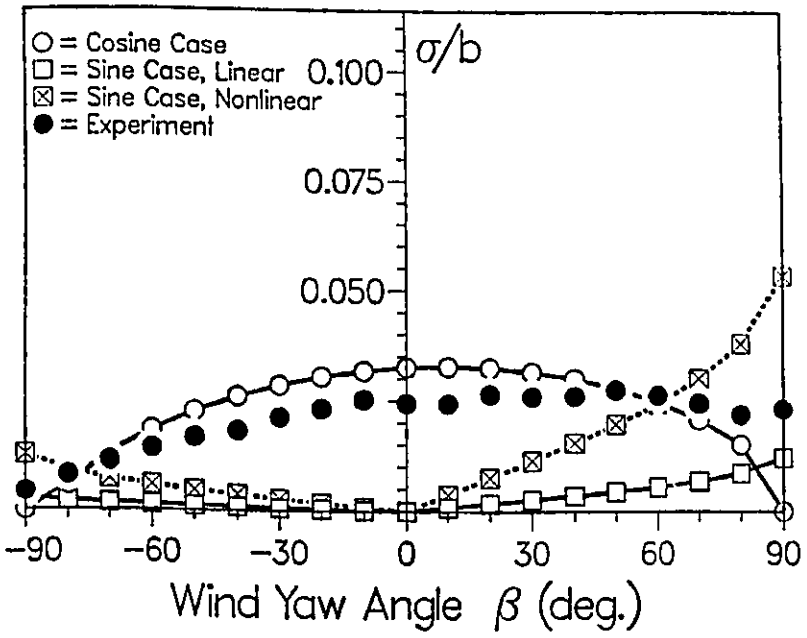

(e) Model AL, b = 50.8 mm, Grid CI, U = 3.0 m/s

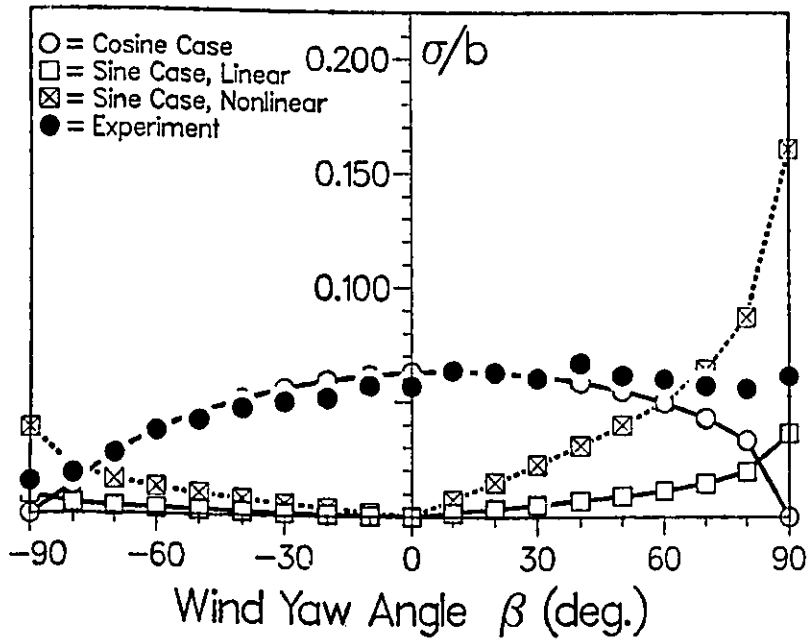

(f) Model AL, b = 50.8 mm, Grid CI, U = 6.1 m/s

Fig. 4.5. Results of Modified Buffeting Analysis (Continued)

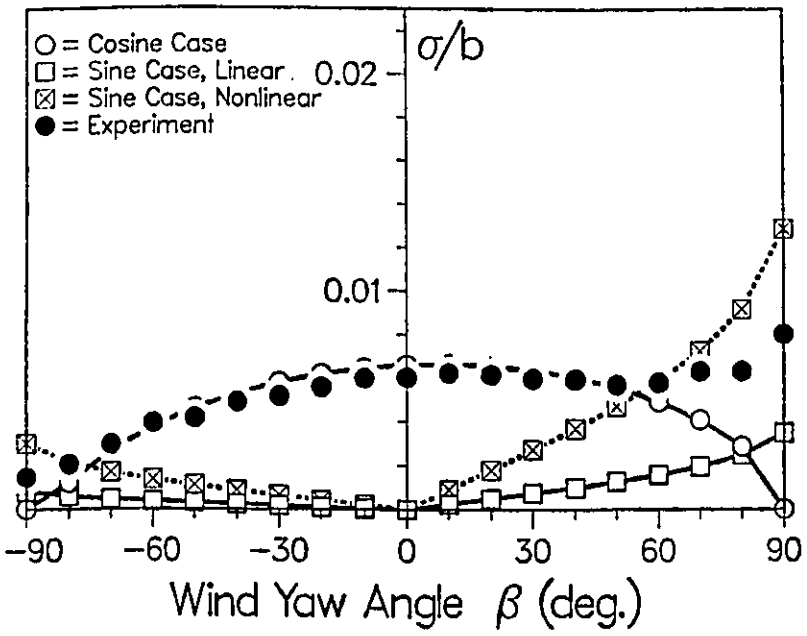

(g) Model AL, b = 50.8 mm, Grid CIII, U = 3.0 m/s

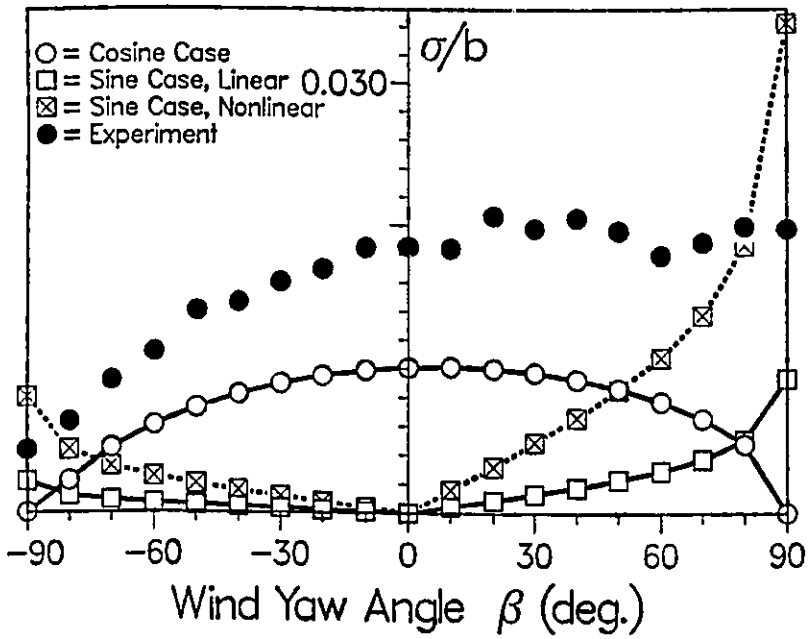

(h) Model AL, b = 50.8 mm, Grid CIII, U = 6.1 m/s

Fig. 4.5. Results of Modified Buffeting Analysis (Continued)

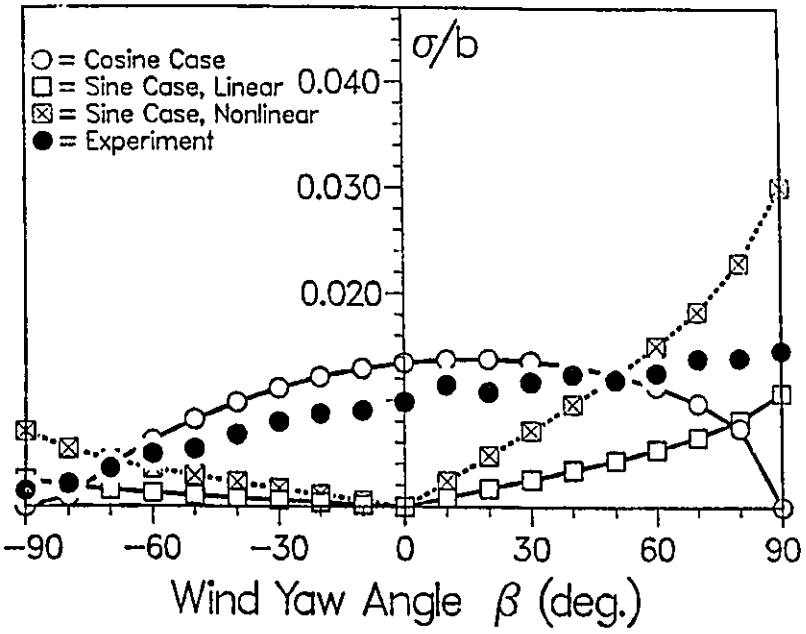

(i) Model AM, b = 102 mm, Grid CI, U = 3.0 m/s

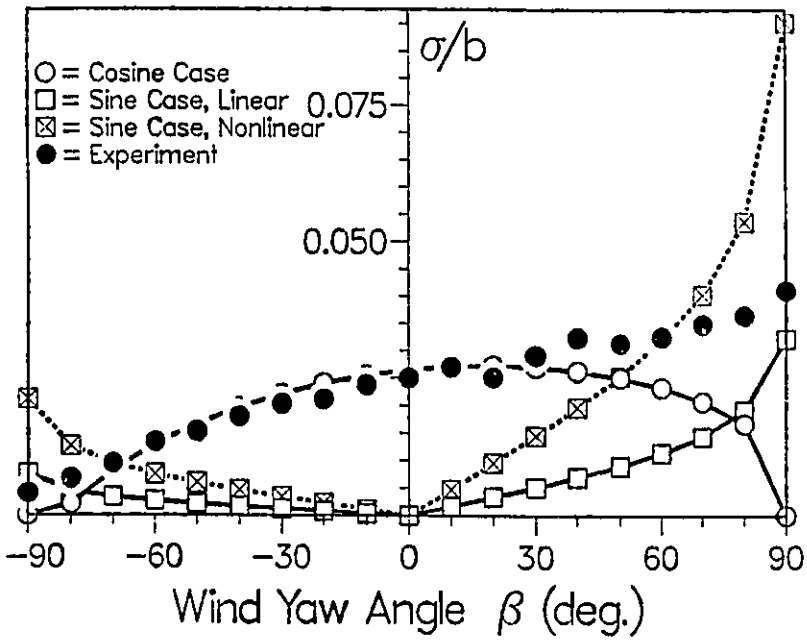

(j) Model AM, b = 102 mm, Grid CI, U = 6.1 m/s

Fig. 4.5. Results of Modified Buffeting Analysis (Continued)

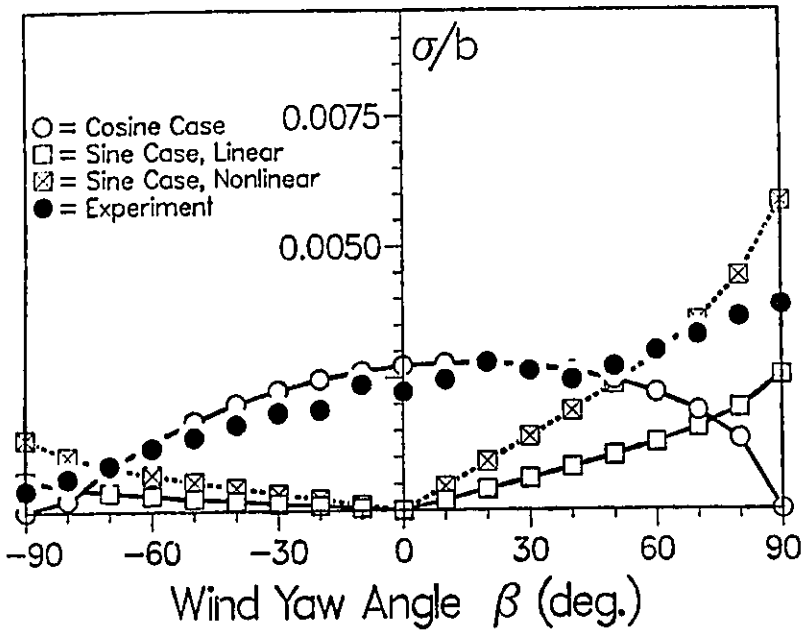

(k) Model AM, b = 102 mm, Grid CIII, U = 3.0 m/s

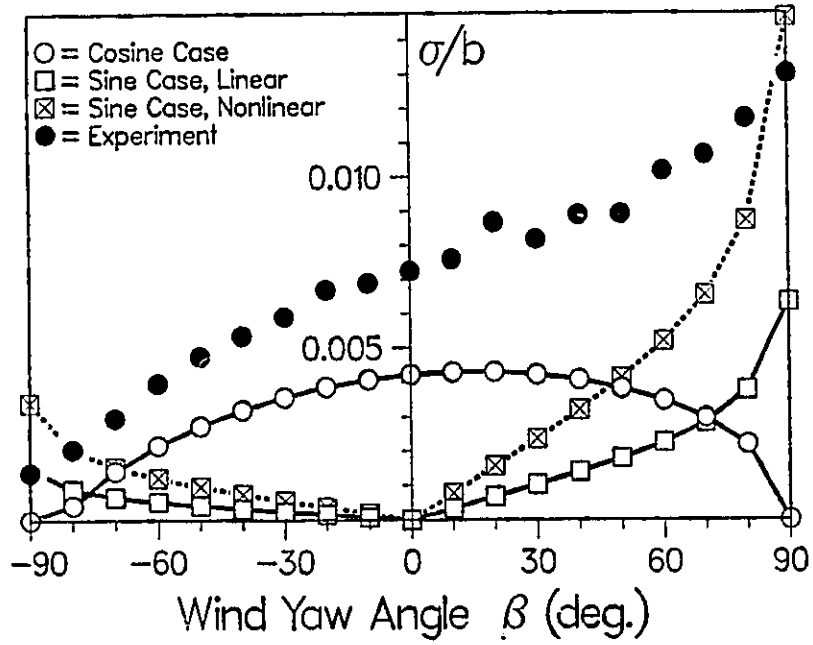

(l) Model AM, b = 102 mm, Grid CIII, U = 6.1 m/s

Fig. 4.5. Results of Modified Buffeting Analysis (Continued)

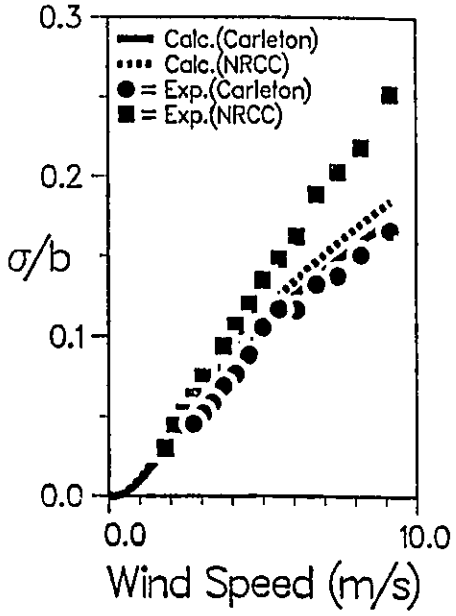

(a) β = 0°, Grid NI and CI

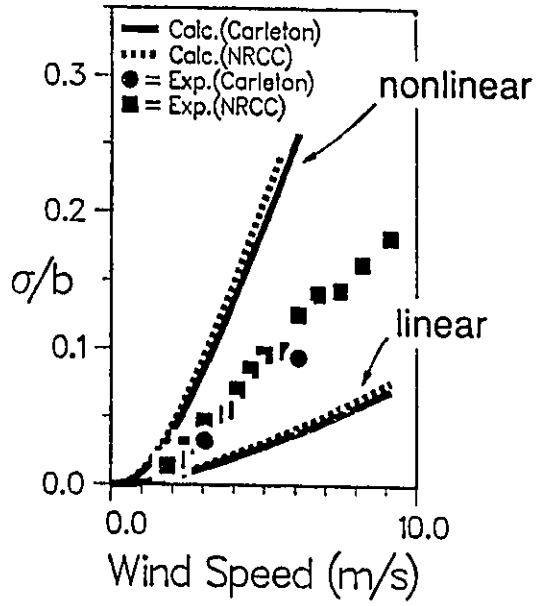

(b) β = 90°, Grid NI and CI

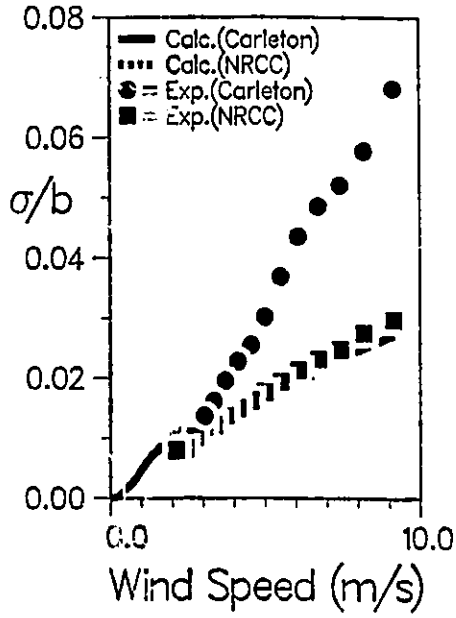

(c) β = 0°, Grid NIII and CIII

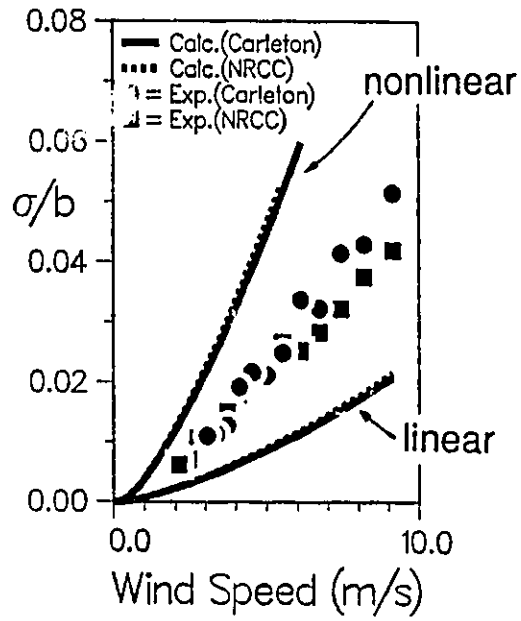

(d) β = 90°, Grid NIII and CIII

Fig. 4.6. Results of Analysis vs. Wind Speed, Model AC, b = 25.4 mm

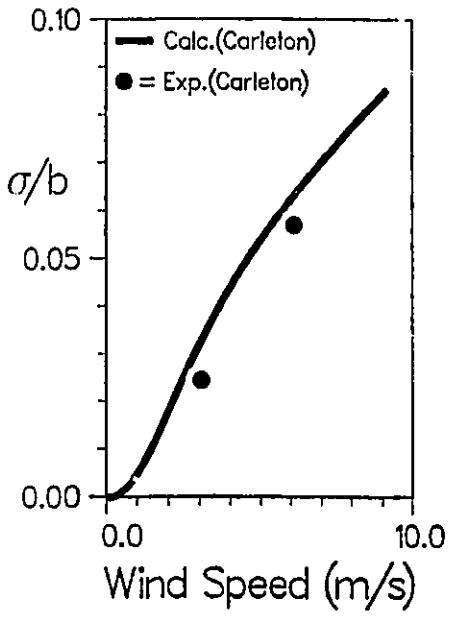

(e) β = 0°, Grid CI

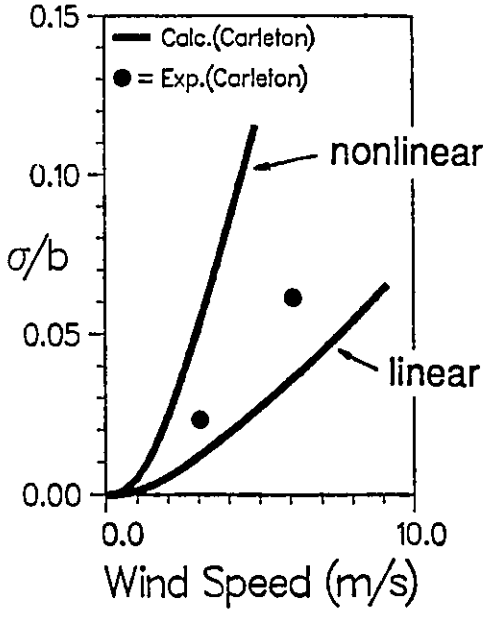

(f) β = 90°, Grid CI

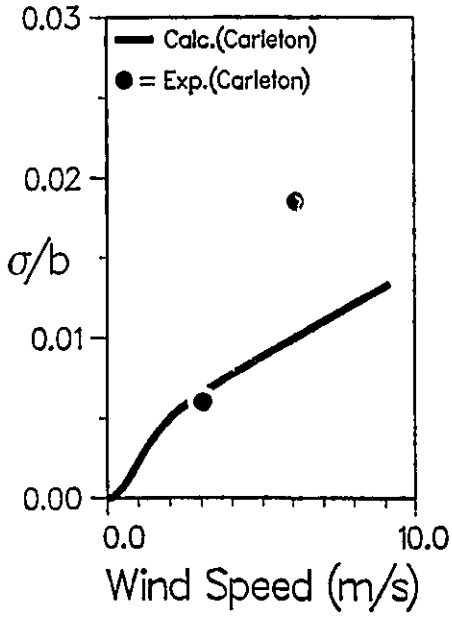

(g) β = 0°, Grid CIII

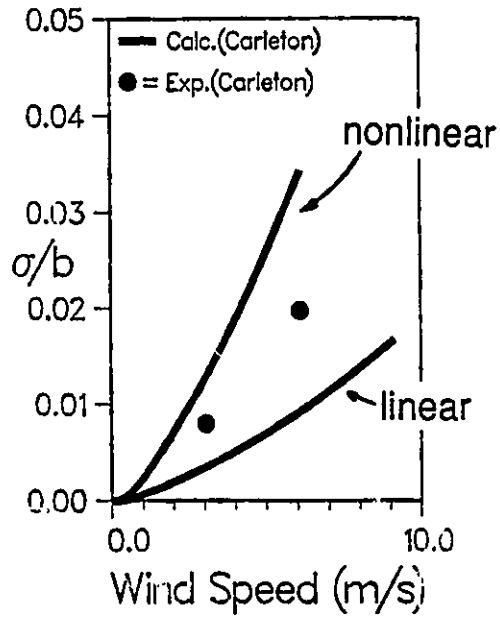

(h) β = 90°, Grid CIII

Fig. 4.6. Results of Analysis vs. Wind Speed, Model AL, b = 50.8 mm (Continued)

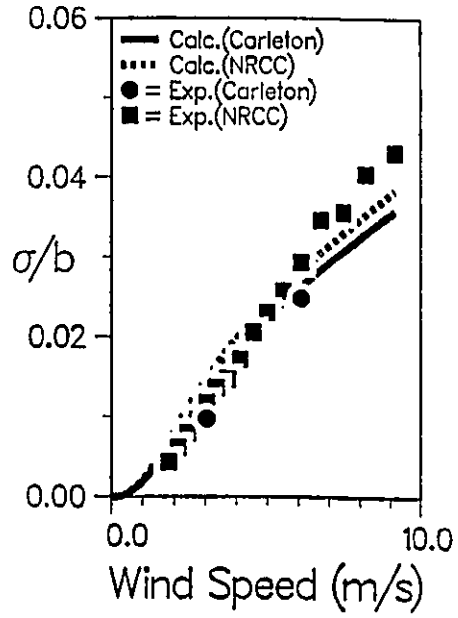

(i) β = 0°, Grid NI and CI

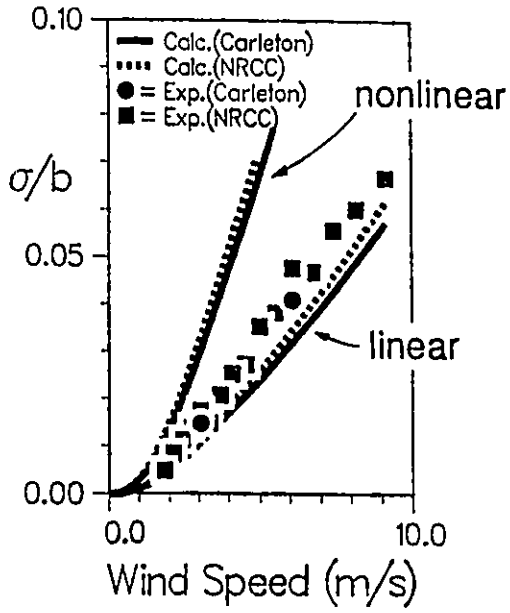

(j) β = 90°, Grid NI and CI

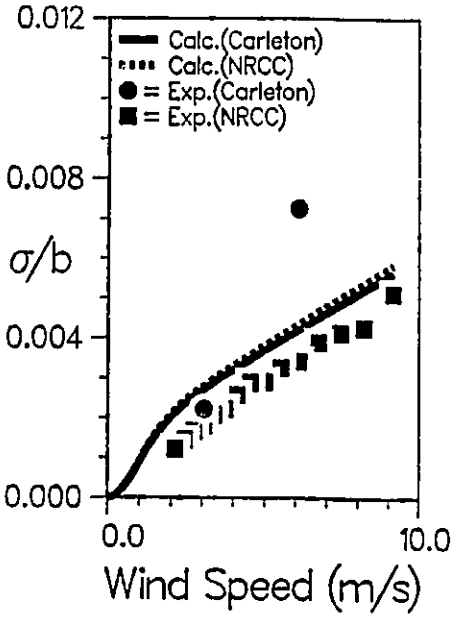

(k) β = 0°, Grid NIII and CIII

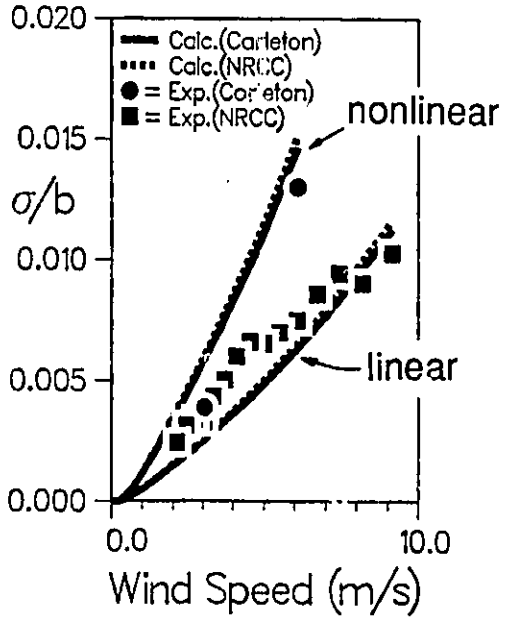

(l) β = 90°, Grid NIII and CIII

Fig. 4.6. Results of Analysis vs. Wind Speed, Model AM, b = 102 mm (Continued)

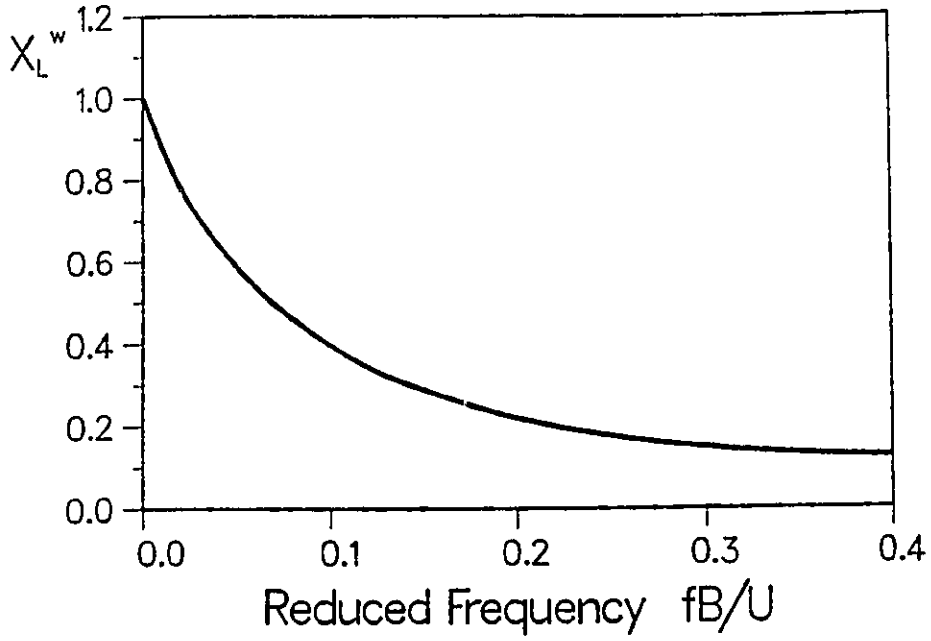

Fig. 5.1. Sears Function

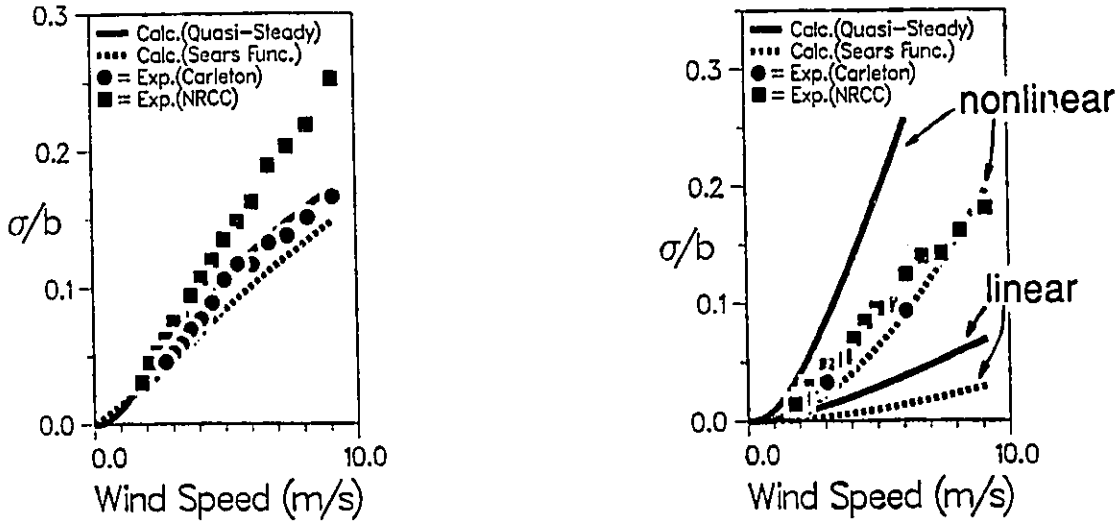

(a) β = 0°

(b) β = 90°

Fig. 5.2. Results with Aerodynamic Admittance, Model AC, Grid CI

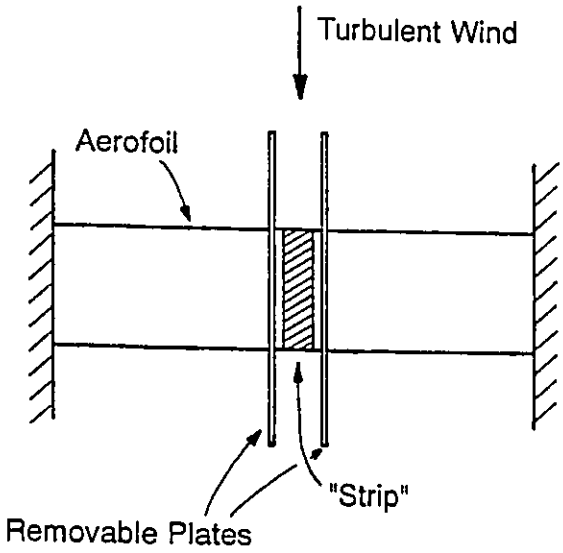

Fig. 5.3. Measurement of Fluctuating Lift Force on a Strip (Lamson, 1948)

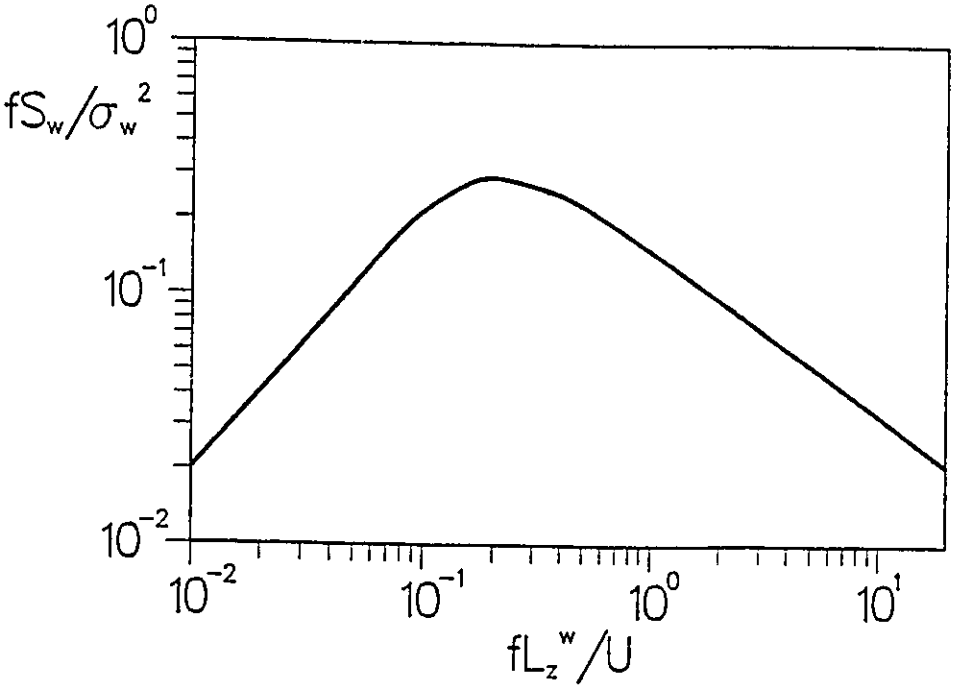

Fig. 5.4. Dimensionless von Kármán Spectrum for w-Component

PLATES

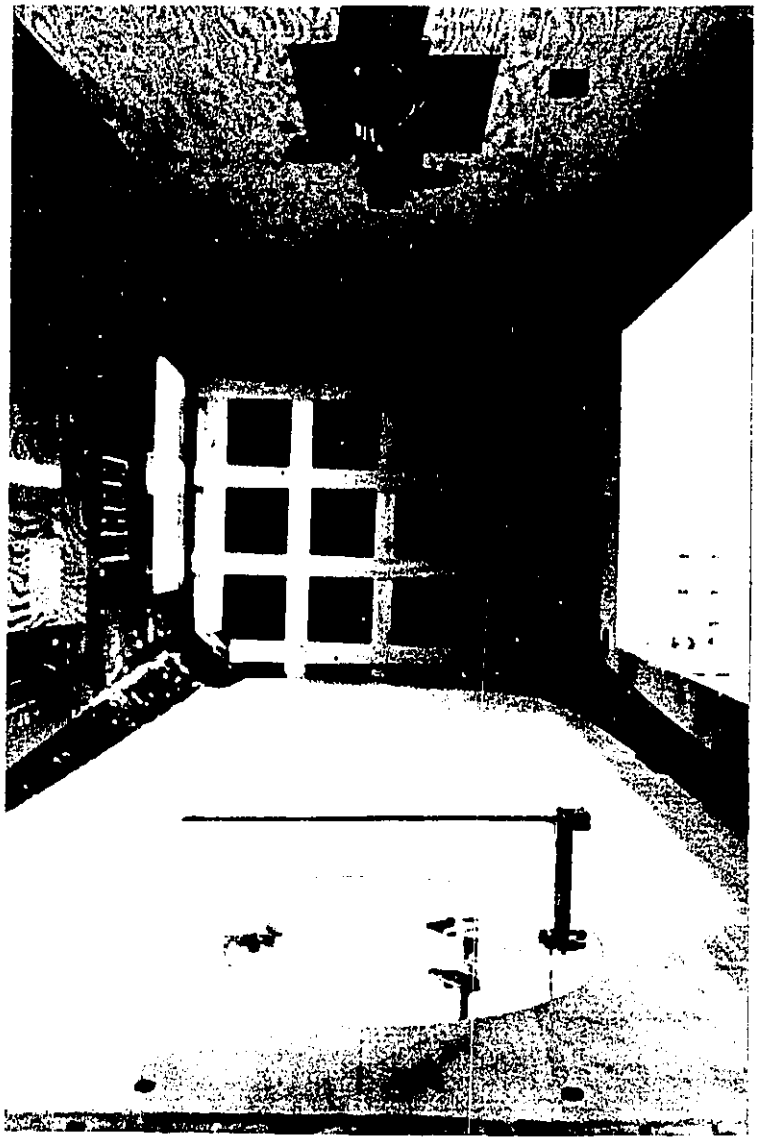

Plate 3.1. Experimental Set Up of Model SB with Grid NI

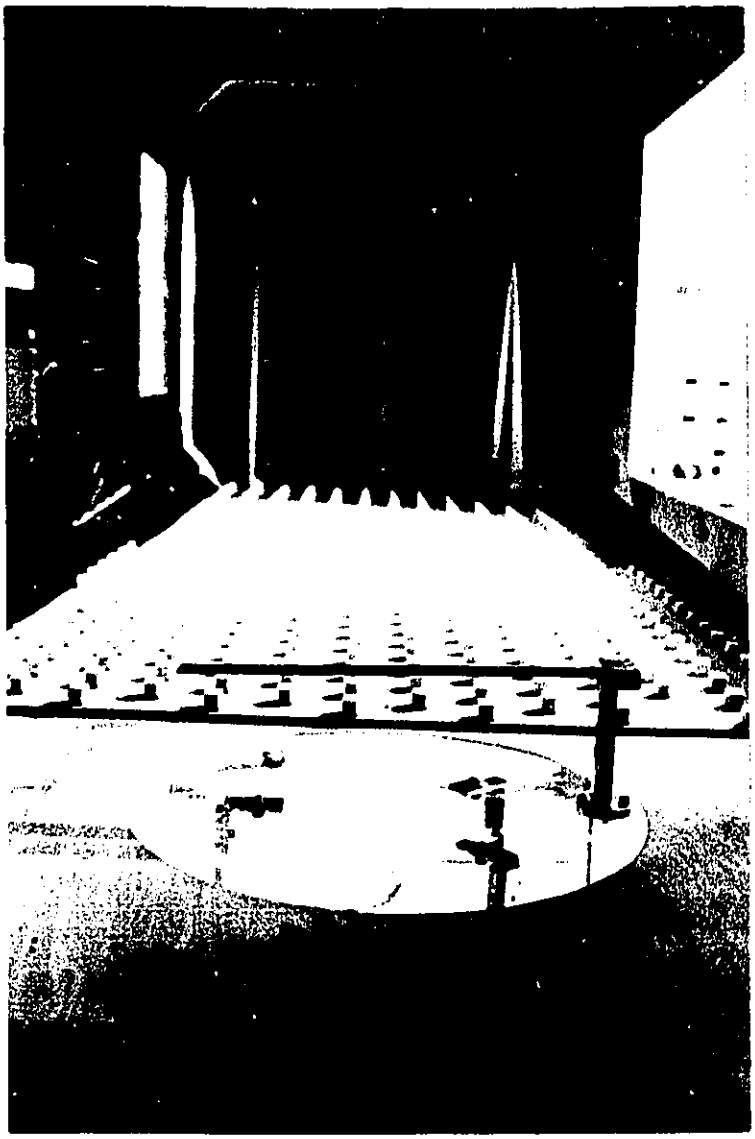

Plate 3.2. Experimental Set Up of Model SC with Spires and Roughness Blocks

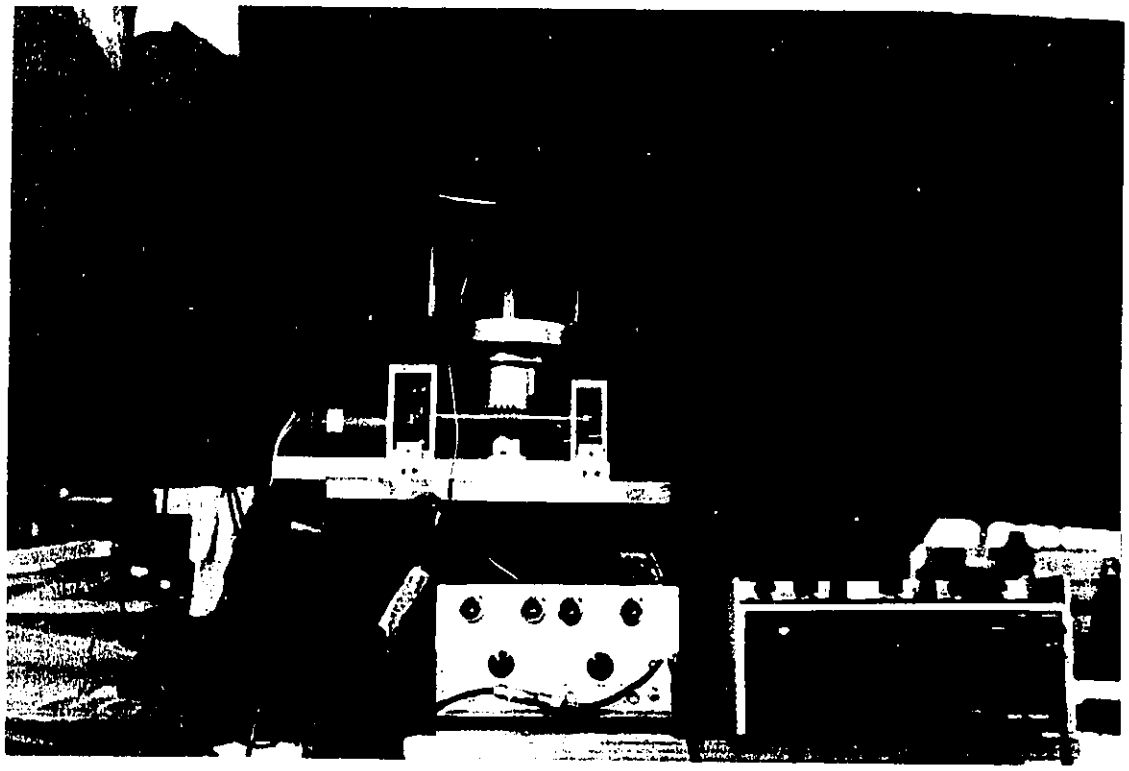

Plate 3.3. Supporting Mechanism for Steel Models

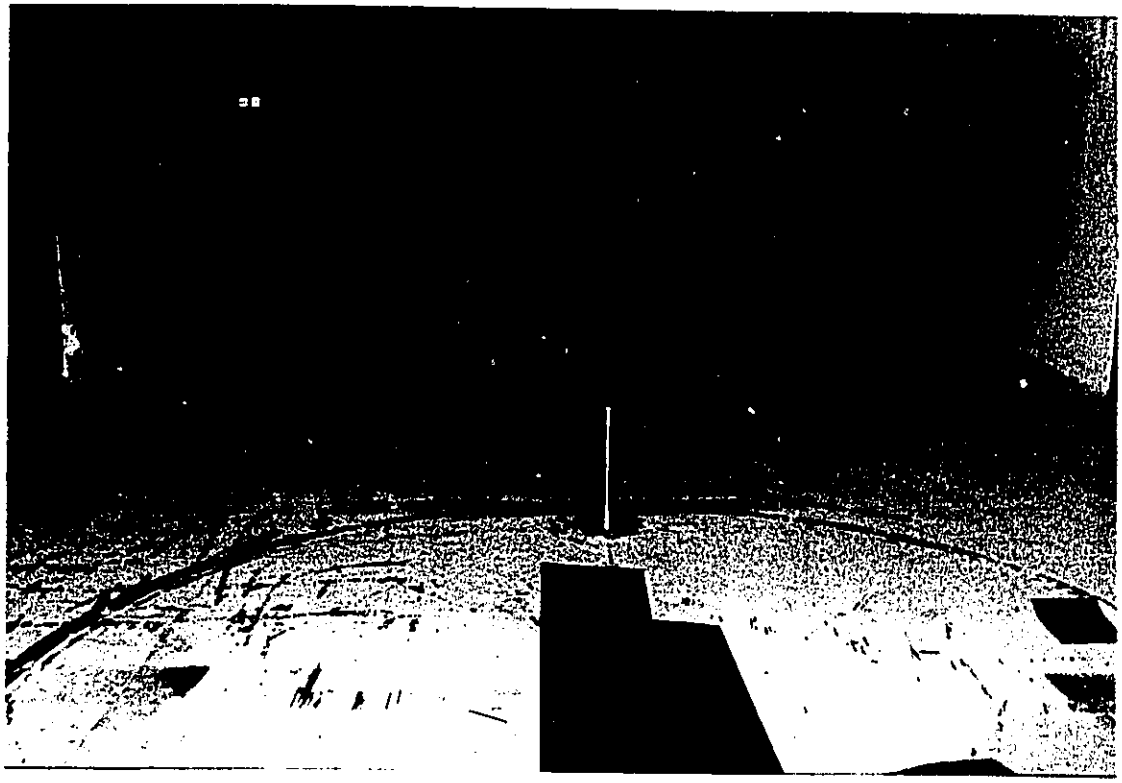

Plate 3.4. Experimental Set Up of Model AC with Grid CI

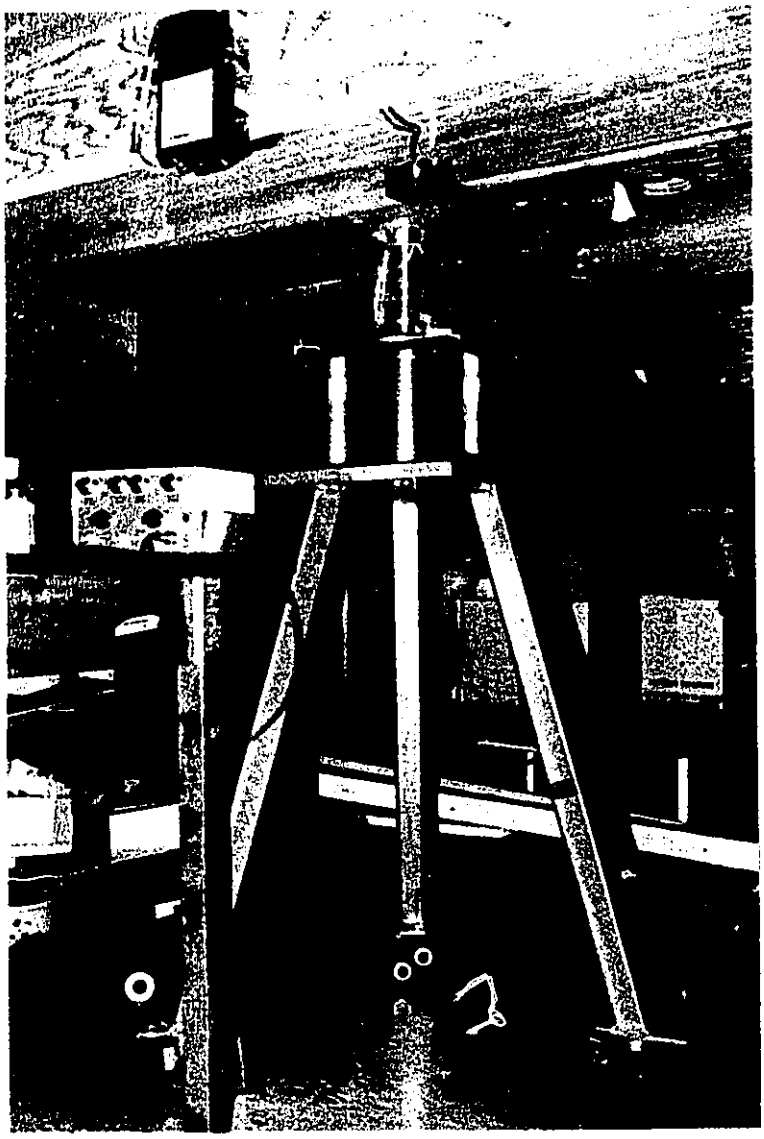

Plate 3.5. Supporting Mechanism for Aluminium Models

Plate 3.6. Sharp-Edged Model

APPENDIX A. MODEL RESPONSE RESULTS

Experimental results of the model response are tabulated in this appendix. The title of a case consists of the model name, flow name, type of the response and response measurement device, with this order. In the description of the response measurement device, HP ANALYZER means the Hewlett Packard Structural Dynamics Analyzer and HP D.V.M. means the Hewlett Packard digital voltmeter with dedicated desktop computer. The explanation of these devices is given in Section 3.2.5.

In the following, the vertical bending response results are listed first and then the torsional response of wider aluminium models. Within the same type of the response, responses of steel models are listed first. The models are arranged in alphabetical order. For the same model, responses in Grid CI are given first, then Grid NI, Grid NII, Grid CIII, Grid NIII, Shear Flow and Smooth Flow. For the same model and flow condition, a table of response vs. wind yaw angle is given first then response vs. wind speed.

The unit is tip deflection divided by the model width for the vertical bending response and degree at the tip for the torsional response. The r.m.s. responses are given for all cases and the peak responses are also given when available. Although the significant figures in the measurement were two or three, more digits are listed because of the convenience for printing. The ratio of the noise to the measurement in terms of r.m.s. (σ_n/σ_m) is used as the index for the noise level (see Section 3.2.5), and the maximum of the ratio in the corresponding column is given at the bottom of the table. In the row of the noise, "..." means the maximum of the ratio is less than 1%.

MODEL SA, FLOW: GRID NI, VERTICAL BENDING, TSI VOLTMETER

WIND YAW ANGLE(DEG.)	U=3.7 M/SEC R.M.S.	U=6.4 M/SEC R.M.S.	U=9.1 M/SEC R.M.S.
-90	0.12848	0.16544	0.25696
-80	0.13640	0.23584	0.26752
-70	0.14168	0.24640	0.32736
-60	0.16632	0.28864	0.46464
-50	0.17776	0.33792	0.52448
-40	0.20768	0.36608	0.54208
-30	0.21736	0.43648	0.58432
-20	0.19800	0.44352	0.67232
-10	0.21736	0.47520	0.69344
0	0.23760	0.49280	0.71104
10	0.19800	0.51392	0.70048
20	0.20768	0.43648	0.67232
30	0.21736	0.45408	0.68288
40	0.20768	0.47520	0.62304
50	0.20768	0.41536	0.64416
60	0.19800	0.38720	0.51392
70	0.17776	0.32736	0.45408
80	0.14344	0.27808	0.45408
90	0.13552	0.21824	0.32736
NOISE(%)	...	...	...

MODEL SA, FLOW: GRID NIII, VERTICAL BENDING, TSI VOLTMETER

WIND YAW ANGLE(DEG.)	U=3.7 M/SEC R.M.S.	U=6.4 M/SEC R.M.S.	U=9.1 M/SEC R.M.S.
-90	0.00760	0.01528	0.03133
-80	0.01795	0.03235	0.06114
-70	0.02246	0.04432	0.06410
-60	0.02545	0.04826	0.07899
-50	0.02844	0.05322	0.09282
-40	0.03242	0.05819	0.09085
-30	0.03443	0.06611	0.09976
-20	0.03443	0.07107	0.10571
-10	0.03344	0.07603	0.10373
0	0.03640	0.07304	0.10768
10	0.03242	0.07403	0.10866
20	0.03242	0.07008	0.11461
30	0.02946	0.06709	0.09976
40	0.02946	0.06118	0.09282
50	0.02647	0.05421	0.08490
60	0.02647	0.04928	0.08096
70	0.02246	0.05322	0.06906
80	0.02045	0.04530	0.06512
90	0.02045	0.04432	0.05618
NOISE(%)	...	...	...

MODEL SA, FLOW: GRID NII, VERTICAL BENDING, HP ANALYZER

WIND YAW ANGLE(DEG.)	U=3.7 M/SEC R.M.S.	U=6.4 M/SEC R.M.S.	U=9.1 M/SEC R.M.S.
-90	0.02008	0.03164	0.04786
-80	0.02488	0.06557	0.09251
-70	0.04473	0.08195	0.11443
-60	0.05620	0.10104	0.14092
-50	0.06296	0.11716	0.14978
-40	0.06723	0.12856	0.16203
-30	0.08148	0.14014	0.17096
-20	0.07735	0.13701	0.16730
-10	0.08156	0.14120	0.17060
0	0.08728	0.13651	0.17384
10	0.08848	0.13835	0.17666
20	0.08432	0.14189	0.17525
30	0.08095	0.13505	0.16767
40	0.06977	0.13269	0.16841
50	0.06696	0.12365	0.16126
60	0.05313	0.10996	0.14859
70	0.04949	0.09556	0.14406
80	0.03027	0.08440	0.11405
90	0.02651	0.05088	0.08791
NOISE(%)	1.7 MAX.	...	...

MODEL SA, FLOW: SHEAR FLOW, VERTICAL BENDING, HP ANALYZER

WIND YAW ANGLE(DEG.)	U=3.7 M/SEC R.M.S.	U=6.4 M/SEC R.M.S.	U=9.1 M/SEC R.M.S.
-90	0.04449	0.11183	0.17875
-80	0.06860	0.12697	0.21952
-70	0.08441	0.22229	0.28897
-60	0.10986	0.26872	0.38702
-50	0.12426	0.29635	0.44939
-40	0.13668	0.32581	0.49416
-30	0.16051	0.35756	0.52563
-20	0.15854	0.35056	0.51492
-10	0.16583	0.35721	0.53383
0	0.16203	0.36798	0.53383
10	0.15974	0.36798	0.55655
20	0.15636	0.36840	0.55432
30	0.15541	0.34880	0.54644
40	0.15974	0.33595	0.51130
50	0.14319	0.35721	0.52563
60	0.12324	0.32257	0.48390
70	0.09969	0.25911	0.41879
80	0.08585	0.21578	0.33336
90	0.06097	0.19452	0.30188
NOISE(%)	...	...	...

MODEL SB, FLOW: GRID NI, VERTICAL BENDING, HP ANALYZER

WIND YAW ANGLE(DEG.)	U=3.7 M/SEC R.M.S.	U=6.4 M/SEC R.M.S.	U=9.1 M/SEC R.M.S.
-90	0.02424	0.06388	0.09410
-80	0.03647	0.07480	0.12013
-70	0.06093	0.11402	0.17826
-60	0.05729	0.13596	0.19367
-50	0.07654	0.16611	0.22627
-40	0.08529	0.17251	0.22811
-30	0.08510	0.16545	0.25013
-20	0.09410	0.19390	0.25260
-10	0.09344	0.19746	0.26516
0	0.09475	0.19124	0.28105
10	0.10153	0.19581	0.28159
20	0.09621	0.18995	0.28324
30	0.10108	0.18423	0.27772
40	0.09109	0.18888	0.26807
50	0.09159	0.18118	0.26865
60	0.07594	0.16915	0.24639
70	0.06961	0.16271	0.22940
80	0.05798	0.11998	0.20020
90	0.05075	0.11497	0.18458
NOISE(%)	...	...	...

MODEL SB, FLOW: GRID NII, VERTICAL BENDING, HP ANALYZER

WIND YAW ANGLE(DEG.)	U=3.7 M/SEC R.M.S.	U=6.4 M/SEC R.M.S.	U=9.1 M/SEC R.M.S.
-90	0.01118	0.02115	0.02971
-80	0.01864	0.03186	0.04320
-70	0.02362	0.04466	0.05379
-60	0.02972	0.05665	0.06773
-50	0.03444	0.06081	0.07461
-40	0.04029	0.06636	0.07570
-30	0.04379	0.06731	0.08044
-20	0.04132	0.07064	0.08530
-10	0.04379	0.07582	0.09024
0	0.04640	0.07704	0.08421
10	0.04358	0.07392	0.08674
20	0.04491	0.07212	0.08763
30	0.04029	0.07601	0.08833
40	0.03927	0.06989	0.08457
50	0.03916	0.06671	0.08158
60	0.03119	0.05802	0.07322
70	0.02732	0.04832	0.06893
80	0.02248	0.04946	0.05681
90	0.02270	0.03986	0.05107
NOISE(%)	1.2 MAX.	...	...

MODEL SB, FLOW: GRID NIII, VERTICAL BENDING, HP ANALYZER

WIND YAW ANGLE(DEG.)	U=3.7 M/SEC R.M.S.	U=6.4 M/SEC R.M.S.	U=9.1 M/SEC R.M.S.
-90	0.00498	0.01207	0.01975
-80	0.00869	0.02078	0.02944
-70	0.01206	0.02333	0.03301
-60	0.01463	0.02537	0.03403
-50	0.01514	0.02588	0.03657
-40	0.01412	0.02537	0.03759
-30	0.01514	0.02639	0.03708
-20	0.01514	0.02639	0.03912
-10	0.01463	0.02791	0.03912
0	0.01668	0.02842	0.04014
10	0.01617	0.02791	0.04014
20	0.01565	0.02791	0.03963
30	0.01617	0.02588	0.03912
40	0.01463	0.02486	0.03810
50	0.01412	0.02486	0.03810
60	0.01412	0.02282	0.03555
70	0.01206	0.02282	0.03504
80	0.01206	0.02333	0.03250
90	0.01154	0.02027	0.03097
NOISE(%)	6.7 MAX.	1.1 MAX.	...

MODEL SB, FLOW: SHEAR FLOW, VERTICAL BENDING, HP ANALYZER

WIND YAW ANGLE(DEG.)	U=3.7 M/SEC R.M.S.	U=6.4 M/SEC R.M.S.	U=9.1 M/SEC R.M.S.
-90	0.02045	0.06146	0.09638
-80	0.02455	0.07416	0.13122
-70	0.04379	0.11336	0.16481
-60	0.05613	0.13620	0.19415
-50	0.06536	0.13505	0.21177
-40	0.08439	0.16206	0.20994
-30	0.07543	0.16167	0.25137
-20	0.07986	0.16677	0.24500
-10	0.07947	0.17713	0.25745
0	0.08439	0.17162	0.25806
10	0.07909	0.16518	0.25806
20	0.08530	0.17431	0.26516
30	0.07229	0.19327	0.27660
40	0.07888	0.18094	0.25745
50	0.07485	0.16042	0.25443
60	0.07011	0.15492	0.25321
70	0.05194	0.14242	0.21119
80	0.04538	0.12629	0.21258
90	0.03888	0.10660	0.14808
NOISE(%)	...	...	...

MODEL SC, FLOW: GRID NI, VERTICAL BENDING, TSI VOLTMETER

WIND YAW ANGLE(DEG.)	U=3.7 M/SEC R.M.S.	U=6.4 M/SEC R.M.S.	U=9.1 M/SEC R.M.S.
-90	0.01388	0.02449	0.04385
-80	0.01517	0.04514	0.05418
-70	0.02448	0.05160	0.07741
-60	0.02680	0.05676	0.10580
-50	0.03791	0.08516	0.11096
-40	0.03868	0.09289	0.11870
-30	0.04437	0.09031	0.13935
-20	0.04127	0.10064	0.13677
-10	0.04850	0.10838	0.14451
0	0.05159	0.11355	0.14451
10	0.05159	0.10838	0.14709
20	0.05159	0.10838	0.15741
30	0.05418	0.10838	0.15999
40	0.05159	0.10838	0.15484
50	0.04644	0.11096	0.14967
60	0.04514	0.09289	0.14709
70	0.04257	0.09548	0.13419
80	0.03353	0.08516	0.10838
90	0.02965	0.08257	0.11354
NOISE(%)	...	...	...

MODEL SC, FLOW: GRID NII, VERTICAL BENDING, HP ANALYZER

WIND YAW ANGLE(DEG.)	U=3.7 M/SEC R.M.S.	U=6.4 M/SEC R.M.S.	U=9.1 M/SEC R.M.S.
-90	0.00486	0.00737	0.01114
-80	0.00668	0.01280	0.01955
-70	0.01104	0.01941	0.02542
-60	0.01287	0.02462	0.03191
-50	0.01772	0.02619	0.03274
-40	0.01772	0.02965	0.03418
-30	0.01797	0.02937	0.03679
-20	0.01854	0.03182	0.03679
-10	0.01786	0.03146	0.03848
0	0.01922	0.03398	0.03748
10	0.02124	0.03236	0.03437
20	0.01891	0.03169	0.03661
30	0.01962	0.03531	0.04070
40	0.01874	0.03119	0.03921
50	0.01697	0.02915	0.03824
60	0.01511	0.02871	0.03638
70	0.01429	0.02563	0.03626
80	0.01215	0.02291	0.02846
90	0.01127	0.02272	0.03687
NOISE(%)	2.0 MAX.	...	...

MODEL SC, FLOW: GRID NIII, VERTICAL BENDING, TSI VOLTMETER

WIND YAW ANGLE(DEG.)	U=3.7 M/SEC R.M.S.	U=6.4 M/SEC R.M.S.	U=9.1 M/SEC R.M.S.
-90	0.00200	0.00453	0.00742
-80	0.00508	0.00742	0.01338
-70	0.00561	0.00898	0.01338
-60	0.00665	0.01001	0.01441
-50	0.00612	0.01027	0.01520
-40	0.00612	0.01079	0.01623
-30	0.00561	0.01079	0.01597
-20	0.00691	0.01183	0.01752
-10	0.00665	0.01157	0.01881
0	0.00691	0.01209	0.01907
10	0.00665	0.01209	0.01959
20	0.00665	0.01209	0.01830
30	0.00691	0.01183	0.01907
40	0.00665	0.01183	0.01881
50	0.00587	0.01131	0.01778
60	0.00534	0.01131	0.01778
70	0.00587	0.01183	0.01959
80	0.00612	0.01209	0.01984
90	0.00587	0.01338	0.02166
NOISE(%)	9.0 MAX.	2.5 MAX.	...

MODEL SC, FLOW: SHEAR FLOW, VERTICAL BENDING, HP ANALYZER

WIND YAW ANGLE(DEG.)	U=3.7 M/SEC R.M.S.	U=6.4 M/SEC R.M.S.	U=9.1 M/SEC R.M.S.
-90	0.01162	0.02661	0.04118
-80	0.01718	0.03650	0.05183
-70	0.02347	0.05402	0.07841
-60	0.02915	0.06265	0.09457
-50	0.03145	0.06648	0.10695
-40	0.03581	0.07579	0.10702
-30	0.03597	0.08236	0.11030
-20	0.03854	0.07944	0.11638
-10	0.03688	0.08305	0.11959
0	0.03631	0.07953	0.12001
10	0.03808	0.08422	0.12900
20	0.03736	0.08385	0.12345
30	0.03771	0.09333	0.13287
40	0.03722	0.08764	0.12873
50	0.04060	0.08422	0.13432
60	0.03315	0.07953	0.12376
70	0.03127	0.06489	0.13403
80	0.03045	0.07277	0.11259
90	0.02520	0.06102	0.11037
NOISE(%)	...	...	...

MODEL SD, FLOW: GRID NI, VERTICAL BENDING, TSI VOLTMETER

WIND YAW ANGLE(DEG.)	U=3.7 M/SEC R.M.S.	U=6.4 M/SEC R.M.S.	U=9.1 M/SEC R.M.S.
-90	0.06479	0.03702	0.06159
-80	0.06301	0.05411	0.09470
-70	0.04735	0.06159	0.12175
-60	0.03738	0.09434	0.15771
-50	0.04165	0.10787	0.21182
-40	0.03916	0.13492	0.22535
-30	0.04699	0.15308	0.27946
-20	0.05340	0.14418	0.27020
-10	0.05091	0.15771	0.27483
0	0.05376	0.17124	0.29299
10	0.05376	0.16661	0.27483
20	0.05767	0.15308	0.27946
30	0.06052	0.16198	0.27946
40	0.05874	0.14418	0.27483
50	0.03738	0.11250	0.22998
60	0.04343	0.11250	0.22072
70	0.03311	0.09434	0.18939
80	0.02599	0.08010	0.12602
90	0.02207	0.05162	0.11250
NOISE(%)	...	...	...

MODEL SD, FLOW: GRID NII, VERTICAL BENDING, HP ANALYZER

WIND YAW ANGLE(DEG.)	U=3.7 M/SEC R.M.S.	U=9.1 M/SEC R.M.S.
-90	0.00610	0.01965
-80	0.00809	0.03734
-70	0.01355	0.05148
-60	0.01870	0.06857
-50	0.02446	0.07485
-40	0.02798	0.08289
-30	0.03072	0.09284
-20	0.03490	0.09559
-10	0.03453	0.09453
0	0.03630	0.10519
10	0.03739	0.10057
20	0.03477	0.09613
30	0.03186	0.09147
40	0.02995	0.09513
50	0.02582	0.08418
60	0.02094	0.07236
70	0.01533	0.06000
80	0.01035	0.04289
90	0.00728	0.02993
NOISE(%)	14.0 MAX.	29. MAX.

MODEL SD, FLOW: GRID NIII, VERTICAL BENDING, HP ANALYZER

WIND YAW ANGLE(DEG.)	U=3.7 M/SEC R.M.S.	U=6.4 M/SEC R.M.S.	U=9.1 M/SEC R.M.S.
-90	0.00531	0.00858	0.01553
-80	0.00927	0.01674	0.02733
-70	0.01056	0.02260	0.03441
-60	0.01420	0.02973	0.03759
-50	0.01659	0.03091	0.03996
-40	0.01826	0.03353	0.04515
-30	0.01992	0.03497	0.04612
-20	0.02136	0.03599	0.04592
-10	0.02201	0.03641	0.04458
0	0.02058	0.03444	0.04415
10	0.02160	0.03371	0.04809
20	0.02100	0.03488	0.04612
30	0.01794	0.03225	0.04503
40	0.01686	0.03142	0.04485
50	0.01461	0.03067	0.04162
60	0.01424	0.02799	0.04231
70	0.01068	0.02192	0.03579
80	0.00737	0.01604	0.02693
90	0.00507	0.00899	0.01871
NOISE(%)	13.6 MAX.	28. MAX.	34. MAX.

MODEL SD, FLOW: SHEAR FLOW, VERTICAL BENDING, HP ANALYZER

WIND YAW ANGLE(DEG.)	U=3.7 M/SEC R.M.S.	U=6.4 M/SEC R.M.S.	U=9.1 M/SEC R.M.S.
-90	0.00933	0.03200	0.05522
-80	0.01253	0.04179	0.08277
-70	0.02058	0.06771	0.11210
-60	0.02706	0.08416	0.13279
-50	0.03389	0.10584	0.17270
-40	0.03706	0.11011	0.18729
-30	0.04422	0.12404	0.19388
-20	0.05162	0.13500	0.20712
-10	0.05198	0.13645	0.22638
0	0.05020	0.14080	0.22193
10	0.04802	0.14706	0.22246
20	0.04931	0.13574	0.22364
30	0.04635	0.12428	0.21566
40	0.04204	0.12243	0.19608
50	0.03496	0.11919	0.17750
60	0.03496	0.10000	0.16248
70	0.02449	0.07465	0.13507
80	0.01663	0.05614	0.09541
90	0.01043	0.04920	0.07195
NOISE(%)	...	...	...

MODEL SE, FLOW: CRID NI, VERTICAL BENDING, HP ANALYZER

WIND YAW ANGLE(DEG.)	U=3.7 M/SEC R.M.S.	U=6.4 M/SEC R.M.S.	U=9.1 M/SEC R.M.S.
-90	0.00541	0.01581	0.03681
-80	0.00625	0.02156	0.04609
-70	0.00960	0.03502	0.06132
-60	0.01459	0.04521	0.08443
-50	0.01784	0.05278	0.09384
-40	0.01906	0.05541	0.10271
-30	0.02379	0.06695	0.12229
-20	0.02215	0.06667	0.11341
-10	0.02380	0.06774	0.11563
0	0.02690	0.07383	0.12189
10	0.02508	0.07058	0.11767
20	0.02619	0.06970	0.13019
30	0.02674	0.07229	0.11563
40	0.02227	0.06850	0.11522
50	0.02028	0.05944	0.10709
60	0.01823	0.05863	0.09452
70	0.01414	0.04608	0.08683
80	0.01140	0.03957	0.06857
90	0.00874	0.02936	0.05789
NOISE(%)	28. MAX.	2.4 MAX.	...

MODEL SE, FLOW: GRID NIII, VERTICAL BENDING, HP ANALYZER

WIND YAW ANGLE(DEG.)	U=3.7 M/SEC R.M.S.	U=6.4 M/SEC R.M.S.	U=9.1 M/SEC R.M.S.
-90	0.00217	0.00594	0.00199
-80	0.00351	0.00812	0.00547
-70	0.00530	0.01110	0.01262
-60	0.00641	0.01196	0.01447
-50	0.00800	0.01439	0.01631
-40	0.00802	0.01507	0.01574
-30	0.00947	0.01415	0.01655
-20	0.00860	0.01458	0.01703
-10	0.00991	0.01501	0.01665
0	0.01063	0.01477	0.01711
10	0.00928	0.01529	0.01606
20	0.00878	0.01347	0.01483
30	0.00816	0.01420	0.01531
40	0.00821	0.01382	0.01785
50	0.00755	0.01384	0.01680
60	0.00678	0.01220	0.01790
70	0.00509	0.01060	0.01627
80	0.00381	0.00804	0.01277
90	0.00305	0.00585	0.01036
NOISE(%)	22. MAX.	9.2 MAX.	83. MAX.

MODEL SE, FLOW: GRID NII, VERTICAL BENDING, HP ANALYZER

WIND YAW ANGLE(DEG.)	U=3.7 M/SEC R.M.S.	U=6.4 M/SEC R.M.S.	U=9.1 M/SEC R.M.S.
-90	0.00279	0.00967	0.00928
-80	0.00460	0.01282	0.01653
-70	0.00755	0.02041	0.02496
-60	0.01034	0.02034	0.03040
-50	0.01226	0.02701	0.03371
-40	0.01360	0.02617	0.03812
-30	0.01468	0.02948	0.03669
-20	0.01514	0.02816	0.03799
-10	0.01658	0.02883	0.04089
0	0.01582	0.03012	0.04058
10	0.01631	0.02877	0.04026
20	0.01594	0.02787	0.03878
30	0.01512	0.02838	0.03816
40	0.01371	0.02736	0.03694
50	0.01174	0.02405	0.03404
60	0.01088	0.02357	0.03118
70	0.00886	0.01724	0.02721
80	0.00599	0.01310	0.02235
90	0.00487	0.01081	0.01769
NOISE(%)	16.1 MAX.	11.0 MAX.	40. MAX.

MODEL SE, FLOW: SHEAR FLOW, VERTICAL BENDING, HP ANALYZER

WIND YAW ANGLE(DEG.)	U=3.7 M/SEC R.M.S.	U=6.4 M/SEC R.M.S.	U=9.1 M/SEC R.M.S.
-90	0.00417	0.01755	0.02713
-80	0.00580	0.02242	0.04213
-70	0.00878	0.03341	0.05621
-60	0.01269	0.04114	0.06897
-50	0.01573	0.04479	0.08419
-40	0.01865	0.05218	0.08494
-30	0.02210	0.06334	0.09713
-20	0.02045	0.05821	0.09875
-10	0.02126	0.06097	0.10344
0	0.02266	0.06349	0.10983
10	0.02286	0.06309	0.10221
20	0.02089	0.06268	0.09859
30	0.01997	0.05655	0.09548
40	0.01845	0.05464	0.09713
50	0.01622	0.05073	0.09278
60	0.01418	0.05007	0.07849
70	0.01048	0.03777	0.06431
80	0.00779	0.03279	0.05245
90	0.00640	0.02666	0.04899
NOISE(%)	9.1 MAX.	...	2.6 MAX.

MODEL SF, FLOW: GRID NI, VERTICAL BENDING, TSI VOLTMETER

WIND YAW ANGLE(DEG.)	U=3.7 M/SEC R.M.S.	U=6.4 M/SEC R.M.S.	U=9.1 M/SEC R.M.S.
-90	0.00635	0.00973	0.01519
-80	0.00635	0.01056	0.02221
-70	0.00683	0.01507	0.03040
-60	0.00789	0.02036	0.03976
-50	0.00906	0.02799	0.04444
-40	0.00977	0.03034	0.04912
-30	0.01024	0.03268	0.06198
-20	0.01177	0.03268	0.06198
-10	0.01258	0.03386	0.06081
0	0.01282	0.03854	0.06666
10	0.01341	0.03737	0.06900
20	0.01224	0.03854	0.05081
30	0.01142	0.03737	0.05964
40	0.01224	0.03971	0.05730
50	0.01071	0.03268	0.05730
60	0.00953	0.03151	0.05497
70	0.00813	0.02917	0.05497
80	0.00611	0.02213	0.04444
90	0.00635	0.02036	0.04444
NOISE(%)	1.5 MAX.	2.2 MAX.	...

MODEL SF, FLOW: GRID NIII, VERTICAL BENDING, HP ANALYZER

WIND YAW ANGLE(DEG.)	U=3.7 M/SEC R.M.S.	U=6.4 M/SEC R.M.S.
-90	0.00112	0.00133
-80	0.00159	0.00283
-70	0.00222	0.00411
-60	0.00271	0.00528
-50	0.00316	0.00509
-40	0.00352	0.00553
-30	0.00373	0.00627
-20	0.00360	0.00582
-10	0.00380	0.00668
0	0.00424	0.00630
10	0.00431	0.00656
20	0.00411	0.00586
30	0.00371	0.00651
40	0.00356	0.00625
50	0.00386	0.00619
60	0.00312	0.00633
70	0.00307	0.00512
80	0.00238	0.00471
90	0.00222	0.00438
NOISE(%)	26. MAX.	46. MAX.

MODEL SF, FLOW: GRID NII, VERTICAL BENDING, HP ANALYZER

WIND YAW ANGLE(DEG.)	U=3.7 M/SEC R.M.S.	U=6.4 M/SEC R.M.S.	U=9.1 M/SEC R.M.S.
-90	0.00160	0.00384	0.00463
-80	0.00213	0.00583	0.00604
-70	0.00352	0.00820	0.01005
-60	0.00457	0.01041	0.01219
-50	0.00522	0.01173	0.01232
-40	0.00623	0.01234	0.01517
-30	0.00678	0.01363	0.01535
-20	0.00715	0.01384	0.01815
-10	0.00783	0.01338	0.01695
0	0.00808	0.01427	0.01943
10	0.00753	0.01429	0.01857
20	0.00757	0.01407	0.01830
30	0.00738	0.01381	0.01891
40	0.00715	0.01361	0.01922
50	0.00716	0.01238	0.01935
60	0.00572	0.01221	0.01933
70	0.00526	0.01053	0.02215
80	0.00396	0.01004	0.01927
90	0.00404	0.00728	0.02035
NOISE(%)	11.3 MAX.	9.5 MAX.	60. MAX.

MODEL SF, FLOW: SHEAR FLOW, VERTICAL BENDING, HP ANALYZER

WIND YAW ANGLE(DEG.)	U=3.7 M/SEC R.M.S.	U=6.4 M/SEC R.M.S.	U=9.1 M/SEC R.M.S.
-90	0.00227	0.00760	0.01287
-80	0.00336	0.01199	0.01970
-70	0.00522	0.01551	0.02731
-60	0.00625	0.01984	0.03289
-50	0.00759	0.02310	0.03718
-40	0.00813	0.02586	0.04137
-30	0.00960	0.02544	0.04793
-20	0.01007	0.02959	0.04591
-10	0.00994	0.02795	0.04964
0	0.01079	0.02925	0.04923
10	0.01032	0.03030	0.05019
20	0.01032	0.02824	0.04980
30	0.00904	0.02653	0.05105
40	0.00975	0.02783	0.04801
50	0.00754	0.02561	0.04883
60	0.00815	0.02571	0.04710
70	0.00585	0.02141	0.03899
80	0.00548	0.01768	0.03418
90	0.00540	0.01667	0.03282
NOISE(%)	5.6 MAX.	...	4.5 MAX.

MODEL AC, FLOW: GRID CI, VERTICAL BENDING, HP D.V.M.

WIND YAW ANGLE(DEG.)	U=3.0 M/SEC R.M.S.	U=3.0 M/SEC PEAK	U=6.1 M/SEC R.M.S.	U=6.1 M/SEC PEAK
-90	0.00942	0.03520	0.03124	0.13728
-80	0.01355	0.04664	0.04391	0.13464
-70	0.02358	0.08448	0.07066	0.26664
-60	0.03036	0.12320	0.08078	0.28864
-50	0.03414	0.10912	0.09038	0.34672
-40	0.04171	0.14080	0.10375	0.38632
-30	0.04585	0.20064	0.10358	0.42240
-20	0.04673	0.18656	0.10912	0.45056
-10	0.05148	0.21824	0.11906	0.40656
0	0.04884	0.17864	0.12619	0.56496
10	0.05333	0.21736	0.12241	0.44264
20	0.05227	0.19008	0.12470	0.45056
30	0.04972	0.18920	0.12417	0.51216
40	0.05254	0.20944	0.12355	0.45144
50	0.04611	0.18128	0.11766	0.45320
60	0.04303	0.15928	0.11510	0.45848
70	0.03582	0.12056	0.10058	0.44176
80	0.03538	0.13816	0.08712	0.35816
90	0.03256	0.11440	0.09363	0.37136
NOISE(%)	...		...	

MODEL AC, FLOW: GRID CI, VERTICAL BENDING, HP D.V.M.

WIND VEL. (M/SEC)	YAW ANGLE=0 DEG. R.M.S.	YAW ANGLE=0 DEG. PEAK
2.7	0.04550	0.15576
3.0	0.05192	0.19008
3.4	0.05861	0.23056
3.7	0.06926	0.24552
4.1	0.07674	0.38720
4.5	0.08853	0.32912
5.0	0.10578	0.39336
5.5	0.11713	0.42416
6.1	0.11678	0.49192
6.7	0.13262	0.50336
7.4	0.13781	0.56408
8.2	0.15110	0.59312
9.1	0.16614	0.62480
NOISE(%)	...	

MODEL AC, FLOW: GRID NI, VERTICAL BENDING, HP D.V.M.

WIND VEL. (M/SEC)	YAW ANGLE=-45 DEG. R.M.S.	PEAK	YAW ANGLE=0 DEG. R.M.S.	PEAK	YAW ANGLE=+45 DEG. R.M.S.	PEAK	YAW ANGLE=+90 DEG. R.M.S.	PEAK
1.8	0.02420	0.08747	0.03030	0.10164	0.02763	0.10384	0.01385	0.04083
2.1	0.03326	0.12408	0.04468	0.19527	0.03705	0.18744	0.01812	0.06494
2.4	0.03758	0.14608	0.05235	0.20618	0.04506	0.16808	0.02869	0.09002
2.7	0.05130	0.18392	0.06200	0.23478	0.05562	0.22088	0.03133	0.10472
3.0	0.05456	0.16808	0.07447	0.28503	0.06318	0.24464	0.04673	0.18216
3.4	0.06521	0.23144	0.07735	0.26831	0.07366	0.26664	0.05210	0.18128
3.7	0.07603	0.25960	0.09428	0.36335	0.08413	0.37752	0.05482	0.21120
4.1	0.08263	0.32736	0.10680	0.39653	0.09662	0.37928	0.06987	0.27192
4.5	0.09592	0.35376	0.11985	0.44546	0.11220	0.40920	0.08466	0.27016
5.0	0.11009	0.54032	0.13501	0.55722	0.12610	0.48400	0.09566	0.33616
5.5	0.11739	0.44352	0.14809	0.59866	0.14142	0.56408	0.09847	0.42504
6.1	0.13570	0.53416	0.16232	0.57376	0.15532	0.54120	0.12514	0.43648
6.7	0.14582	0.63536	0.18921	0.75117	0.16966	0.65472	0.14036	0.53064
7.4	0.17116	0.67584	0.20337	0.77238	0.19756	0.97328	0.14291	0.51128
8.2	0.17424	0.65472	0.21883	0.75874	0.22361	0.80960	0.16236	0.54032
9.1	0.19316	0.70048	0.25239	1.07580	0.23276	0.86592	0.18172	0.66792
NOISE(%)	...		...		...		...	

MODEL AC, FLOW: GRID CIII, VERTICAL BENDING, HP D.V.M.

WIND YAW ANGLE(DEG.)	U=3.0 M/SEC R.M.S.	PEAK	U=6.1 M/SEC R.M.S.	PEAK
-90	0.00378	0.01144	0.00986	0.03520
-80	0.00546	0.02024	0.01804	0.08096
-70	0.00766	0.03784	0.02367	0.09680
-60	0.00986	0.03520	0.02842	0.09944
-50	0.01144	0.04664	0.03495	0.12760
-40	0.01197	0.05456	0.03810	0.13024
-30	0.01258	0.04576	0.03925	0.19888
-20	0.01355	0.05104	0.04127	0.15488
-10	0.01417	0.04928	0.04171	0.16456
0	0.01399	0.05632	0.04426	0.20504
10	0.01390	0.05104	0.04409	0.19096
20	0.01399	0.05896	0.04479	0.15136
30	0.01390	0.04928	0.04462	0.17512
40	0.01320	0.04664	0.04312	0.17776
50	0.01258	0.04312	0.04330	0.15664
60	0.01320	0.05720	0.03863	0.13288
70	0.01162	0.04224	0.03467	0.13728
80	0.01074	0.03608	0.03247	0.11704
[illegible]	0.01012	0.03520	0.02781	0.10384
NOISE(%)	...		...	

MODEL AC, FLOW: GRID CIII, VERTICAL BENDING, HP D.V.M.

WIND VEL. (M/SEC)	YAW ANGLE=0 DEG. R.M.S.	PEAK	YAW ANGLE=+45 DEG. R.M.S.	PEAK	YAW ANGLE=+90 DEG. R.M.S.	PEAK
3.0	0.01373	0.05896	0.01285	0.04928	0.01100	0.03960
3.4	0.01619	0.06600	0.01470	0.05984	0.01126	0.03432
3.7	0.01962	0.08800	0.01742	0.06248	0.01267	0.05192
4.1	0.02288	0.10120	0.01910	0.07304	0.01910	0.05808
4.5	0.02552	0.08976	0.02482	0.09680	0.02156	0.08448
5.0	0.03027	0.11176	0.02763	0.10824	0.02103	0.07040
5.5	0.03696	0.16368	0.03256	0.12408	0.02482	0.08888
6.1	0.04356	0.16632	0.04101	0.17248	0.03362	0.10032
6.7	0.04858	0.19800	0.04620	0.16104	0.03221	0.10560
7.4	0.05210	0.19976	0.05430	0.22528	0.04145	0.16808
8.2	0.05782	0.22880	0.05817	0.21912	0.04294	0.14960
9.1	0.06820	0.29216	0.07022	0.28688	0.05148	0.19272
NOISE(%)	...		...		...	

MODEL AC, FLOW: GRID NIII, VERTICAL BENDING, HP D.V.M.

WIND VEL. (M/SEC)	YAW ANGLE=-45 DEG. R.M.S.	PEAK	YAW ANGLE=0 DEG. R.M.S.	PEAK	YAW ANGLE=+45 DEG. R.M.S.	PEAK	YAW ANGLE=+90 DEG. R.M.S.	PEAK
2.1	0.00686	0.02138	0.00798	0.03124	0.00824	0.03045	0.00620	0.02050
2.4	0.00828	0.03344	0.00827	0.02922	0.00955	0.04101	0.00709	0.02209
2.7	0.00897	0.03150	0.01021	0.03634	0.01111	0.03934	0.01057	0.03696
3.0	0.01042	0.03766	0.01183	0.05509	0.01294	0.04849	0.01062	0.03529
3.4	0.01068	0.03599	0.01222	0.05403	0.01280	0.04717	0.01180	0.04391
3.7	0.01225	0.04312	0.01379	0.05157	0.01387	0.06389	0.01492	0.05474
4.1	0.01346	0.05078	0.01502	0.06618	0.01602	0.06072	0.01790	0.06406
4.5	0.01472	0.05526	0.01630	0.06618	0.01611	0.06239	0.02109	0.08210
5.0	0.01613	0.06389	0.01768	0.06829	0.01884	0.07322	0.02024	0.06864
5.5	0.01704	0.06424	0.01944	0.08228	0.01971	0.07735	0.02651	0.09293
6.1	0.01917	0.06926	0.02143	0.08474	0.02224	0.09874	0.02519	0.10058
6.7	0.02035	0.07480	0.02322	0.09821	0.02575	0.09143	0.02831	0.11202
7.4	0.02213	0.08158	0.02481	0.08906	0.02776	0.09275	0.03220	0.12003
8.2	0.02434	0.09381	0.02762	0.11097	0.02992	0.11704	0.03751	0.14555
9.1	0.02674	0.09803	0.02982	0.12311	0.03445	0.15673	0.04191	0.13684
NOISE(%)	...		...		...		...	

MODEL AC, FLOW: SMOOTH FLOW, VERTICAL BENDING, HP D.V.M.

WIND YAW ANGLE(DEG.)	U=3.0 M/SEC R.M.S.	U=3.0 M/SEC PEAK	U=6.1 M/SEC R.M.S.	U=6.1 M/SEC PEAK
-90	0.00311	0.01214	0.00835	0.02763
-80	0.00216	0.00827	0.00448	0.01681
-70	0.00139	0.00502	0.00295	0.01206
-60	0.00091	0.00422	0.00290	0.01153
-50	0.00123	0.00686	0.00290	0.01118
-40	0.00106	0.00414	0.00260	0.01021
-30	0.00107	0.00449	0.00260	0.01091
-20	0.00103	0.00361	0.00280	0.01021
-10	0.00101	0.00361	0.00305	0.01074
0	0.00096	0.00352	0.00306	0.01091
10	0.00100	0.00378	0.00312	0.01214
20	0.00103	0.00361	0.00308	0.01153
30	0.00104	0.00396	0.00300	0.01126
40	0.00111	0.00449	0.00243	0.00986
50	0.00128	0.00519	0.00265	0.01153
60	0.00093	0.00414	0.00223	0.00827
70	0.00138	0.00519	0.00180	0.00722
80	0.00129	0.00519	0.00187	0.00686
90	0.00184	0.00634	0.00286	0.00994
NOISE(%)	1.4 MAX.		...	

MODEL AC, FLOW: SMOOTH FLOW, VERTICAL BENDING, HP D.V.M.

WIND VEL. (M/SEC)	YAW ANGLE=0 DEG. R.M.S.	YAW ANGLE=0 DEG. PEAK	YAW ANGLE=+45 DEG. R.M.S.	YAW ANGLE=+45 DEG. PEAK	YAW ANGLE=+90 DEG. R.M.S.	YAW ANGLE=+90 DEG. PEAK
3.0	0.00100	0.00370	0.00116	0.00378	0.00244	0.00686
3.4	0.00109	0.00475	0.00114	0.00510	0.00274	0.00854
3.7	0.00120	0.00449	0.00129	0.00510	0.00230	0.00827
4.1	0.00144	0.00634	0.00137	0.00519	0.00275	0.00810
4.5	0.00163	0.00660	0.00161	0.00686	0.00253	0.00836
5.0	0.00195	0.00695	0.00180	0.00774	0.00241	0.00906
5.5	0.00244	0.00827	0.00202	0.00915	0.00285	0.00818
6.1	0.00280	0.01021	0.00231	0.00862	0.00274	0.01012
6.7	0.00348	0.01232	0.00281	0.01065	0.00280	0.00862
7.4	0.00380	0.01320	0.00338	0.01258	0.00334	0.01030
8.2	0.00432	0.01637	0.00400	0.01734	0.00365	0.01250
9.1	0.00534	0.01839	0.00512	0.01804	0.00448	0.01637
NOISE(%)	...		...		...	

MODEL AD, FLOW: GRID CI, VERTICAL BENDING, HP D.V.M.

WIND YAW ANGLE(DEG.)	U=3.0 M/SEC R.M.S.	PEAK	U=6.1 M/SEC R.M.S.	PEAK
-90	0.01382	0.04488	0.03388	0.11440
-80	0.01901	0.06952	0.04418	0.14520
-70	0.02737	0.09856	0.07216	0.26400
-60	0.03678	0.15224	0.08360	0.32208
-50	0.04224	0.14696	0.10111	0.38896
-40	0.04629	0.18656	0.11009	0.41712
-30	0.05201	0.17688	0.11766	0.47608
-20	0.05394	0.21648	0.11449	0.49896
-10	0.05315	0.18480	0.11475	0.42152
0	0.05914	0.23232	0.12690	0.47872
10	0.05861	0.21736	0.13332	0.53856
20	0.05826	0.22968	0.12487	0.61248
30	0.05799	0.22792	0.12452	0.52536
40	0.05386	0.21208	0.13156	0.56232
50	0.05254	0.18304	0.12945	0.51216
60	0.04682	0.21912	0.12021	0.48488
70	0.04567	0.18216	0.10754	0.35992
80	0.03881	0.11528	0.09970	0.36432
90	0.03511	0.14872	0.10278	0.35376
NOISE(%)	...		...	

MODEL AE, FLOW: GRID CI, VERTICAL BENDING, HP D.V.M.

WIND YAW ANGLE(DEG.)	U=3.0 M/SEC R.M.S.	PEAK	U=5.8 M/SEC R.M.S.	PEAK
-90	0.00123	0.00440	0.00651	0.02640
-80	0.00229	0.00792	0.01051	0.03238
-70	0.00449	0.01408	0.01955	0.08034
-60	0.00669	0.02288	0.02495	0.09918
-50	0.00818	0.03168	0.02655	0.10666
-40	0.01012	0.04224	0.03173	0.13376
-30	0.01109	0.03784	0.03184	0.11854
-20	0.01214	0.04136	0.03928	0.16931
-10	0.01250	0.04928	0.03661	0.14432
0	0.01258	0.05016	0.03858	0.15840
10	0.01294	0.04488	0.04061	0.14397
20	0.01311	0.05104	0.04290	0.20645
30	0.01294	0.05016	0.04024	0.14089
40	0.01135	0.03608	0.03692	0.12338
50	0.01012	0.03960	0.03717	0.13878
60	0.00986	0.03344	0.03090	0.11704
70	0.00766	0.02992	0.02471	0.09319
80	0.00783	0.02376	0.03084	0.11880
90	0.00642	0.01848	0.02301	0.07638
NOISE(%)	...		...	

MODEL AD, FLOW: GRID CIII, VERTICAL BENDING, HP D.V.M.

WIND YAW ANGLE(DEG.)	U=3.0 M/SEC R.M.S.	PEAK	U=6.1 M/SEC R.M.S.	PEAK
-90	0.00352	0.01056	0.01065	0.03520
-80	0.00598	0.02024	0.01936	0.07480
-70	0.00845	0.02992	0.02534	0.09592
-60	0.00994	0.04136	0.03098	0.11968
-50	0.01065	0.04136	0.03309	0.14696
-40	0.01197	0.04928	0.03546	0.13816
-30	0.01258	0.05280	0.03969	0.15928
-20	0.01434	0.05544	0.04022	0.16984
-10	0.01417	0.04928	0.04198	0.15752
0	0.01461	0.05456	0.04382	0.16192
10	0.01505	0.06072	0.04074	0.16632
20	0.01434	0.05192	0.04277	0.16984
30	0.01346	0.05544	0.04127	0.15752
40	0.01390	0.04664	0.03986	0.14960
50	0.01294	0.04488	0.03793	0.13464
60	0.01294	0.04576	0.03749	0.14872
70	0.01214	0.04752	0.03705	0.15400
80	0.01302	0.04664	0.03423	0.11704
90	0.01250	0.04840	0.03168	0.11528
NOISE(%)	...		...	

MODEL AE, FLOW: GRID CIII, VERTICAL BENDING, HP D.V.M.

WIND YAW ANGLE(DEG.)	U=3.0 M/SEC R.M.S.	PEAK	U=5.8 M/SEC R.M.S.	PEAK
-90	0.00044	0.00176	0.00229	0.00880
-80	0.00079	0.00352	0.00378	0.01496
-70	0.00141	0.00440	0.00625	0.02112
-60	0.00185	0.00792	0.00766	0.02552
-50	0.00273	0.01056	0.00810	0.02816
-40	0.00299	0.01056	0.00827	0.03344
-30	0.00308	0.01144	0.00950	0.03520
-20	0.00361	0.01144	0.01056	0.03872
-10	0.00370	0.01320	0.01021	0.04224
0	0.00405	0.01496	0.01074	0.04048
10	0.00387	0.01408	0.01012	0.04224
20	0.00370	0.01144	0.01118	0.04664
30	0.00361	0.01320	0.01021	0.03960
40	0.00361	0.01408	0.00986	0.04048
50	0.00352	0.01232	0.00871	0.03608
60	0.00343	0.01144	0.00942	0.04224
70	0.00264	0.01056	0.00915	0.02816
80	0.00202	0.00792	0.00801	0.02992
90	0.00238	0.00880	0.00572	0.02200
NOISE(%)	...		...	

MODEL AF, FLOW: GRID CI, VERTICAL BENDING, HP D.V.M.

WIND YAW ANGLE(DEG.)	U=6.1 M/SEC R.M.S.	PEAK	U=11.9 M/SEC R.M.S.	PEAK
-90	0.00070	0.00220	0.00348	0.01355
-80	0.00103	0.00326	0.00784	0.02446
-70	0.00233	0.00915	0.01068	0.03898
-60	0.00372	0.01390	0.01624	0.04998
-50	0.00493	0.01558	0.01939	0.07225
-40	0.00587	0.02174	0.02198	0.08466
-30	0.00693	0.02552	0.02340	0.08474
-20	0.00786	0.03062	0.02620	0.09750
-10	0.00790	0.02939	0.02731	0.10613
0	0.00810	0.02904	0.02787	0.10437
10	0.00876	0.03634	0.02720	0.10067
20	0.00818	0.02992	0.02881	0.11810
30	0.00809	0.03062	0.02607	0.09733
40	0.00796	0.02728	0.02419	0.09407
50	0.00592	0.01989	0.02459	0.08694
60	0.00574	0.02279	0.01981	0.07198
70	0.00454	0.01566	0.01808	0.07251
80	0.00309	0.01109	0.01313	0.04541
90	0.00266	0.00968	0.01217	0.03978
NOISE(%)	...		...	

MODEL AF', FLOW: GRID CI, VERTICAL BENDING, HP D.V.M.

WIND YAW ANGLE(DEG.)	U=4.6 M/SEC R.M.S.	PEAK	U=8.8 M/SEC R.M.S.	PEAK
-90	0.00054	0.00210	0.00369	0.01550
-80	0.00141	0.00520	0.00655	0.02150
-70	0.00266	0.00820	0.01021	0.03400
-60	0.00443	0.01460	0.01460	0.05420
-50	0.00484	0.01770	0.02049	0.09690
-40	0.00631	0.02290	0.02414	0.09140
-30	0.00750	0.02430	0.02473	0.08870
-20	0.00742	0.02660	0.02546	0.08940
-10	0.00804	0.03110	0.02841	0.12740
0	0.00858	0.02870	0.02887	0.12340
10	0.00898	0.03400	0.02784	0.12420
20	0.00908	0.03540	0.02902	0.09920
30	0.00792	0.02790	0.02921	0.09340
40	0.00866	0.03850	0.02832	0.09100
50	0.00620	0.02230	0.02491	0.08680
60	0.00544	0.01730	0.02021	0.07400
70	0.00419	0.01590	0.01682	0.06250
80	0.00301	0.01330	0.01162	0.05050
90	0.00268	0.00890	0.01199	0.03930
NOISE(%)	...		...	

MODEL AF, FLOW: GRID CIII, VERTICAL BENDING, HP D.V.M.

WIND YAW ANGLE(DEG.)	U=6.1 M/SEC R.M.S.	PEAK	U=11.9 M/SEC R.M.S.	PEAK
-90	0.00028	0.00088	0.00123	0.00466
-80	0.00053	0.00167	0.00246	0.00845
-70	0.00095	0.00326	0.00392	0.01399
-60	0.00152	0.00581	0.00490	0.01690
-50	0.00202	0.00792	0.00570	0.01936
-40	0.00229	0.00792	0.00623	0.02781
-30	0.00238	0.00933	0.00661	0.02517
-20	0.00249	0.00906	0.00753	0.02816
-10	0.00265	0.00968	0.00685	0.02508
0	0.00295	0.01003	0.00699	0.02508
10	0.00288	0.01126	0.00730	0.02781
20	0.00269	0.01021	0.00707	0.02684
30	0.00279	0.00933	0.00696	0.02517
40	0.00243	0.00950	0.00675	0.02297
50	0.00238	0.00871	0.00601	0.02658
60	0.00252	0.00836	0.00579	0.02033
70	0.00195	0.00713	0.00508	0.01690
80	0.00170	0.00519	0.00473	0.01646
90	0.00100	0.00334	0.00370	0.01382
NOISE(%)	3.0 MAX.		...	

MODEL AF', FLOW: GRID CIII, VERTICAL BENDING, HP D.V.M.

WIND YAW ANGLE(DEG.)	U=4.6 M/SEC R.M.S.	PEAK	U=8.8 M/SEC R.M.S.	PEAK
-90	0.00025	0.00090	0.00138	0.00400
-80	0.00049	0.00160	0.00270	0.00860
-70	0.00092	0.00310	0.00423	0.01590
-60	0.00143	0.00500	0.00468	0.01780
-50	0.00172	0.00650	0.00547	0.02270
-40	0.00208	0.00820	0.00636	0.02390
-30	0.00233	0.00890	0.00636	0.02550
-20	0.00238	0.00830	0.00689	0.02420
-10	0.00275	0.00960	0.00721	0.03030
0	0.00246	0.00820	0.00742	0.02780
10	0.00258	0.00900	0.00702	0.02630
20	0.00279	0.00870	0.00787	0.02760
30	0.00266	0.00910	0.00676	0.02730
40	0.00231	0.00810	0.00650	0.02350
50	0.00208	0.00790	0.00723	0.02400
60	0.00204	0.00730	0.00674	0.02500
70	0.00160	0.00580	0.00546	0.01710
80	0.00108	0.00400	0.00473	0.01610
90	0.00099	0.00320	0.00333	0.01180
NOISE(%)	...		...	

MODEL AG, FLOW: GRID CI, VERTICAL BENDING, HP D.V.M.

WIND YAW ANGLE(DEG.)	U=3.7 M/SEC R.M.S.	U=3.7 M/SEC PEAK	U=7.0 M/SEC R.M.S.	U=7.0 M/SEC PEAK
-90	0.00037	0.00150	0.00176	0.00620
-80	0.00083	0.00320	0.00431	0.01540
-70	0.00134	0.00450	0.00638	0.02160
-60	0.00225	0.00750	0.00851	0.02910
-50	0.00290	0.00970	0.01096	0.04010
-40	0.00386	0.01480	0.01409	0.04760
-30	0.00527	0.01930	0.01760	0.05700
-20	0.00484	0.01690	0.01883	0.05730
-10	0.00632	0.02500	0.01798	0.06000
0	0.00562	0.02010	0.01916	0.07840
10	0.00508	0.01760	0.01788	0.06120
20	0.00546	0.02050	0.01765	0.06370
30	0.00576	0.02430	0.01745	0.05650
40	0.00540	0.01790	0.01524	0.06290
50	0.00415	0.01290	0.01684	0.06050
60	0.00318	0.01010	0.01373	0.04720
70	0.00206	0.00720	0.01108	0.04060
80	0.00142	0.00600	0.00836	0.02980
90	0.00107	0.00350	0.00593	0.01940
NOISE(%)	...		...	

MODEL AG, FLOW: GRID CIII, VERTICAL BENDING, HP D.V.M.

WIND YAW ANGLE(DEG.)	U=3.7 M/SEC R.M.S.	U=3.7 M/SEC PEAK	U=7.0 M/SEC R.M.S.	U=7.0 M/SEC PEAK
-90	0.00014	0.00050	0.00069	0.00240
-80	0.00023	0.00070	0.00145	0.00460
-70	0.00045	0.00170	0.00208	0.00730
-60	0.00082	0.00280	0.00317	0.01040
-50	0.00121	0.00370	0.00353	0.01280
-40	0.00138	0.00460	0.00414	0.01530
-30	0.00158	0.00500	0.00465	0.01610
-20	0.00169	0.00570	0.00475	0.02040
-10	0.00178	0.00640	0.00480	0.02080
0	0.00194	0.00750	0.00557	0.01990
10	0.00222	0.00770	0.00486	0.01980
20	0.00182	0.00710	0.00469	0.01430
30	0.00171	0.00610	0.00470	0.02060
40	0.00145	0.00470	0.00470	0.01680
50	0.00141	0.00540	0.00397	0.01380
60	0.00127	0.00470	0.00408	0.01270
70	0.00075	0.00260	0.00285	0.01010
80	0.00045	0.00170	0.00285	0.01000
90	0.00046	0.00140	0.00141	0.00550
NOISE(%)	...		...	

MODEL AH, FLOW: GRID CI, VERTICAL BENDING, HP D.V.M.

WIND YAW ANGLE(DEG.)	U=3.0 M/SEC R.M.S.	U=3.0 M/SEC PEAK	U=4.9 M/SEC R.M.S.	U=4.9 M/SEC PEAK
-90	0.00029	0.00100	0.00105	0.00340
-80	0.00055	0.00160	0.00284	0.00860
-70	0.00132	0.00420	0.00440	0.01340
-60	0.00248	0.00680	0.00780	0.02640
-50	0.00358	0.01170	0.00742	0.02620
-40	0.00432	0.01260	0.00834	0.03030
-30	0.00461	0.01470	0.00847	0.03070
-20	0.00652	0.01830	0.01179	0.03750
-10	0.00637	0.01930	0.01338	0.03640
0	0.00683	0.01990	0.01215	0.03650
10	0.00599	0.02160	0.01032	0.03630
20	0.00463	0.01420	0.01193	0.04270
30	0.00526	0.01980	0.01416	0.04720
40	0.00439	0.01590	0.01266	0.04570
50	0.00376	0.01120	0.01227	0.04040
60	0.00265	0.00920	0.00942	0.03520
70	0.00197	0.00770	0.00627	0.01910
80	0.00125	0.00470	0.00405	0.01390
90	0.00090	0.00270	0.00456	0.01310
NOISE(%)	...		...	

MODEL AH, FLOW: GRID NI, VERTICAL BENDING, HP D.V.M.

WIND VEL. (M/SEC)	YAW ANGLE=-40 DEG. R.M.S.	YAW ANGLE=-40 DEG. PEAK	YAW ANGLE=0 DEG. R.M.S.	YAW ANGLE=0 DEG. PEAK	YAW ANGLE=+40 DEG. R.M.S.	YAW ANGLE=+40 DEG. PEAK	YAW ANGLE=+90 DEG. R.M.S.	YAW ANGLE=+90 DEG. PEAK
1.8	0.00199	0.00600	0.00210	0.00710	0.00160	0.00640	0.00029	0.00110
2.1	0.00229	0.00720	0.00352	0.01080	0.00247	0.00950	0.00063	0.00190
2.4	0.00369	0.01200	0.00486	0.01760	0.00379	0.01220	0.00083	0.00260
2.7	0.00365	0.01280	0.00653	0.02160	0.00408	0.01410	0.00094	0.00430
3.0	0.00537	0.01880	0.00787	0.02570	0.00576	0.01790	0.00117	0.00370
3.4	0.00697	0.02140	0.00872	0.02690	0.00706	0.02180	0.00136	0.00570
3.7	0.00674	0.02470	0.00972	0.03190	0.00892	0.02720	0.00151	0.00480
4.1	0.00971	0.03020	0.01201	0.03440	0.00922	0.02890	0.00246	0.00780
4.5	0.00841	0.03140	0.01380	0.04500	0.01174	0.04490	0.00242	0.00840
5.0	0.01068	0.04050	0.01298	0.05080	0.01203	0.04220	0.00330	0.00980
5.5	0.01502	0.04520	0.01353	0.04500	0.01541	0.04850	0.00516	0.01800
6.1	0.01456	0.05270	0.01503	0.04550	0.01714	0.05840	0.00482	0.01790
6.7	0.01718	0.05600	0.01929	0.06300	0.01942	0.08440	0.00553	0.01770
7.4	0.02056	0.06200	0.01888	0.06820	0.02171	0.07120	0.00606	0.01690
8.2	0.01810	0.06790	0.02335	0.08560	0.02337	0.08150	0.00751	0.02820
9.1	0.02348	0.09[illegible]0	0.02369	0.08790	0.02778	0.09270	0.01011	0.03250
NOISE(%)	...		...		...		14.7 MAX.	

MODEL AH, FLOW: GRID CIII, VERTICAL BENDING, HP D.V.M.

WIND YAW ANGLE(DEG.)	U=3.0 M/SEC R.M.S.	PEAK	U=4.9 M/SEC R.M.S.	PEAK
-90	0.00009	0.00030	0.00035	0.00120
-80	0.00015	0.00050	0.00091	0.00250
-70	0.00051	0.00170	0.00150	0.00500
-60	0.00073	0.00230	0.00214	0.00650
-50	0.00089	0.00320	0.00289	0.00880
-40	0.00128	0.00450	0.00267	0.00880
-30	0.00178	0.00630	0.00339	0.01370
-20	0.00214	0.00670	0.00520	0.01650
-10	0.00252	0.00840	0.00757	0.02330
0	0.00230	0.00970	0.00497	0.01640
10	0.00224	0.00710	0.00533	0.01720
20	0.00171	0.00590	0.00333	0.00980
30	0.00173	0.00590	0.00398	0.01560
40	0.00129	0.00420	0.00315	0.01130
50	0.00125	0.00410	0.00246	0.00880
60	0.00092	0.00310	0.00231	0.00850
70	0.00057	0.00180	0.00141	0.00540
80	0.00049	0.00140	0.00097	0.00330
90	0.00023	0.00080	0.00095	0.00300
NOISE(%)	...		...	

MODEL AH, FLOW: GRID NIII, VERTICAL BENDING, HP D.V.M.

WIND VEL. (M/SEC)	YAW ANGLE=-40 DEG. R.M.S.	PEAK	YAW ANGLE=0 DEG. R.M.S.	PEAK	YAW ANGLE=+40 DEG. R.M.S.	PEAK	YAW ANGLE=+90 DEG. R.M.S.	PEAK
2.1	0.00104	0.00330	0.00153	0.00440	0.00070	0.00260	0.00021	0.00080
2.4	0.00118	0.00410	0.00159	0.00510	0.00089	0.00330	0.00027	0.00110
2.7	0.00142	0.00580	0.00227	0.00790	0.00150	0.00500	0.00028	0.00110
3.0	0.00161	0.00530	0.00233	0.00770	0.00156	0.00560	0.00043	0.00140
3.4	0.00146	0.00580	0.00284	0.01030	0.00180	0.00560	0.00039	0.00160
3.7	0.00214	0.00780	0.00313	0.01120	0.00190	0.00630	0.00062	0.00230
4.1	0.00242	0.00840	0.00372	0.01280	0.00198	0.00630	0.00066	0.00230
4.5	0.00264	0.00920	0.00362	0.01230	0.00236	0.00730	0.00070	0.00260
5.0	0.00231	0.01070	0.00448	0.01470	0.00266	0.00890	0.00121	0.00410
5.5	0.00263	0.00890	0.00470	0.01840	0.00257	0.00840	0.00102	0.00420
6.1	0.00278	0.00930	0.00543	0.01780	0.00335	0.01140	0.00125	0.00430
6.7	0.00331	0.01240	0.00897	0.02580	0.00299	0.01140	0.00144	0.00530
7.4	0.00352	0.01120	0.00788	0.02970	0.00311	0.01000	0.00159	0.00510
8.2	0.00338	0.01120	0.00978	0.02630	0.00371	0.01100	0.00156	0.00560
9.1	0.00345	0.01010	0.00879	0.02600	0.00365	0.01350	0.00233	0.00790
NOISE(%)	1.9 MAX.		...		1.4 MAX.		16.0 MAX.	

MODEL AI, FLOW: GRID CI, VERTICAL BENDING, HP D.V.M.

WIND YAW ANGLE(DEG.)	U=3.7 M/SEC R.M.S.	PEAK	U=7.3 M/SEC R.M.S.	PEAK
-90	0.00064	0.00170	0.00269	0.00800
-80	0.00153	0.00500	0.00582	0.01990
-70	0.00314	0.00840	0.00899	0.02820
-60	0.00405	0.01420	0.01098	0.03860
-50	0.00723	0.02320	0.01079	0.04000
-40	0.01073	0.03490	0.01660	0.04860
-30	0.01054	0.02930	0.01278	0.04080
-20	0.01240	0.02980	0.03899	0.08290
-10	0.01499	0.04190	0.03736	0.08190
0	0.01931	0.05120	0.02715	0.06870
10	0.01237	0.03830	0.01818	0.05790
20	0.01229	0.03340	0.01501	0.04350
30	0.01348	0.04050	0.01532	0.05250
40	0.00815	0.03160	0.01658	0.05000
50	0.00772	0.02420	0.01815	0.05300
60	0.00599	0.02230	0.01954	0.05930
70	0.00549	0.01500	0.01310	0.04010
80	0.00255	0.00810	0.00816	0.02360
90	0.00258	0.00680	0.00496	0.01730
NOISE(%)	...		...	

MODEL AJ, FLOW: GRID CI, VERTICAL BENDING, HP D.V.M.

WIND YAW ANGLE(DEG.)	U=7.0 M/SEC R.M.S.	PEAK
-90	0.01241	0.04850
-80	0.01642	0.06043
-70	0.02622	0.11873
-60	0.03374	0.11463
-50	0.04230	0.15335
-40	0.04748	0.17026
-30	0.05101	0.25294
-20	0.05375	0.19082
-10	0.05579	0.24591
0	0.05789	0.22748
10	0.06174	0.19927
20	0.05934	0.21725
30	0.05962	0.22428
40	0.05821	0.22766
50	0.05729	0.24511
60	0.05316	0.21698
70	0.05241	0.21627
80	0.04391	0.16590
90	0.03941	0.16963
NOISE(%)	...	

MODEL AI, FLOW: GRID CIII, VERTICAL BENDING, HP D.V.M.

WIND YAW ANGLE(DEG.)	U=3.7 M/SEC R.M.S.	PEAK	U=7.3 M/SEC R.M.S.	PEAK
-90	0.00028	0.00240	0.00083	0.00230
-80	0.00058	0.00160	0.00255	0.00650
-70	0.00159	0.00470	0.00425	0.01430
-60	0.00199	0.00620	0.00423	0.01290
-50	0.00363	0.01090	0.00876	0.02740
-40	0.00648	0.02310	0.01787	0.04030
-30	0.01006	0.02480	0.01633	0.03750
-20	0.00689	0.01820	0.01825	0.04790
-10	0.00476	0.01390	0.01390	0.03190
0	0.00691	0.01860	0.02285	0.04750
10	0.00736	0.02460	0.01821	0.04890
20	0.00764	0.01930	0.01330	0.04100
30	0.00657	0.01960	0.00999	0.03120
40	0.00498	0.01690	0.00854	0.03030
50	0.00297	0.00870	0.00599	0.02090
60	0.00193	0.00570	0.00612	0.02340
70	0.00129	0.00420	0.00564	0.01800
80	0.00055	0.00180	0.00334	0.01010
90	0.00047	0.00160	0.00161	0.00540
NOISE(%)	...		...	

MODEL AJ, FLOW: GRID CIII, VERTICAL BENDING, HP D.V.M.

WIND YAW ANGLE(DEG.)	U=7.0 M/SEC R.M.S.	PEAK
-90	0.00496	0.02065
-80	0.00581	0.02234
-70	0.00821	0.02999
-60	0.01036	0.04219
-50	0.01155	0.03987
-40	0.01282	0.04939
-30	0.01345	0.04824
-20	0.0147	0.05794
-10	0.01509	0.06586
0	0.01546	0.06782
10	0.01635	0.06986
20	0.01620	0.06915
30	0.01575	0.05830
40	0.01680	0.06355
50	0.01594	0.05865
60	0.01559	0.06595
70	0.01486	0.05589
80	0.01410	0.04904
90	0.01271	0.03934
NOISE(%)	...	

MODEL AK, FLOW: GRID CI, VERTICAL BENDING, HP D.V.M.

WIND YAW ANGLE(DEG.)	U=9.1 M/SEC R.M.S.	PEAK
-90	0.00174	0.00679
-80	0.00215	0.00902
-70	0.00306	0.01293
-60	0.00392	0.01776
-50	.00458	0.01609
-40	0.00556	0.02743
-30	0.00588	0.02427
-20	0.00658	0.02846
-10	0.00724	0.03292
0	0.00758	0.02790
10	0.00765	0.03227
20	0.00790	0.03125
30	0.00742	0.03106
40	0.00738	0.02902
50	0.00710	0.03274
60	0.00658	0.02604
70	0.00602	0.02232
80	0.00578	0.02334
90	0.00560	0.02241
NOISE(%)	...	

MODEL AL, FLOW: GRID CI, VERTICAL BENDING, HP D.V.M.

WIND YAW ANGLE(DEG.)	U=3.0 M/SEC R.M.S.	PEAK	U=6.1 M/SEC R.M.S.	PEAK
-90	0.00428	0.01465	0.01412	0.05126
-80	0.00779	0.02763	0.01750	0.06824
-70	0.01114	0.04409	0.02628	0.10661
-60	0.01392	0.05729	0.03630	0.13394
-50	0.01651	0.06358	0.04114	0.16826
-40	0.01796	0.07357	0.04662	0.20302
-30	0.02112	0.07867	0.04969	0.20284
-20	0.02314	0.09491	0.05137	0.23712
-10	0.02529	0.09372	0.05706	0.20112
0	0.02439	0.08342	0.05685	0.22242
10	0.02437	0.09583	0.06378	0.22568
20	0.02642	0.09447	0.06296	0.22986
30	0.02595	0.10595	0.06039	0.21380
40	0.02600	0.12954	0.06706	0.25142
50	0.02741	0.10705	0.06164	0.21564
60	0.02622	0.08536	0.06007	0.23685
70	0.02438	0.08818	0.05717	0.25410
80	0.02189	0.07374	0.05587	0.20170
90	0.02316	0.07625	0.06150	0.21199
NOISE(%)	...		...	

MODEL AK, FLOW: GRID CIII, VERTICAL BENDING, HP D.V.M.

WIND YAW ANGLE(DEG.)	U=9.1 M/SEC R.M.S.	PEAK
-90	0.00089	0.00335
-80	0.00113	0.00428
-70	0.00146	0.00614
-60	0.00179	0.00716
-50	0.00205	0.00939
-40	0.00225	0.00874
-30	0.00257	0.01004
-20	0.00274	0.01069
-10	0.00308	0.01339
0	0.00329	0.01321
10	0.00313	0.01218
20	0.00331	0.01497
30	0.00337	0.01395
40	0.00342	0.01255
50	0.00314	0.01135
60	0.00315	0.01144
70	0.00300	0.01051
80	0.00269	0.00976
90	0.00259	.01042
NOISE(%)	...	

MODEL AL, FLOW: GRID CIII, VERTICAL BENDING, HP D.V.M.

WIND YAW ANGLE(DEG.)	U=3.0 M/SEC R.M.S.	PEAK	U=6.1 M/SEC R.M.S.	PEAK
-90	0.00146	0.00510	0.00433	0.01826
-80	0.00204	0.00757	0.00632	0.02275
-70	0.00295	0.01082	0.00917	0.03458
-60	0.00391	0.01346	0.01115	0.04400
-50	0.00414	0.01439	0.01400	0.04976
-40	0.00488	0.02130	0.01462	0.05174
-30	0.00514	0.01716	0.01602	0.07093
-20	0.00556	0.02046	0.01693	0.06692
-10	0.00598	0.02416	0.01844	0.07022
0	0.00601	0.02336	0.01852	0.06274
10	0.00620	0.02165	0.01837	0.06582
20	0.00613	0.02323	0.02066	0.08870
30	0.00594	0.02103	0.01977	0.07740
40	0.00593	0.02055	0.02053	0.07335
50	0.00567	0.02297	0.01962	0.07480
60	0.00577	0.02103	0.01792	0.06666
70	0.00627	0.02552	0.01881	0.06151
80	0.00628	0.01993	0.01992	0.08967
90	0.00800	.01954	0.01976	0.06851
NOISE(%)	...		...	

MODEL AL, FLOW: SMOOTH FLOW, VERTICAL BENDING, HP D.V.M.

WIND VEL. (M/SEC)	YAW ANGLE=0 DEG. R.M.S.	PEAK	YAW ANGLE=+45 DEG. R.M.S.	PEAK	YAW ANGLE=+90 DEG. R.M.S.	PEAK
2.7	0.00031	0.00123	0.00049	0.00207	0.00099	0.00326
3.0	0.00039	0.00158	0.00046	0.00167	0.00113	0.00343
3.4	0.00041	0.00167	0.00049	0.00180	0.00103	0.00308
3.7	0.00048	0.00172	0.00055	0.00356	0.00168	0.00506
4.1	0.00052	0.00194	0.00061	0.00242	0.00150	0.00440
4.5	0.00062	0.00260	0.00062	0.00246	0.00125	0.00427
5.0	0.00074	0.00273	0.00072	0.00268	0.00104	0.00374
5.5	0.00083	0.00334	0.00083	0.00312	0.00150	0.00554
6.1	0.00109	0.00434	0.00097	0.00392	0.00153	0.00519
6.7	0.00124	0.00484	0.00115	0.00515	0.00209	0.00695
7.4	0.00146	0.00603	0.00133	0.00625	0.00243	0.00744
8.2	0.00176	0.00673	0.00166	0.00625	0.00273	0.01052
9.1	0.00227	0.00770	0.00212	0.01038	0.00283	0.00942
NOISE(%)	2.8 MAX.		...		...	

MODEL AM, FLOW: GRID CI, VERTICAL BENDING, HP D.V.M.

WIND YAW ANGLE(DEG.)	U=3.0 M/SEC R.M.S.	PEAK	U=6.1 M/SEC R.M.S.	PEAK
-90	0.00146	0.00480	0.00406	0.01690
-80	0.00209	0.00798	0.00664	0.02275
-70	0.00351	0.01131	0.00939	0.03381
-60	0.00487	0.01729	0.01330	0.05029
-50	0.00534	0.02272	0.01520	0.05616
-40	0.00672	0.03302	0.01795	0.07652
-30	0.00793	0.03417	0.02028	0.09950
-20	0.00869	0.03253	0.02102	0.07262
-10	0.00901	0.03670	0.02374	0.09853
0	0.00983	0.03384	0.02501	0.08687
10	0.01142	0.03773	0.02698	0.10531
20	0.01074	0.03900	0.02509	0.10333
30	0.01168	0.04061	0.02913	0.11147
40	0.01238	0.04770	0.03233	0.10821
50	0.01192	0.03966	0.03125	0.10403
60	0.01257	0.04387	0.03244	0.12954
70	0.01395	0.05027	0.03481	0.11433
80	0.01400	0.04446	0.03637	0.12828
90	0.01470	0.04833	0.04104	0.14091
NOISE(%)	...		...	

MODEL AM, FLOW: GRID NI, VERTICAL BENDING, HP D.V.M.

WIND VEL. (M/SEC)	YAW ANGLE=-45 DEG. R.M.S.	PEAK	YAW ANGLE=0 DEG. R.M.S.	PEAK	YAW ANGLE=+45 DEG. R.M.S.	PEAK	YAW ANGLE=+90 DEG. R.M.S.	PEAK
1.8	0.00282	0.00996	0.00438	0.01690	0.00635	0.02627	0.00477	0.01951
2.1	0.00439	0.01654	0.00620	0.02159	0.00816	0.02942	0.00833	0.02682
2.4	0.00519	0.02006	0.00801	0.02775	0.01040	0.03417	0.01118	0.04089
2.7	0.00708	0.02548	0.00970	0.03604	0.01119	0.03976	0.01368	0.04393
3.0	0.00723	0.02620	0.01181	0.04554	0.01419	0.05170	0.01738	0.05085
3.4	0.00855	0.03278	0.01370	0.05016	0.01663	0.05654	0.01489	0.05104
3.7	0.01045	0.03426	0.01476	0.05016	0.01801	0.06380	0.02072	0.07348
4.1	0.01150	0.03846	0.01727	0.06270	0.02028	0.07920	0.02521	0.08338
4.5	0.01364	0.05192	0.02072	0.07040	0.02382	0.09614	0.02725	0.09460
5.0	0.01577	0.05786	0.02321	0.10692	0.02763	0.10758	0.03539	0.11396
5.5	0.01800	0.07392	0.02589	0.08646	0.03201	0.13948	0.03825	0.13706
6.1	0.02094	0.07458	0.02948	0.11330	0.03548	0.13288	0.04778	0.16478
6.7	0.02235	0.07766	0.03473	0.14520	0.04243	0.15004	0.04688	0.16280
7.4	0.02385	0.10274	0.03573	0.15378	0.04257	0.15884	0.05563	0.18260
8.2	0.02659	0.10494	0.04050	0.13992	0.05110	0.21186	0.06015	0.24156
9.1	0.02857	0.11066	0.04318	0.17930	0.05233	0.19470	0.06681	0.27358
NOISE(%)	...		...		...		...	

MODEL AM, FLOW: GRID CIII, VERTICAL BENDING, HP D.V.M.

WIND YAW ANGLE(DEG.)	U=3.0 M/SEC R.M.S.	PEAK	U=6.1 M/SEC R.M.S.	PEAK
-90	0.00040	0.00163	0.00138	0.00559
-80	0.00062	0.00242	0.00206	0.00759
-70	0.00086	0.00327	0.00297	0.01062
-60	0.00119	0.00475	0.00397	0.01386
-50	0.00139	0.00561	0.00477	0.02040
-40	0.00163	0.00635	0.00536	0.01964
-30	0.00185	0.00781	0.00592	0.02209
-20	0.00189	0.00750	0.00671	0.02549
-10	0.00237	0.00798	0.00691	0.03062
0	0.00223	0.00860	0.00725	0.03014
10	0.00246	0.00952	0.00760	0.03049
20	0.00278	0.01062	0.00866	0.03221
30	0.00262	0.00959	0.00818	0.03228
40	0.00245	0.00972	0.00888	0.03179
50	0.00269	0.01185	0.00891	0.03536
60	0.00299	0.01047	0.01017	0.03472
70	0.00329	0.01008	0.01065	0.03988
80	0.00363	0.01012	0.01179	0.03923
90	0.00386	0.01360	0.01[illegible]	0.04035
NOISE(%)	2.6 MAX.		...	

MODEL AM, FLOW: GRID NIII, VERTICAL BENDING, HP D.V.M.

WIND VEL. (M/SEC)	YAW ANGLE=-45 DEG. R.M.S.	PEAK	YAW ANGLE=0 DEG. R.M.S.	PEAK	YAW ANGLE=+45 DEG. R.M.S.	PEAK	YAW ANGLE=+90 DEG. R.M.S.	PEAK
2.1	0.00084	0.00270	0.00122	0.00429	0.00150	0.00477	0.00241	0.00796
2.4	0.00097	0.00376	0.00145	0.00541	0.00172	0.00662	0.00312	0.01128
2.7	0.00119	0.00447	0.00167	0.00745	0.00232	0.00759	0.00335	0.01175
3.0	0.00124	0.00484	0.00181	0.00688	0.00238	0.00882	0.00327	0.00988
3.4	0.00153	0.00569	0.00208	0.00700	0.00244	0.00895	0.00432	0.01333
3.7	0.00158	0.00620	0.00223	0.00864	0.00260	0.01005	0.00501	0.01692
4.1	0.00179	0.00651	0.00258	0.00884	0.00298	0.01085	0.00600	0.02024
4.5	0.00195	0.00675	0.00289	0.01269	0.00341	0.01212	0.00660	0.02297
5.0	0.00198	0.00688	0.00291	0.01261	0.00341	0.01265	0.00653	0.02187
5.5	0.00222	0.00847	0.00326	0.01201	0.00384	0.01701	0.00699	0.02350
6.1	0.00255	0.00974	0.00343	0.01265	0.00417	0.01571	0.00749	0.02414
6.7	0.00272	0.01028	0.00390	0.01676	0.00480	0.02143	0.00858	0.03113
7.4	0.00292	0.01221	0.00414	0.01452	0.00502	0.01961	0.00943	0.02875
8.2	0.00315	0.01164	0.00427	0.01716	0.00524	0.01910	0.00904	0.03344
9.1	0.00359	0.01382	0.00513	0.02233	0.00610	0.02380	0.01029	0.04246
NOISE(%)	...		...		...		...	

MODEL AM, FLOW: SMOOTH FLOW, VERTICAL BENDING, HP D.V.M.

WIND YAW ANGLE(DEG.)	U=3.0 M/SEC R.M.S.	PEAK	U=6.1 M/SEC R.M.S.	PEAK
-90	0.00036	0.00141	0.00081	0.00308
-80	0.00033	0.00121	0.00070	0.00282
-70	0.00018	0.00077	0.00051	0.00216
-60	0.00015	0.00060	0.00048	0.00187
-50	0.00015	0.00057	0.00044	0.00187
-40	0.00014	0.00053	0.00039	0.00152
-30	0.00013	0.00055	0.00037	0.00157
-20	0.00013	0.00057	0.00037	0.00136
-10	0.00014	0.00053	0.00036	0.00141
0	0.00016	0.00062	0.00036	0.00132
10	0.00014	0.00066	0.00039	0.00141
20	0.00014	0.00057	0.00042	0.00167
30	0.00016	0.00066	0.00044	0.00173
40	0.00018	0.00075	0.00038	0.00143
50	0.00021	0.00090	0.00042	0.00198
60	0.00021	0.00084	0.00046	0.00185
70	0.00029	0.00121	0.00043	0.00169
80	0.00045	0.00123	0.00059	0.00245
90	0.00048	0.00150	0.00084	0.00319
NOISE(%)	10.0 MAX.		2.1 MAX.	

MODEL AM, FLOW: SMOOTH FLOW, VERTICAL BENDING, HP D.V.M.

WIND VEL. (M/SEC)	YAW ANGLE=0 DEG. R.M.S.	YAW ANGLE=0 DEG. PEAK	YAW ANGLE=+45 DEG. R.M.S.	YAW ANGLE=+45 DEG. PEAK	YAW ANGLE=+90 DEG. R.M.S.	YAW ANGLE=+90 DEG. PEAK
2.7	0.00012	0.00053	0.00019	0.00075	0.00036	0.00110
3.0	0.00016	0.00066	0.00019	0.00077	0.00043	0.00182
3.4	0.00017	0.00070	0.00019	0.00075	0.00036	0.00129
3.7	0.00019	0.00092	0.00022	0.00088	0.00047	0.00172
4.1	0.00021	0.00090	0.00024	0.00104	0.00047	0.00167
4.5	0.00024	0.00101	0.00026	0.00114	0.00048	0.00169
5.0	0.00028	0.00113	0.00030	0.00128	0.00055	0.00176
5.5	0.00032	0.00117	0.00035	0.00134	0.00068	0.00253
5.8	—	—	—	—	0.00061	0.00224
5.9	—	—	—	—	0.00087	0.00277
6.1	0.00040	0.00173	0.00043	0.00233	0.00108	0.00321
6.7	0.00045	0.00176	0.00048	0.00187	0.00123	0.00444
7.4	0.00050	0.00194	0.00062	0.00235	0.00147	0.00495
8.2	0.00062	0.00306	0.00077	0.00317	0.00189	0.00686
9.1	0.00075	0.00275	0.00096	0.00361	0.00211	0.00759
NOISE(%)	15.2 MAX.		8.3 MAX.		2.4 MAX.	

MODEL AN, FLOW: GRID CI, VERTICAL BENDING, HP D.V.M.

WIND YAW ANGLE(DEG.)	U=3.0 M/SEC R.M.S.	U=3.0 M/SEC PEAK	U=6.1 M/SEC R.M.S.	U=6.1 M/SEC PEAK
-90	0.00057	0.00260	0.00141	0.00537
-80	0.00067	0.00246	0.00180	0.00622
-70	0.00104	0.00444	0.00276	0.01006
-60	0.00142	0.00483	0.00387	0.01404
-50	0.00171	0.00669	0.00456	0.01861
-40	0.00200	0.00875	0.00582	0.02204
-30	0.00249	0.01016	0.00687	0.02761
-20	0.00275	0.01235	0.00772	0.02771
-10	0.00290	0.01162	0.00814	0.02962
0	0.00348	0.01148	0.01015	0.03392
10	0.00362	0.01305	0.01041	0.03656
20	0.00444	0.01503	0.01245	0.04883
30	0.00506	0.01693	0.01302	0.05606
40	0.00503	0.01925	0.01396	0.05504
50	0.00567	0.01893	0.01640	0.06372
60	0.00675	0.02474	0.01819	0.07011
70	0.00897	0.02913	0.02048	0.07561
80	0.00793	0.02785	0.02326	0.07249
90	0.00906	0.03090	0.02594	0.08104
NOISE(%)	...		...	

MODEL AN, FLOW: GRID CIII, VERTICAL BENDING, HP D.V.M.

WIND YAW ANGLE(DEG.)	U=3.0 M/SEC R.M.S.	U=3.0 M/SEC PEAK	U=6.1 M/SEC R.M.S.	U=6.1 M/SEC PEAK
-90	0.00029	0.00115	0.00077	0.00326
-80	0.00025	0.00098	0.00075	0.00322
-70	0.00030	0.00119	0.00093	0.00328
-60	0.00034	0.00123	0.00117	0.00428
-50	0.00044	0.00178	0.00149	0.00541
-40	0.00050	0.00224	0.00163	0.00689
-30	0.00057	0.00202	0.00200	0.00750
-20	0.00065	0.00236	0.00227	0.00852
-10	0.00079	0.00373	0.00234	0.00930
0	0.00091	0.00341	0.00289	0.01097
10	0.00084	0.00290	0.00305	0.01193
20	0.00097	0.00339	0.00334	0.01197
30	0.00111	0.00386	0.00383	0.01588
40	0.00116	0.00382	0.00428	0.01407
50	0.00118	0.00442	0.00441	0.01703
60	0.00131	0.00501	0.00472	0.01765
70	0.00152	0.00534	0.00559	0.02212
80	0.00181	0.00533	0.00627	0.02125
90	0.00217	0.00683	0.00718	0.02077
NOISE(%)	1.1 MAX.		...	

MODEL AO, FLOW: GRID CIII, VERTICAL BENDING, HP D.V.M.

WIND YAW ANGLE(DEG.)	U=3.0 M/SEC R.M.S.	U=3.0 M/SEC PEAK
-90	0.00013	0.00057
-80	0.00014	0.00055
-70	0.00014	0.00059
-60	0.00017	0.00066
-50	0.00020	0.00076
-40	0.00024	0.00091
-30	0.00028	0.00124
-20	0.00031	0.00110
-10	0.00035	0.00143
0	0.00041	0.00148
10	0.00045	0.00171
20	0.00054	0.00207
30	0.00055	0.00189
40	0.00074	0.00327
50	0.00092	0.00320
60	0.00092	0.00311
70	0.00089	0.00379
80	0.00134	0.00480
90	0.00116	0.00426
NOISE(%)	4.6 MAX.	

MODEL AO, FLOW: GRID CI, VERTICAL BENDING, HP D.V.M.

WIND YAW ANGLE(DEG.)	U=3.0 M/SEC R.M.S.	U=3.0 M/SEC PEAK
-90	0.00031	0.00119
-80	0.00036	0.00167
-70	0.00044	0.00181
-60	0.00057	0.00193
-50	0.00083	0.00308
-40	0.00089	0.00363
-30	0.00114	0.00477
-20	0.00126	0.00594
-10	0.00149	0.00534
0	0.00185	0.00761
10	0.00205	0.00801
20	0.00234	0.00781
30	0.00250	0.00961
40	0.00320	0.01150
50	0.00357	0.01237
60	0.00414	0.01414
70	0.00529	0.01910
80	0.00576	0.02588
90	0.00510	0.01781
NOISE(%)	...	

MODEL AP, FLOW: GRID CI, VERTICAL BENDING, HP D.V.M.

WIND YAW ANGLE(DEG.)	U=7.0 M/SEC R.M.S.	U=7.0 M/SEC PEAK
-90	0.00043	0.00163
-80	0.00046	0.00169
-70	0.00053	0.00190
-60	0.00063	0.00243
-50	0.00075	0.00303
-40	0.00087	0.00367
-30	0.00105	0.00457
-20	0.00124	0.00491
-10	0.00148	0.00579
0	0.00171	0.00643
10	0.00189	0.00748
20	0.00238	0.00918
30	0.00324	0.01352
40	0.00432	0.01511
50	0.00459	0.01699
60	0.00570	0.02449
70	0.00660	0.02221
80	0.00732	0.02820
90	0.00684	0.02676
NOISE(%)	...	

MODEL AP, FLOW: GRID CIII, VERTICAL BENDING, HP D.V.M.

WIND YAW ANGLE(DEG.)	U=7.0 M/SEC R.M.S.	PEAK
-90	0.00020	0.00076
-80	0.00018	0.00076
-70	0.00017	0.00073
-60	0.00019	0.00068
-50	0.00021	0.00086
-40	0.00025	0.00095
-30	0.00029	0.00116
-20	0.00032	0.00120
-10	0.00040	0.00156
0	0.00046	0.00176
10	0.00045	0.00184
20	0.00056	0.00222
30	0.00080	0.00327
40	0.00097	0.00332
50	0.00115	0.00449
60	0.00126	0.00497
70	0.00138	0.00542
80	0.00154	0.00473
90	0.00168	0.00595
NOISE(%)	1.5 MAX.	

MODEL AM, FLOW: GRID CI, TORSION, HP D.V.M.

WIND YAW ANGLE(DEG.)	U=3.0 M/SEC R.M.S.	PEAK	U=6.1 M/SEC R.M.S.	PEAK
-90	0.00257	0.01069	0.01258	0.06195
-80	0.00397	0.01715	0.01771	0.08314
-70	0.00641	0.03117	0.03352	0.15277
-60	0.01178	0.05088	0.05740	0.23603
-50	0.01405	0.05683	0.08564	0.34080
-40	0.02031	0.09613	0.11327	0.43885
-30	0.02420	0.09082	0.12412	0.49293
-20	0.02786	0.12186	0.14182	0.52538
-10	0.03094	0.12966	0.15507	0.58131
0	0.03180	0.13261	0.16731	0.65472
10	0.03204	0.12090	0.17462	0.70982
20	0.03074	0.14387	0.15074	0.61933
30	0.03107	0.12435	0.15074	0.62720
40	0.02596	0.13101	0.13617	0.58605
50	0.02097	0.08870	0.12299	0.48320
60	0.01913	0.08179	0.08931	0.36083
70	0.01687	0.06317	0.08015	0.30304
80	0.01700	0.06266	0.07568	0.31610
90	0.01558	0.05504	0.07345	0.21600
NOISE(%)	5.3 MAX.		...	

MODEL AM, FLOW: GRID NI, TORSION, TSI VOLTMETER

WIND VEL. (M/SEC)	YAW ANGLE=-45 DEG. R.M.S.	YAW ANGLE=0 DEG. R.M.S.	YAW ANGLE=+45 DEG. R.M.S.	YAW ANGLE=+90 DEG. R.M.S.
1.8	0.00723	0.01180	0.00843	0.00555
2.1	0.01064	0.01780	0.01296	0.00726
2.4	0.01542	0.02456	0.01832	0.01204
2.7	0.02062	0.03600	0.02459	0.01346
3.0	0.02533	0.04554	0.02882	0.01786
3.4	0.03317	0.05492	0.03711	0.02163
3.7	0.04334	0.07101	0.04556	0.02883
4.1	0.05538	0.09366	0.05931	0.03274
4.5	0.07491	0.11709	0.07571	0.04603
5.0	0.09366	0.14833	0.09680	0.05072
5.5	0.12100	0.18113	0.12647	0.06556
6.1	0.16863	0.22330	0.15302	0.07805
6.7	0.20924	0.29670	0.19831	0.09524
7.4	0.25921	0.34355	0.25297	0.12257
8.2	0.33574	0.41226	0.32012	0.14678
9.1	0.39820	0.51844	0.40601	0.18582
NOISE(%)	5.5 MAX.	1.9 MAX.	2.7 MAX.	5.2 MAX.

MODEL AM, FLOW: GRID CIII, TORSION, HP D.V.M.

WIND YAW ANGLE(DEG.)	U=3.0 M/SEC R.M.S.	U=3.0 M/SEC PEAK	U=6.1 M/SEC R.M.S.	U=6.1 M/SEC PEAK
-90	0.00143	0.00653	0.00970	0.03757
-80	0.00207	0.01082	0.01030	0.04122
-70	0.00294	0.01338	0.01654	0.06918
-60	0.00527	0.02272	0.02913	0.11238
-50	0.00751	0.03290	0.03811	0.14291
-40	0.01016	0.04320	0.05359	0.20845
-30	0.01142	0.05139	0.05481	0.22099
-20	0.01273	0.04589	0.06135	0.26618
-10	0.01480	0.05376	0.06390	0.27162
0	0.01428	0.05606	0.06764	0.29069
10	0.01481	0.05459	0.06556	0.23648
20	0.01542	0.05286	0.06612	0.25958
30	0.01475	0.05779	0.06557	0.29715
40	0.01394	0.06138	0.06361	0.26976
50	0.01146	0.04250	0.05328	0.22106
60	0.01132	0.04653	0.04500	0.16352
70	0.01063	0.04947	0.03935	0.15187
80	0.01119	0.03597	0.03702	0.14061
90	0.01136	0.03251	0.03878	0.14790
NOISE(%)	14.1 MAX.		...	

MODEL AM, FLOW: GRID NIII, TORSION, TSI VOLTMETER

WIND VEL. (M/SEC)	YAW ANGLE=-45 DEG. R.M.S.	YAW ANGLE=0 DEG. R.M.S.	YAW ANGLE=+45 DEG. R.M.S.	YAW ANGLE=+90 DEG. R.M.S.
2.1	0.00375	0.00717	0.00705	0.00924
2.4	0.00524	0.01050	0.00947	0.01306
2.7	0.00749	0.01554	0.01359	0.01465
3.0	0.00956	0.01977	0.01737	0.01670
3.4	0.01192	0.02509	0.02130	0.02252
3.7	0.01444	0.03119	0.02647	0.02723
4.1	0.0204C	0.03745	0.03273	0.03083
4.5	0.02493	0.04370	0.04055	0.03428
5.0	0.02994	0.05464	0.04836	0.03741
5.5	0.03745	0.06244	0.05306	0.04679
6.1	0.04760	0.07338	0.06399	0.05148
6.7	0.05385	0.08588	0.07649	0.05617
7.4	0.06479	0.09681	0.08274	0.06711
8.2	0.07963	0.11086	0.09836	0.07180
9.1	0.09524	0.12961	0.11085	0.08273
NOISE(%)	7.6 MAX.	2.2 MAX.	3.9 MAX.	3.1 MAX.

MODEL AN, FLOW: GRID CI, TORSION, TSI VOLTMETER

WIND YAW ANGLE(DEG.)	U=3.0 M/SEC R.M.S.	U=6.1 M/SEC R.M.S.
-90	0.00446	0.02069
-80	0.00468	0.02921
-70	0.00863	0.05045
-60	0.01367	0.06763
-50	0.01937	0.10400
-40	0.02516	0.14036
-30	0.03326	0.14642
-20	0.03528	0.17672
-10	0.04034	0.18177
0	0.04236	0.19692
10	0.04236	0.19996
20	0.04540	0.21308
30	0.03933	0.19692
40	0.04034	0.20197
50	0.03832	0.17470
60	0.03933	0.17672
70	0.04034	0.16965
80	0.03933	0.16864
90	0.04337	0.16662
NOISE(%)	9.9 MAX.	...

MODEL AN, FLOW: GRID CIII, TORSION, TSI VOLTMETER

WIND YAW ANGLE(DEG.)	U=3.0 M/SEC R.M.S.	U=6.1 M/SEC R.M.S.
-90	0.00223	0.01704
-80	0.00276	0.01551
-70	0.00397	0.02211
-60	0.00586	0.02789
-50	0.00913	0.03629
-40	0.01192	0.04641
-30	0.01396	0.04944
-20	0.01580	0.05551
-10	0.01550	0.06157
0	0.01743	0.06258
10	0.01774	0.06763
20	0.01702	0.06763
30	0.01784	0.06763
40	0.01774	0.06561
50	0.01886	0.06460
60	0.01631	0.06763
70	0.01702	0.06258
80	0.01896	0.06561
90	0.02109	0.07470
NOISE(%)	2.9 MAX.	...

MODEL AO, FLOW: GRID CI, TORSION, TSI VOLTMETER

WIND YAW ANGLE(DEG.)	U=3.0 M/SEC R.M.S.
-90	0.00548
-80	0.00793
-70	0.01214
-60	0.01939
-50	0.02718
-40	0.03608
-30	0.04275
-20	0.04942
-10	0.05443
0	0.06720
10	0.06109
20	0.05443
30	0.06665
40	0.06332
50	0.06220
60	0.06109
70	0.06887
80	0.05998
90	0.07498
NOISE(%)	3.2 MAX.

MODEL AO, FLOW: GRID CIII, TORSION, TSI VOLTMETER

WIND YAW ANGLE(DEG.)	U=3.0 M/SEC R.M.S.
-90	0.00383
-80	0.00360
-70	0.00507
-60	0.00741
-50	0.00950
-40	0.01213
-30	0.01381
-20	0.01548
-10	0.01716
0	0.01772
10	0.01883
20	0.01939
30	0.02050
40	0.01939
50	0.02050
60	0.02328
70	0.02217
80	0.03052
90	0.02885
NOISE(%)	7.5 MAX.

MODEL AP, FLOW: GRID CI, TORSION, TSI VOLTMETER

WIND YAW ANGLE(DEG.)	U=7.0 M/SEC R.M.S.
-90	0.01323
-80	0.01517
-70	0.02326
-60	0.03199
-50	0.04072
-40	0.04912
-30	0.06140
-20	0.06787
-10	0.07595
0	0.08079
10	0.10019
20	0.10019
30	0.10666
40	0.11635
50	0.11958
60	0.12928
70	0.13574
80	0.13898
90	0.13898
NOISE(%)	...

MODEL AP, FLOW: GRID CIII, TORSION, TSI VOLTMETER

WIND YAW ANGLE(DEG.)	U=7.0 M/SEC R.M.S.
-90	0.00674
-80	0.00771
-70	0.00901
-60	0.01096
-50	0.01355
-40	0.01743
-30	0.01841
-20	0.02132
-10	0.02422
0	0.02682
10	0.02908
20	0.03069
30	0.03489
40	0.03942
50	0.03651
60	0.04201
70	0.04201
80	0.05009
90	0.06140
NOISE(%)	...

APPENDIX B. AERODYNAMIC DAMPING RESULTS

The results of the aerodynamic damping measurement are tabulated in this appendix. Description of the measuring procedure is given in Section 3.5.

MODEL AC, AERODYNAMIC DAMPING RATIO

WIND VEL. (M/SEC)	YAW ANGLE=-45 DEG.	YAW ANGLE=0 DEG.	YAW ANGLE=+45 DEG.	YAW ANGLE=+90 DEG.
2.1	0.0134	0.0221	0.0143	-0.0024
3.0	0.0224	0.0361	0.0263	-0.0024
4.1	0.0334	0.0511	0.0403	-0.0022
5.0	0.0424	0.0661	0.0523	-0.0020
6.1	0.0524	0.0851	0.0693	-0.0016
7.4	0.0674	0.1101	0.0963	-0.0007
9.1	0.0814	0.1351	0.1343	0.0001

MODEL AC, AERODYNAMIC DAMPING RATIO

WIND YAW ANGLE(DEG.)	U=3.0 M/SEC	U=6.1 M/SEC
-90	0.0064	0.0139
-80	0.0077	0.0164
-70	0.0114	0.0280
-60	0.0162	0.0390
-50	0.0218	0.0496
-40	0.0260	0.0597
-30	0.0319	0.0707
-20	0.0353	0.0790
-10	0.0378	0.0867
0	0.0409	0.0922
10	0.0413	0.0966
20	0.0399	0.0921
30	0.0369	0.0911
40	0.0318	0.0811
50	0.0269	0.0678
60	0.0192	0.0509
70	0.0122	0.0314
80	0.0044	0.0130
90	-0.0005	0.0005

MODEL AL, AERODYNAMIC DAMPING RATIO

WIND YAW ANGLE(DEG.)	U=3.0 M/SEC	U=6.1 M/SEC
-90	0.0088	0.0191
-80	0.0106	0.0225
-70	0.0123	0.0294
-60	0.0157	0.0359
-50	0.0189	0.0427
-40	0.0214	0.0497
-30	0.0237	0.0552
-20	0.0257	0.0597
-10	0.0265	0.0603
0	0.0267	0.0622
10	0.0269	0.0629
20	0.0265	0.0652
30	0.0248	0.0627
40	0.0218	0.0566
50	0.0184	0.0474
60	0.0135	0.0366
70	0.0088	0.0238
80	0.0034	0.0104
90	-0.0005	0.0000

MODEL AH, AERODYNAMIC DAMPING RATIO

WIND YAW ANGLE(DEG.)	U=3.0 M/SEC	U=6.1 M/SEC
-90	-0.00020	0.00080
-80	0.00140	0.00190
-70	-0.00020	0.00060
-60	0.00110	0.00210
-50	0.00440	0.00200
-40	-0.00030	-0.00154
-30	-0.00159	-0.00122
-20	-0.00151	-0.00148
-10	-0.00151	-0.00192
0	-0.00098	-0.00146
10	-0.00050	-0.00129
20	-0.00095	-0.00162
30	0.00020	-0.00108
40	0.00130	0.00110
50	0.00220	0.00250
60	0.00100	0.00220
70	0.00000	0.00050
80	-0.00020	-0.00010
90	-0.00030	-0.00020

MODEL AM, AERODYNAMIC DAMPING RATIO

WIND YAW ANGLE(DEG.)	U=3.0 M/SEC	U=6.1 M/SEC
-90	0.0115	0.0265
-80	0.0140	0.0325
-70	0.0154	0.0367
-60	0.0164	0.0412
-50	0.0182	0.0438
-40	0.0189	0.0460
-30	0.0194	0.0476
-20	0.0193	0.0469
-10	0.0170	0.0448
0	0.0170	0.0425
10	0.0169	0.0431
20	0.0166	0.0444
30	0.0156	0.0428
40	0.0140	0.0394
50	0.0116	0.0331
60	0.0087	0.0274
70	0.0053	0.0176
80	0.0016	0.0071
90	-0.0010	-0.0011